DIOXYGEN ACTIVATION AND SUBSTRATE HYDROXYLATION BY THE HYDROXYLASE COMPONENT OF TOLUENE/*O*-XYLENE MONOOXYGENASE FROM *PSEUDOMONAS* SPORIUM OX1

by

Leslie Justin Murray
B.A. Chemistry, B.A. Biology
Swarthmore College, 2002

SUBMITTED TO THE DEPARTMENT OF CHEMISTRY IN PARTIAL FULFILLMENT OF THE REQUIREMENTS FOR THE DEGREE OF

DOCTOR OF PHILOSOPHY OF INORGANIC CHEMISTRY
AT THE
MASSACHUSETTS INSTITUTE OF TECHNOLOGY

SEPTEMBER 2007

Signature of Author: _____
Department of Chemistry
August 02, 2007

Certified by: _____
Stephen J. Lippard
Arthur Amos Noyes Professor of Chemistry
Thesis Supervisor

Accepted by: _____
Robert W. Field
Haslem and Dewey Professor of Chemistry
Chairman, Departmental Committee on Graduate Studies

This doctoral thesis has been examined by a Committee of the Department of Chemistry as follows:

Daniel G. Nocera
W. M. Keck Professor of Energy and Professor of Chemistry
Committee Chairman

Stephen J. Lippard
Arthur Amos Noyes Professor of Chemistry
Thesis Supervisor

Stuart S. Licht
Assistant Professor of Chemistry

DIOXYGEN ACTIVATION AND SUBSTRATE HYDROXYLATION BY THE HYDROXYLASE COMPONENT OF TOLUENE/*O*-XYLENE MONOOXYGENASE FROM *PSEUDOMONAS* SPORIUM OX1

by

Leslie Justin Murray

Submitted to the Department of Chemistry
on 02 August, 2007
In Partial Fulfillment of the Requirements for the
Degree of Doctor of Philosophy in Chemistry

ABSTRACT

Non-heme carboxylate-bridged diiron centers in the hydroxylase components of the bacterial multicomponent monooxygenases activate dioxygen at structurally homologous active sites. Catalysis requires the management of four substrates: electrons, protons, dioxygen, and hydrocarbons. Protein component complexes control the delivery of these substrates to the diiron center in the hydroxylase ensuring selective hydrocarbon oxidation. A detailed mechanistic understanding of structural and chemical consequences of such interactions is a significant challenge.

This thesis begins with an overview of our current understanding of these processes. The discussion is primarily on the methane monooxygenase systems (MMO) because these have been the most extensively studied BMMs to date. Recent results for the toluene/*o*-xylene monooxygenase (ToMO) and phenol hydroxylase systems from *Pseudomonas* sporium OX1 are also briefly summarized, the former being the research focus of this dissertation.

Restricting access to the diiron center in ToMOH and other non-heme carboxylate-bridged diiron proteins was proposed to facilitate observation of oxygenated intermediates. To examine this hypothesis, dioxygen activation in ToMOH mutants that were predicted to occlude this channel was investigated by rapid-freeze quench (RFQ) EPR, Mössbauer, and ENDOR spectroscopy and stopped-flow optical spectroscopy. For the I100W mutant, a transient species is observed with an absorption maximum at 500 nm. EPR and Mössbauer spectra of RFQ samples identified this species as a diiron(III,IV) cluster spin-coupled to a neutral W radical. ENDOR spectra of this intermediate confirmed the protonation state and type of the amino acid radical and also identified a labile terminal water or hydroxide on the diiron center. Decay of this intermediate results in hydroxylation of the W radical. A diamagnetic precursor to the mixed-valent diiron(III,IV) center was also observed at an earlier time-point, with Mössbauer parameters typical of high-spin Fe^{III}. We have tentatively assigned this antiferromagnetically-coupled diiron(III) intermediate as a peroxo-bridged cluster.

A similar diiron(III) species is observed in RFQ Mössbauer samples from the reaction of reduced wild type hydroxylase with dioxygen. Substrate accelerates the decay rate of this species, providing evidence for the diiron(III) transient as the active oxidant. Under steady state conditions, hydrogen peroxide was generated in the absence of substrate. The oxidized hydroxylase also decomposed hydrogen peroxide to liberate dioxygen if no reducing equivalents were present. This

catalase activity suggests that dioxygen activation could be reversible. The linear free energy relationship determined from steady state hydroxylation of *para* substituted phenols has a negative slope. A value of $\rho < 0$ is indicative of electrophilic attack on the aromatic substrate by the oxidizing diiron(III) intermediate. The results from these steady state and pre-steady experiments provide compelling evidence that the diiron(III) transient is the active oxidant in ToMO and is a peroxodiiron(III) transient, despite differences between the optical and Mössbauer spectroscopic parameters and those of other peroxodiiron(III) centers.

Enzymatic oxidation of the radical clock substrate probe, norcarane, by ToMO gives rise to both desaturation and hydroxylation products, norcarenes and norcaranols respectively. Norcarenes are better substrates for this enzyme system than norcarane, producing additional oxidation products. In all, more than twenty oxidation products were characterized in these reaction mixtures, half of which arose from norcarene oxidation. Accounting for these secondary oxidation products, we determined that no substrate radical intermediates with a significant lifetime ($\tau < 25$ ps) are formed during catalysis.

Thesis Supervisor: Stephen J. Lippard
Title: Arthur Amos Noyes Professor of Chemistry

To my teachers

ACKNOWLEDGEMENTS

My completion of graduate school would have been impossible without my parents, my brother, and Sophia. Their emotional support through the early times at MIT and in the dash at the death was immensely important and uplifting. Their support and love have been like a puppeteer's strings that have kept me standing upright when I've felt like collapsing to the floor. We did it!

Early in my graduate career, I was without a lab to call home and my advisor, Professor Stephen Lippard, placed his faith and trust in me to undertake a project that was far removed from my research interests at that time. Accidents invariably flower into beautiful experiences, and my time in his lab is an experience that I would *never* trade. Intellectually, I have gained a profound awe and respect of enzymatic catalysis. His weekly, monthly, or biannual intellectual or scientific nitpickings and his demand for perfection, or what he perceived it as, were invaluable and annoying all at once. I am indebted to him for his guidance and support over the past five years. Useful, interesting, and challenging discussions were always on the menu in Professor Daniel Nocera's office. He instructed me during both of my oral examinations on photoinduced electron-transfer and charge separation. Now I know more than nothing! The remaining inorganic faculty, Professors Dick Schrock, Kit Cummins, Alan Davison, and Joseph Sadighi have provided me with the platform to understand, question, and appreciate the wealth of chemistry that falls under the veil of inorganic. And last, but not least, I thank Professor Stuart Licht for agreeing to sit on my thesis committee as I struggled to make the availabilities of various professors magically align.

Swarthmore College is a small place and it is odd to stay close to friends as one moves from undergraduate to graduate institutions. Tushar Parlikar has been a brother to me since my first days at Swarthmore and having him at MIT to share a drink, meal, ice cream, conversation, or anything else was wonderfully rejuvenating and relaxing. No matter how bad the day, a friendly face was just around the corner in electrical engineering. The walk to/from campus or Sunday morning dim sum was always in the company of Simon Kaufman, Aliki Bonarou, Russell Gordley, and Imo Akpan. I'm truly fortunate to have had their friendship while at MIT even if I've not been the most stellar correspondent.

For two summers, I worked at some iteration of Glaxo. I learned an enormous amount from Graham Robinett, Bill Zuercher, Stephen Reister, and Phil Turnbull, to name a few, while I was there. These experiences heightened my chemical interest and guided me toward graduate school. In my first summer, I worked for Sam Gerritz who always hoped secretly that I'd go to his graduate alma mater. He's talked me through a few rough times at M.I.T., and it has been good to have a friendly ear who knows what life in MIT Chemistry is like. Day trips with Sophia in August to visit the Gerritz family at Manchester-by-Sea to sit by the water, chat about life, and relax have been eagerly anticipated off-days many a summer.

I've spent more time in lab than anywhere else in the last few years. Fittingly, the people with whom I've worked have helped me all along the way. Matt Sazinsky and Laurance Beauvais took me under their wings as I floundered through protein expressions and purifications. I watched Euro 2006 with Dr. Viviane Izzo, screaming our hearts out as our teams played good, then bad, then lost. Colleague, classmate, and friend equal Mi Hee Lim. These coworkers have been great friends who've shared multiple scorpion bowls, swigs of rum, and late night dinners. Woon Ju Song, who is taking up the reigns on ToMO, has been immensely helpful to me as I was writing. The remainder of my subgroup past and present – Jessica Blazyk, Lisa Chatwood, Erik Dill, Mike McCormick, and Christy Tinberg – for their invaluable intellectual support and camaraderie over these five years.

My teachers from primary and secondary school in Trinidad – Mrs. Farinha, Mrs. Mitchell, Mrs. Camille Warwick, Mrs. Judy Lee Pow, Mr. Clifford Pierre, and Mr. Rajnatsingh – and my professors at Swarthmore College – Bob Paley, Bob Pasternack, Ahamindra Jain, Michael Wedlock, Paul

Rablen, Tom Stephenson, and Liz Vallen – were instrumental. This thesis acknowledges their tireless efforts as educators.

My research in the Lippard lab would have been impossible without our collaborators. Professor Brian Hoffman, Roman Davydov, Sun-Hee Kim, and Judy Nocek at Northwestern University have been amazing coworkers throughout my MIT career. Brian and Roman, in particular, have always given freely of their time to ensure that I understood the science. On my eight or so visits to Emory, I've had multiple dinners and lunches where the discussion has ranged from personal to professional with Professor Boi Hanh Vincent Huynh. His postdoctoral associates, Ricardo García-Serres, Sunil Naik, Danilo Ortillo, have been the workhorses behind data collection, processing, and analysis for the rapid freeze quench studies. Their contribution to my graduate work is immeasurable. Ioannis Papayannopoulos in the Proteomics Core Facility in the CCR at MIT examined my samples over and over and over again. Although we weren't able to get the beautiful data for which we were hoping, I'm very grateful to him for patient conversations regarding the experiments and subsequent data analysis.

My undergraduates, Jessica Lee and Eric Brown, who worked under my supervision have contributed greatly to the work that's presented here. Moreover, every time graduate school wore me down and made me question if this chemistry thing was worth it, along came Jessica with questions about her project, and biscotti to boot. Those discussions rejuvenated me on those long days or weeks.

Lastly, the Lippard Lab is filled with fantastic coworkers such as Andy Tennyson, Loi Do, Liz Nolan, Lindsey McQuade, K. Summer Lovejoy, Katie Barnes, Emily Carson, Sungho Yoon, Dong Xu, Dong Wang, Yongwon Jung, Evan Guggenheim, and Lippardites past and present. Cheers to you all!

I'm DONE!

TABLE OF CONTENTS

LIST OF TABLES

LIST OF SCHEMES

LIST OF FIGURES

ABBREVIATIONS

ACP	acyl-carrier protein
BMM	bacterial multicomponent monooxygenase
CBDI	non-heme carboxylate-bridged diiron
COSY	correlation spectroscopy
Δ^9D	stearoyl-ACP Δ^9 desaturase
DFT	density functional theory
dNTP	deoxynucleotide triphosphate
E. coli	*Escherichia coli*
EDTA	ethylenediamine-*N,N,N',N'*-tetraacetic acid
ENDOR	electron nuclear double resonance
EPR	electron paramagnetic resonance
ESI	electrospray ionization in either positive (+) or negative (-) modes
ET	electron transfer
FAD	flavin adenine dinucleotide
FID	flame ionization detection
Ft	ferritin
GC	gas chromatography
H_{mv}	diiron(II,III) hydroxylase component, prefaced with system abbreviation
H_{ox}	oxidized hydroxylase component, prefaced with system abbreviation
H_{peroxo}	peroxodiiron(III) intermediate, prefaced with system abbreviation
H_{red}	reduced hydroxylase component, prefaced with system abbreviation
HPLC	high performance liquid chromatography
ITC	isothermal titration calorimetry
LC/MS	liquid chromatography/mass spectrometry
M. caps.	*Methylococcus capsulatus* (Bath)
M. trich.	*Methylosinus trichosporium* OB3b
MALDI	matrix-assisted laser desorption/ionization
mCPBA	*m*-chloroperoxybenzoic acid
MMO	soluble methane monooxygenase, enzyme system
MMOB	regulatory protein of MMO

MMOH	hydroxylase component of MMO
MMOR	NADH oxidoreductase component of MMO
MMOR-Fd	truncated MMOR containing only a ferredoxin domain
MOPS	*N*-morphilinopropane sulfonic acid
MS/MS	mass spectrometry/mass spectrometry
MWCO	molecular weight cut-off
NADH	reduced form of β-nicotinamide adenine dinucleotide
NHE	normal hydrogen electrode
NMR	nuclear magnetic resonance
NOE	nuclear overhauser effect
PH	phenol hydroxylase from *Pseudomonas* sporium OX1, enzyme system
PHH	hydroxylase component of PH
PHM	regulatory protein of PH
Q	diiron(IV) intermediate formed in MMOH
RCS	radical-clock substrate
RFQ	rapid-freeze quench
RNR-R2	ribonucleotide reductase R2 subunit (Class 1)
rR	resonance Raman
SDS-PAGE	sodium dodecyl sulfate polyacrylamide gel electrophoresis
SKIE	solvent kinetic isotope effect
T4MO	toluene 4-monooxygenase from *Pseudomonas mendocina* KR1, enzyme system
T4MOH	hydroxylase component of T4MO
TFA	trifluoroacetic acid
TOF	time of flight
ToMO	toluene/*o*-xylene monooxygenase from *Pseudomonas* sp. OX1, enzyme system
ToMOC	Rieske component of ToMO
ToMOD	regulatory protein of ToMO
ToMOF	NADH oxidoreductase component of ToMO
ToMOH	hydroxylase component of ToMO
Tris	tris(hydroxymethyl)aminomethane
X	mixed-valent diiron(III,IV) intermediate formed in RNR-R2
XAS	X-ray absorption spectroscopy

CHAPTER 1

SUBSTRATE TRAFFICKING AND DIOXYGEN ACTIVATION IN BACTERIAL MULTICOMPONENT MONOOXYGENASES

INTRODUCTION

The biological activation of small substrates, such as dioxygen and dinitrogen, is carried out by large proteins comprising multiple subunits and containing metal cofactors. Examples of these remarkable enzymes include nitrogenase, cytochromes P450, tyrosinase, hydrogenase, cytochrome *c* oxidase, and the non-heme carboxylate-bridged diiron proteins. Members of the last family, which include the BMMs, RNR-R2, and Δ^9D, activate dioxygen at structurally homologous diiron centers housed within a four-helix bundle. The metal atoms in this bundle are coordinated by the side-chains of two E(D/H)XXH motifs.[1,2] The BMMs exquisitely couple the consumption of electrons and protons to dioxygen activation and substrate hydroxylation. Understanding the management of four substrates (electrons, protons, dioxygen, and hydrocarbons) in these enzyme systems is a central goal of ongoing research.

The mechanism of dioxygen activation in the carboxylate-bridged diiron family of enzymes is the subject of intense investigation. In the systems studied thus far, the resting state of the enzyme is a diiron(III) cluster with bridging oxo or hydroxo ligands, as observed in RNR-R2 and MMOH respectively. This state is unreactive toward dioxygen. Catalysis is initiated by two-electron reduction of the resting state to the reactive diiron(II) state. In systems where structures of the diiron(III) and diiron(II) forms of the enzymes, or analogues thereof, have been solved, reduction is accompanied by reorganization of the dimetallic cluster, whereby a dangling, or non-bonded, oxygen atom of a terminal carboxylate ligand shifts so that it bridges the metal ions. To maintain charge neutrality at the active site, proton transfers are predicted to occur during the reduction process. These protons may protonate the bridging hydroxo or oxo ligands, and the formed water dissociates from the dimetallic center.[3,4] The resulting diiron(II) form rapidly reacts with dioxygen to form a peroxodiiron(III) intermediate, which has been characterized by a number of spectroscopic methods (Table 1.1).[1] In MMO and RNR-R2, this intermediate evolves to higher-valent species Q and X,

Table 1.1. Spectroscopic Parameters for Peroxodiiron(III) Intermediates at Non-heme Diiron Centers

	Optical[a]		Mössbauer[a]		Resonance Raman[a]	
	λ_{max} [nm]	ε [$M^{-1}cm^{-1}$]	δ [mm/s]	ΔE_Q [mm/s]	O-O [cm^{-1}]	Fe-O [cm^{-1}]
MMO (*M. caps.)*	700	1800	0.66	1.51	-	-
MMO (*M. trich.*)	725	2500	0.67	1.51	-	-
RNR-R2[b]	700	1500	0.63	1.74	-	-
RNR-R2 D84E	700	1500	0.63	1.58	890	-
RNR-R2 D84E/W48F	700	-	-	-	870	458
Δ^9D	700	1200	0.68	1.90	898	442
			0.64	1.06		
Frog M Ft	650	-	0.62	1.08	851	458
cis-μ-1,2-peroxo Fe_2^{III}	694	2650	0.66	1.40	888	

[a]All parameters are reported from reference 1. [b] Reported in reference 42.

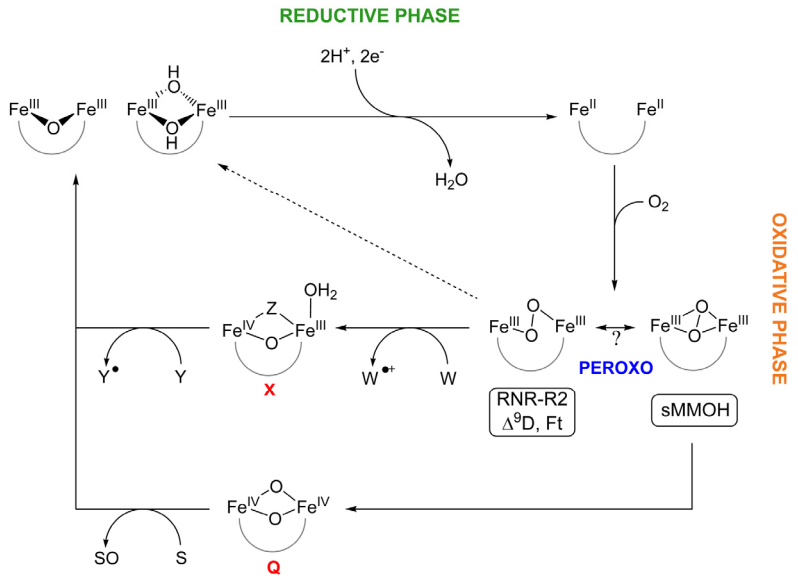

Figure 1.1. Dioxygen activation at non-heme carboxylate-bridged diiron centers. Reaction of the reduced diiron(II) state with dioxygen affords a peroxide-bridged intermediate, which can evolve to a high-valent species or decay to the resting diiron(III) state. In MMOH, intermediate Q can oxidize substrates, denoted as S, or decay via other pathways to the resting state. The peroxo intermediate in RNR-R2 oxidizes Trp48 to form X, which then oxidizes Tyr122 to restore the resting diiron(III) state.

respectively, which carry out methane hydroxylation or the one-electron oxidation of aromatic amino acid residues (Figure 1.1). In MMOH, both the peroxodiiron(III) ($MMOH_{peroxo}$) and Q intermediates are reactive toward substrates,[5] similar to the reactivity observed for oxygenated intermediates in the cytochrome P450 family[6] and some dicopper systems.[7] The catalytic cycle is closed as the

oxygenated intermediates return to the resting diiron(III) state following substrate hydroxylation or electron abstraction. In the absence of substrate, intermediate Q decays by a yet to be determined pathway to the resting state.

This discussion begins with a description of the protein components and their interactions. We then proceed through the stages of the catalytic cycle, examining first the ET events, followed by dioxygen activation and, finally, substrate hydroxylation. The role of protein component interactions in these processes is also highlighted.

BMM PROTEIN COMPONENTS

The BMMs are subdivided into different families, but all contain at least three components in the enzymatic system: a hydroxylase, an NADH oxidoreductase, and a regulatory protein. A fourth, Rieske protein, is also utilized in toluene/alkene monooxygenases.[8] In MMO, ToMO, and PH, the hydroxylase is a dimer of three polypeptide chains, $(\alpha\beta\gamma)_2$, with each α-subunit housing the carboxylate-bridged diiron center, the site of substrate hydroxylation. The hydroxylase molecular mass varies from 220 kDa in ToMO and PH to 251 kDa in MMOH. The 38-kDa oxidoreductase component shuttles electrons from NADH through its bound FAD and [2Fe-2S] cofactors to the hydroxylase either directly, as in MMO and PH, or indirectly via the Rieske component. The 10 to 15-kDa cofactor-less regulatory proteins bind to the hydroxylase and couple electron consumption to hydrocarbon oxidation.[9-11] The precise mechanistic consequences of these protein-protein interactions on ET and dioxygen activation are the subject of ongoing research. Very recently, the structure of PHH complexed to its regulatory protein, PHM, was solved, providing the first detailed picture of such an interaction.[12]

COMPONENT INTERACTIONS

The assembly of protein complexes during the reductive and oxidative phases of the catalytic

cycle must be finely orchestrated to ensure that electron consumption is linked to substrate hydroxylation. For example, reactive oxygenated diiron intermediates in the hydroxylase must not undergo adventitious reduction by the reductase or Rieske protein components.[13] The regulatory protein is proposed to compete with the reductase for a shared binding site on the hydroxylase,[10] thereby protecting oxygenated intermediates formed at the diiron center from undesired reductive quenching following dioxygen activation.[12] On the other hand, ET from these reducing components to the resting, diiron(III) state of the hydroxylase must occur to initiate catalysis. In this section, we first discuss studies of the structures and interactions between the regulatory proteins and their respective hydroxylases and then turn our attention to the ternary system comprising the regulatory, hydroxylase, and reductase/Rieske components.

Crystal structures of BMM hydroxylases from MMO, ToMO, and PH have been solved. Three structurally conserved features of note are hydrocarbon access routes, a likely ET pathway to the diiron core, and a pore through the four-helix bundle housing the diiron center for possible dioxygen or proton translocation. Soaking or pressurizing crystals of these proteins with substrate or product analogues has revealed the first of the three shared features, a potential pathway for the entrance or egress of hydrocarbon substrates or products. Soaking ToMOH crystals with the product analogue *p*-bromophenol revealed a large channel that delineates an access pathway from the exterior of the protein through the α-subunit to the active site (Figure 1.2).[14] When MMOH crystals were treated with xenon, bromomethanes, or iodoethane, these small hydrophobic species were detected in a series of adjacent hydrophobic pockets within the protein that trace a pathway from the protein surface to the diiron center.[15] The distinct pockets are capable of forming a contiguous pathway, as evidenced by structures of crystals soaked with *ω*-halogenated alcohols. In these structures, several residues, including Leu110 and Leu289, shift to allow the substrate analogues to traverse the protein cavities.[16] The structure of MMOH crystals soaked with 6-bromohexan-1-ol revealed another

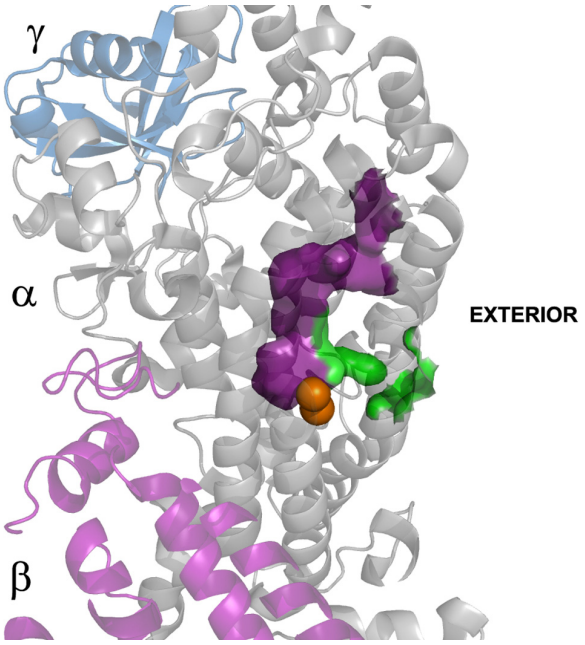

Figure 1.2. Substrate access channel and the conserved pore in ToMOH. The access channel (magenta) delineates a path from the diiron center (orange atoms) to the protein surface through the α-subunit (grey). The conserved pore (green), which is gated by Asn202, extends from the active site pocket to the protein surface. One half of the dimer is depicted.

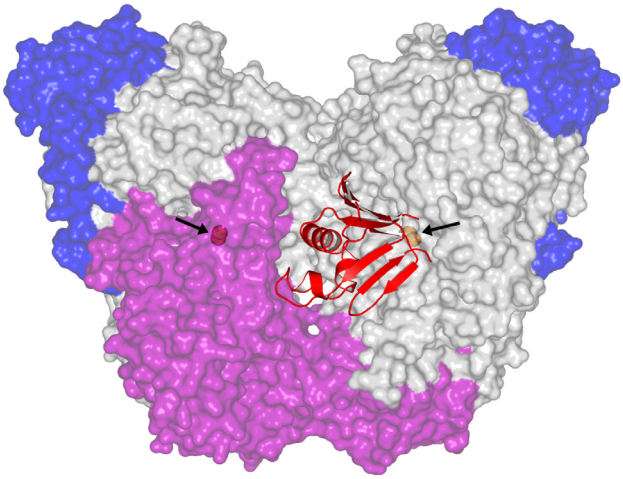

Figure 1.3. Crystal structure of PHH in complex with PHM shows the binding of the regulatory protein in the canyon region. The surface of PHH is rendered translucent with the α-, β-, and γ-subunits depicted in grey, purple, and blue, respectively. The iron atoms are depicted as orange spheres and denoted by arrows. PHM (red) binds to the α-subunit in a location similar to that predicted for binding of other regulatory proteins to their hydroxylases.

property of note. Residues 212-216 in helix E of the α-subunit unwind to extend the π-character of this helix, increasing the active site volume and reorienting Thr213 and Asn214, residues strictly conserved among the BMMs. The structure of PHH complexed to PHM contains a similarly extended π-helix, providing strong evidence that the binding of BMM regulatory proteins to their respective hydroxylases gives rise to specific conformational changes in helix E that directly affect the configuration of the active site pocket.[12] The environment around the diiron cluster was predicted from XAS studies of ToMOH and MMOH in complex with their regulatory proteins[17] to undergo conformational changes, and the PHH-PHM structure provides the first evidence for the nature of these changes.

PHM binds in the canyon region of PHH, specifically on helices E and F, and covers a hydrogen-bonding network that extends from the exterior to the iron-coordinated histidine residues at the active site. This feature is the second one conserved among the BMMs (Figures 1.3 and 1.4). The

locus on PHH where PHM binds, and the predominantly hydrophobic contacts between the proteins, agrees with the predictions of early NMR line-broadening studies carried out on MMOB and MMOH from *M. caps*.[18] The binding site of the regulatory proteins in the BMMs may therefore be conserved throughout the family. The hydrogen-bonding network that is covered by PHM, and presumably MMOB, is spatially homologous to the proposed ET pathway in other non-heme diiron proteins.[14] Binding of the BMM regulatory proteins to this surface, therefore, would interfere with ET for the reasons described above.[13]

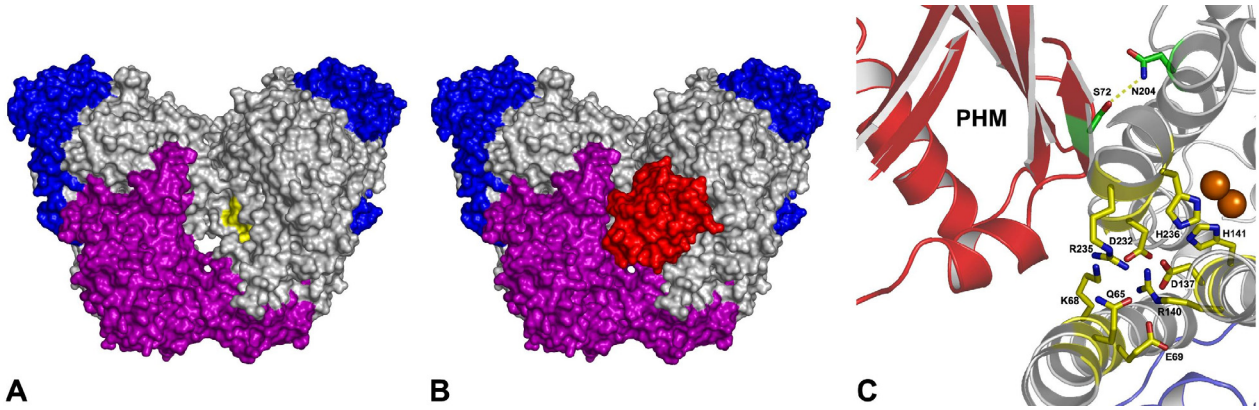

Figure 1.4. PHM binds to PHH at the proposed ET pathway and interacts with Asn204. (A) The surface-exposed residues, Arg235 and Lys68, of the conserved hydrogen-bonding network in the α-subunit are highlighted in yellow on a surface-rendered diagram of PHH. The α-, β-, and γ-subunits are depicted in grey, purple, and blue, respectively. (B) Diagram A with PHM (red) included. PHM covers this network when complexed to PHH and may prevent the reductase from binding at this locus. (C) A cutaway view, perpendicular to that in A and B, shows that this network, which extends from the iron atoms (orange spheres) to the surface, lies at the interface between the two proteins. PHM also interacts with Asn204 (green sticks), the side chain of which is oriented away from the diiron center as in the oxidized form of the hydroxylase and forms a hydrogen bond with Ser72 of the latter.

The third structurally conserved feature among BMMs is a small pore through the four helix bundle, which is proximal to the proposed ET pathway and extends from the active site pocket to the protein surface. In most of the crystal structures of BMM hydroxylases, this pore is closed, with a strictly conserved Asn residue (214, 202, and 204 in MMOH, ToMOH, and PHH respectively) serving as a gate to the opening. Crystallographic studies reveal this Asn residue to shift in a redox-dependent manner. Its side chain is oriented away from the active site in the oxidized form and points inward in the reduced or Mn(II)-reconstituted forms of the hydroxylase. This motion correlates with

the carboxylate shift that occurs upon reduction of the dimetallic center (Figure 1.5).[3,4] DFT calculations predict that dioxygen activation at the diiron(II) core of MMOH is accompanied by dissociation of this carboxylate group from its bridging position.[19] The Asn gate is open and the pore provides direct access to the diiron center in the bromohexanol-soaked structure of MMOH due to the increased π-character of helix E.[16]

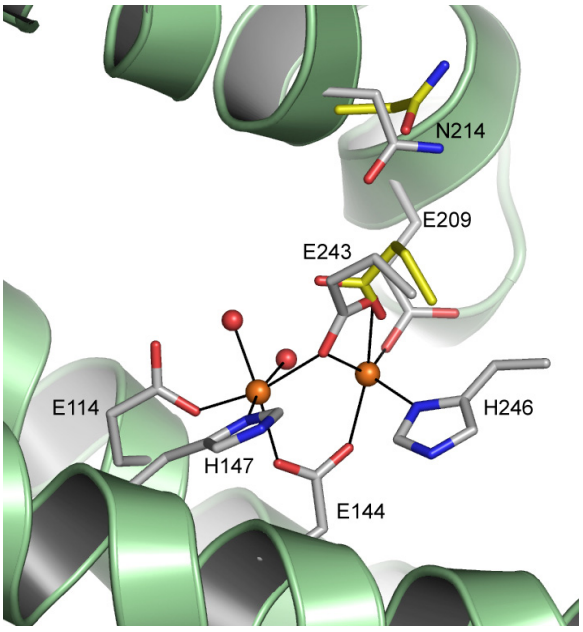

Figure 1.5. Redox-state-dependent conformations of residues in the active site pocket of MMOH. The amino acid residues depicted in gray correspond to the reduced state. Residues Glu243 and Asn214 shift upon oxidation (yellow) with Glu243 changing its coordination mode to the dimetallic center.

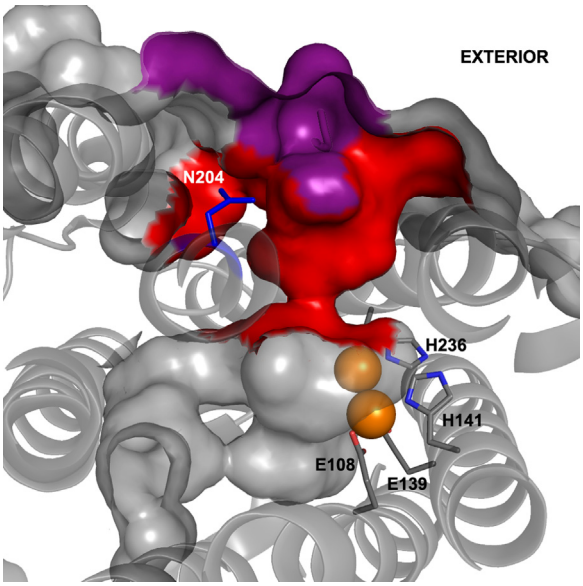

Figure 1.6. A surface-rendered representation of the pore in the α-subunit of PHH to which PHM is *not* bound. Asn204 (blue) is oriented away from the diiron center, opens the pore (red), and allows access from the protein exterior to the diiron center (orange spheres). Four iron-binding ligands, Glu108, Glu139, His236, and His141, are identified. This structural change may arise from PHM binding at the opposing face, interactions with the N-terminus of the β-subunit from the opposing monomer (purple), or packing in the crystal.

In the α-subunits of PHH, helix E adopts π-character similar to that in the MMOH bromohexanol-soaked structure, orients Asn204 away from the active site, and opens the pore.[12] PHM is bound only to one face of the PHH dimer and restricts access through this pore for the α–subunit to which it is bound, but for the other, the pore allows access to the diiron center (Figure 1.6). The opening of the pore by the shift in Asn204 on the face opposite that to which PHM binds may be an allosteric effect transmitted through the protein dimer interface, arise from interactions

with the N-terminus of the α-subunit of the adjacent monomer, or be a consequence of crystal packing. Residue Asn204 in PHH interacts with the hydroxyl side chain of a serine residue of the regulatory protein (Figure 1.4C), suggesting that mechanical strain created when the latter binds to the hydroxylase could promote rearrangement of the shifting carboxylate.[12] The hypothesis[20] that the regulatory protein binds to the MMO hydroxylase and provides a sieve for methane access to the active site at that position is inconsistent with the PHH-PHM structure. Moreover, we have not been able to rationalize this alternative proposal with the observation of CH_2Br_2, Xe, and other methane substrate analogues bound in the hydrophobic cavities of MMOH during structure determinations of crystals exposed to these agents. Finally, we note the possibility that dioxygen or protons may enter the active site via the pore. Additional structures of hydroxylases in complex with their respective regulatory proteins are required to evaluate further these possibilities.

Among the BMMs, component interactions in MMO isolated either from *M. caps.* or *M. trich.* have been the most extensively studied. Similar interactions were proposed for the binding of MMOB and MMOR to MMOH from studies using chemically modified MMOH.[21] The nature of these similar interactions was proposed to be electrostatic in contrast to the NMR line-broadening experiments mentioned above and the crystal structure of PHH-PHM. Whereas the binding face may have predominantly hydrophobic contacts, important electrostatic interactions, possibly to Arg245 and Lys74 in MMOH, may be essential for catalysis. A higher resolution structure of PHH-PHM with greater occupancy of PHM would be invaluable in resolving this apparent contradiction. The efficiency of cross-linking MMOB to MMOH decreases in the presence of MMOR,[9] suggesting that these components may share, either partially or completely, the same binding site on the hydroxylase. Both MMOR and MMOB bind to MMOH with a 2:1 stoichiometry in the *M. caps.* system, with MMOR binding being an order of magnitude stronger to MMOH than MMOB.[10] A 1:1 MMOB:MMOH complex has been proposed for the analogous *M. trich.* enzyme system.[9] In *M.*

trich., MMOB binds thirty-fold more weakly to reduced versus oxidized MMOH.[22] The K_d values determined from the formation and dissociation rate constants of these complexes disagree with the thermodynamic ones, indicative of rapid pre-equilibrium complex formation followed by a slower structural change,[10,22] such as an allosteric effect being transmitted to the other binding site on the dimer. Component binding to one face of the hydroxylase could effect a structural change in the canyon region on the opposite half of the dimer, as noted previously in the PHH-PHM structure. In agreement with the stoichiometry mentioned above, a ratio of 2 MMOB:1 MMOH affords maximal activity for steady-state hydroxylation in the *M. caps.* system. Moreover, enzymatic inhibition occurs at higher ratios of MMOB, suggesting that MMOB saturates the binding sites on MMOH, inhibiting the association of MMOR with MMOH.

ELECTRON TRANSFER TO THE OXIDIZED HYDROXYLASE

An early study of ET from NADH to the diiron(III) centers in oxidized MMOH, premixed with MMOR and variable equivalents of MMOB, demonstrated that all of the ET events from the [2Fe-2S] cluster of MMOR to diiron(III) active sites of MMOH are enhanced by MMOB.[10] More recently, an investigation of the reaction of chemically reduced MMOR or MMOR-Fd with MMOH-MMOB mixtures showed the opposite effect, in which MMOB served to *inhibit* ET.[23] These two apparently contradictory effects of MMOB on ET may be a consequence of a slow structural change associated with MMOB or MMOR binding to MMOH.[23] The conclusion that hysteresis may control the activity of MMOH was similarly drawn from an analysis of the product distributions when various substrates were hydroxylated by MMO from *M. trich*.[24] The interaction of MMOH with either MMOR or MMOB may depend on the presence or absence of the other component. The two may bind either concurrently, on opposing canyon regions of MMOH, or in rapid succession at the same canyon region on one side of the hydroxylase.

These two scenarios for the interaction of the components during the catalytic cycle are

illustrated in Figure 1.7. In the half-sites reactivity mechanism, the reductase binds on one canyon surface for ET while the regulatory protein binds on the other canyon surface for dioxygen activation and substrate hydroxylation (Figure 1.7A). Hysteresis would reflect binding of the regulatory and the reductase components to the opposite faces of the hydroxylase, thereby predisposing each diiron center to traverse opposite segments of the catalytic cycle. RFQ Mössbauer experiments performed to investigate the reaction of reduced MMOH[25] and ToMOH[26-28] with dioxygen have recorded consistently a maximal conversion of ~ 50% of the initial diiron(II) protein to the oxygenated intermediates. This observation suggests that the oxidative phase of the catalytic cycle can occur only at one active site of the dimer, irrespective of whether both active sites are fully reduced. The reaction of reduced ToMOH with dioxygen studied by RFQ Mössbauer spectroscopy will be

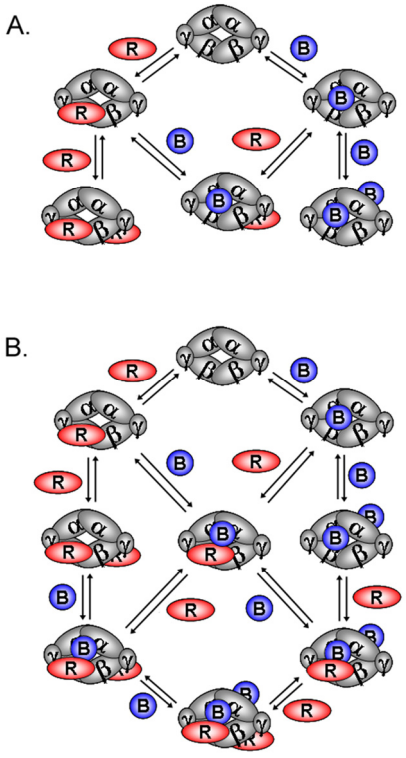

Figure 1.7. Possible scenarios for component interactions in the BMMs depicting a half-sites mechanism (A) and a non-interacting sites model (B). In (A), one active site is undergoing reduction while the second is activating dioxygen. In (B), a ternary complex may form but is not obligatory for catalysis and may have implications for ET and dioxygen activation. Adapted from reference 10.

presented in more detail in Chapters 2 and 3. Half-sites reactivity has also been proposed in other non-heme diiron proteins, in particular Δ^9D[29] and RNR-R2,[30] and may be a conserved feature in these systems. A different scenario, depicted in Figure 1.7B, is that the regulatory protein binds loosely to the hydroxylase and is displaced partially or shifts in the presence of the reductase to form a ternary complex that is competent for ET and catalysis. The inhibitory effect of excess MMOB on steady-state catalysis in MMO is best simulated by a model in which MMOB and MMOR bind to MMOH non-competitively and form a transient ternary complex.[10]

FORMATION AND REACTIVITY OF ACTIVATED DIOXYGEN INTERMEDIATES

Steady-state studies. The mechanism of hydrocarbon hydroxylation by the BMMs under steady-state conditions has been examined with radical clock substrate (RCS) probes. These hydrocarbons often contain strained rings that open with a characteristic lifetime following the loss of a hydrogen atom or ion. Such alternative substrates have been used to probe the mechanism of steady-state catalysis for a variety of enzyme systems including the BMMs.[1,31] Radical-derived ring-opened products will be observed only if their recombination rate is slower than ring expansion, in which case the lifetime of the radical can be estimated from ratios of the rearranged to unrearranged product alcohols. In general, only unrearranged products arising from rapid recombination of bound radical species are observed for most of the RCS probes tested in MMO, and their lifetime has been estimated as being less than 150 fs.[1,31] In addition to ring expansion from H-atom abstraction from the substrate, some RCS probes can ring-open following hydride abstraction to yield products that differ from the radical-derived ones. Norcarane, methylcubane, and 1,1-dimethylcyclopropane are examples of such RCS probes and the major products formed in steady-state catalysis by ToMO[32], T4MO[33], and MMO[1] with these substrates are the unrearranged alcohols. Little or no rearranged products, either radical- or carbocation-derived, are observed for these substrates in reactions with T4MO and MMO, in agreement with the other RCS experiments mentioned above. For the oxidation

of norcarane by MMO, ring-expansion products from both intermediates formed and the product ratios placed a lower limit of 20 ps on the radical lifetime, significantly greater than the value determined from any other probe. Oxidation of this RCS by T4MO afforded a radical-rearranged product (4.5% of the total), and no carbocation-derived product could be detected, contrary to the results from the oxidation of both 1,1-dimethyl- and 1,1-diethylcyclopropane.[33] A recent reexamination of the norcarane reaction for MMO and ToMO revealed that desaturation of the substrate by BMMs can explain these discrepancies.[34] Evidence for both a hydride and an H-atom transfer mechanism suggests that more than one reactive oxygenated intermediate may be involved.

Transient kinetic studies. In the oxidative phase of the catalytic cycle (Figure 1.1), the regulatory protein is required for the formation of detectable intermediates[35] and tunes the regioselectivity of substrate hydroxylation.[36] Transient, pre-steady-state kinetic studies have been performed with chemically reduced mixtures of the hydroxylases and their regulatory proteins to study the reactivity of individual intermediates during the reaction of dioxygen with the reduced BMM hydroxylases. In particular, we have utilized single- and double-mixing stopped-flow methodologies whereby a solution of reduced hydroxylase with its regulatory protein is mixed rapidly with dioxygen, allowed to age for a time period that maximizes the formation of an intermediate of interest, and the aged solution is subsequently mixed with buffer containing a substrate. Loss of an optical absorption band characteristic of the intermediate,[5] or of an infrared band of a substrate,[37] is measured as a function of substrate concentration. Among the BMMs, this strategy has been the most effective for investigating the reactions of MMOH with dioxygen since both $MMOH_{peroxo}$ and Q have characteristic absorption bands. The effect of substrates on the decay rate of each intermediate can be readily monitored by recording a change in these optical features. Initial studies of MMO in which propylene, methane, and acetylene were used as substrates indicated that $MMOH_{peroxo}$ reacts only with propylene whereas Q reacts with all three substrates.[5] Previous steady-state studies revealed that terminal alkenes are epoxidized by MMO with no C–H bond activation.[38,39] Although Q oxidizes propylene faster than

$MMOH_{peroxo}$, a judiciously chosen substrate might react more rapidly with $MMOH_{peroxo}$ than Q to confirm that $MMOH_{peroxo}$ is a reactive species. The oxidation of alternate substrates by these intermediates was therefore explored. Two such substrates, ethyl vinyl ether and diethyl ether, reacted more rapidly with $MMOH_{peroxo}$ than with Q.[40] A comparison of the nucleophilicity of the substrates investigated, and a detailed study of the oxidation of these particular substrates, indicated that $MMOH_{peroxo}$ is a more electrophilic oxidant than Q, preferring to react by a two-electron, or a hydride abstraction, pathway, whereas one-electron oxidation processes are preferred by Q (Figure 1.8). This difference in reactivity may explain the carbocation-derived products in the RCS probe experiments because attack of $MMOH_{peroxo}$ on these substrates is expected to form transient carbocations and Q would yield radical intermediates.

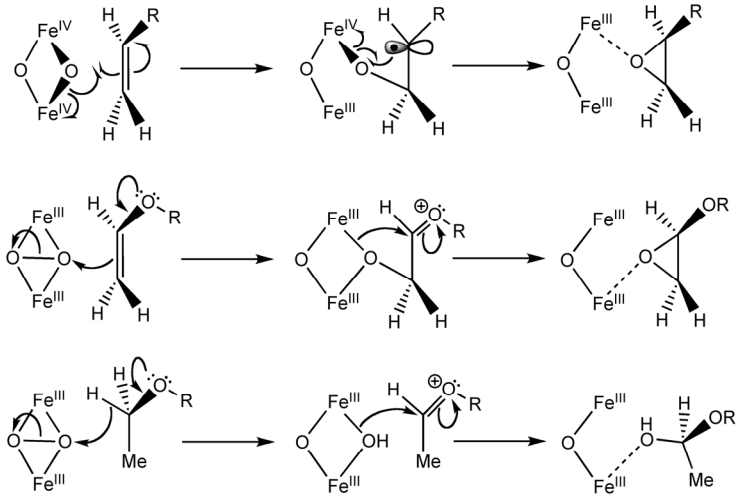

Figure 1.8. Proposed mechanism for reaction of Q and $MMOH_{peroxo}$ with substrates. Q reacts by sequential one-electron oxidations (upper). Reaction of $MMOH_{peroxo}$ with ethyl vinyl ether proceeds by a two-electron mechanism, in which a transient carbocation is stabilized by the proximal oxygen atom (middle). Hydroxylation of diethyl ether by $MMOH_{peroxo}$ is also proposed to proceed by a two-electron process, in which hydride abstraction forms a transient carbocation that recombines with the coordinated hydroxide (lower). Adapted from reference 40.

In contrast to what we observe for $MMOH_{peroxo}$, peroxodiiron(III) intermediates in ferritin,[41] RNR-R2,[42-44] Δ^9D,[29] and synthetic model compounds have no observed reactivity toward hydrocarbons. These peroxo species have been characterized by rR spectroscopy, from which it

appears that the peroxide moiety bridges the dimetallic center in a μ-1,2 fashion. Although a rR spectrum has not yet been obtained for $MMOH_{peroxo}$, computational methods predict that a μ-η^2:η^2-peroxo butterfly structure is more stable than the alternative μ-1,2 geometry of the bound peroxide.[19,40,45] The occurrence of such a binding mode in $MMOH_{peroxo}$ may explain why it reacts with electron-rich hydrocarbons and why a Q-type species is *only* observed in MMO. The difference in reactivity between $MMOH_{peroxo}$ and Q parallels the known differences between (μ-η^2:η^2-peroxo)dicopper(II) species and high-valent di(μ-oxo)dicopper(III) center in the dicopper complexes.[7] The lower-valent complex reacts by two-electron processes compared to the higher-valent counterpart, which prefers sequential one-electron oxidations. Theoretical studies on MMOH revealed that compression of the diiron cluster by the protein scaffold at the active site facilitates formation of a (μ-η^2:η^2-peroxo)diiron(III) structure and its subsequent conversion to Q.[45] It will be interesting to learn whether such an effect may be absent in other BMM hydroxylases which have different spectral parameters for the peroxo species and for which a diiron(IV) species has not yet been observed. A key difference between MMOB and the other BMM regulatory proteins is that the former has an unstructured 35 amino acid N-terminal domain.[18] Truncation of this domain leads to uncoupling of hydroxylation during steady-state turnover.[46] The presence of the N-terminal tail also correlates with the unique ability of MMOH to form Q, and binding of this domain to MMOH might further serve to compress the diiron core. Despite the structural homology between the active site of MMOH and ToMOH, no intermediates were observed by stopped-flow optical spectroscopy in studies of the latter.[26,27]

ORGANIZATION & SCOPE OF THESIS

This thesis addresses the oxidative and reductive phases of the catalytic cycle in the ToMO system. Investigations of dioxygen activation in mutant and native forms of ToMOH are presented in Chapters 2 and 3, respectively. Studies of the steady-state oxidation of the RCS probe norcarane are

described in Chapter 4. Appendix A discusses attempts to photoreduce the oxidized hydroxylase in MMO by tris(bipyridyl)ruthenium(III) complexes tethered to MMOB, and Appendix B details electron transfer from reduced ToMOC to oxidized ToMOH. The work in these appendices is preliminary in nature.

Until recently, no intermediates were reported during stopped-flow optical spectroscopic study of the reactions of reduced ToMOH or PHH, complexed with their respective regulatory proteins, with O_2-saturated buffer. Comparison of the crystal structures of ToMOH and MMOH reveal that residue I100 in the former is analogous to a leucine in the latter that is proposed to gate substrate access to the diiron site during catalysis.[47] As described in Chapter 2, mutations I100W/Y, L208F, and F205W were introduced in the α-subunit of ToMOH with the aim of retarding access at different points along the substrate access channel of any buffer components to the diiron site that might quench high-valent intermediates before they could accumulate to an observable level.[14,47] The reactions of these reduced mutant hydroxylases in complex with ToMOD with dioxygen were studied by stopped-flow optical spectroscopy. This method revealed that, in the ToMOH I100W mutant, a transient species having a maximal absorption at 500 nm formed upon oxygenation. No optically active intermediates were observed for the native or any of the other mutant hydroxylases. The reaction of the I100W mutant with dioxygen was further interrogated by RFQ EPR, ENDOR, and Mössbauer spectroscopy. Two intermediates were observed: a mixed-valent diiron(III,IV) cluster coupled to a neutral tryptophanyl radical, the latter giving rise to the optical absorption at 500 nm, and a diiron(III) species, which has no distinct optical absorption features and forms prior to the mixed-valent diiron(III,IV).[26]

Chapter 3 details our studies of dioxygen activation in the native system under steady-state and pre-steady-state conditions. First, we present the reaction of chemically reduced native ToMOH in complex with ToMOD by RFQ Mössbauer spectroscopy. A diiron(III) intermediate with isomer

shift, δ, and quadrupole splitting, ΔE_Q, parameters similar to those for the I100W diiron(III) transient was discovered.[27] This intermediate is longer-lived than that in the I100W mutant, presumably because it is no longer being quenched by a nearby redox-active residue. The effect of phenol, a substrate for this system, on the decay rate of this oxygenated intermediate was investigated by double-mixing RFQ Mössbauer spectroscopy. The decay is enhanced by more than thirty-fold in the presence of substrate, strongly suggesting that this species is the active oxidant in this system. Steady-state experiments are also described that complement the pre-steady-state investigations. The ToMO enzyme system appears to be incapable of accessing the peroxide shunt pathway for substrate hydroxylation in the absence of reducing equivalents from NADH, unlike MMO.[24] Second, the system generates hydrogen peroxide if substrate is absent from the reaction mixture. Third, the steady-state activity for the hydroxylation of a series of *para*-substituted phenols provided some insight into the nature of the key intermediate in this system. Taken together, these results indicate that a peroxodiiron(III) intermediate is the active oxidant in this system. The peroxide moiety is predicted to have a binding geometry and/or protonation state different from those previously reported in similar carboxylate-bridged diiron systems.

RCS probes have been extensively used to probe enzymatic oxidations under steady-state conditions. In most enzyme systems studied with these substrates, the calculated lifetimes of radical intermediates and the ratios of radical- and cation-derived products are consistent across a variety of different probes. Lifetime calculations from experiments employing norcarane as the RCS probe, however, are inconsistent in most enzyme systems studied thus far. The values obtained from product distributions for norcarane reactions are significantly greater that those from other substrates. A careful examination of the oxidation of norcarane by ToMO determined that more than twenty products form. Almost half of these products arise from oxidation of 2- and 3-norcarene, desaturation products of the parent compound. We therefore conclude that the lifetimes previously estimated in

the homologous T4MO, and for other CBDI enzymes such as MMO,[48,49] greatly overestimated the amount of radical-derived product formed.[32,34] By estimating the correct yields for the radical- and cation-derived products from our analysis, we determined lifetimes that agree with independent measurements carried out with different probes. Desaturation of substrates by this and other enzyme systems requires a judicious choice of RCS probe for which such reactivity is unfavorable.

No intermediates prior to $MMOH_{peroxo}$ have been observed in any carboxylate-bridged diiron proteins to date. DFT methods[19] predict that a short-lived superoxodiiron(II,III) species forms initially after dioxygen binding but that the calculated relative energies of $MMOH_{red}$, $MMOH_{superoxo}$, and $MMOH_{peroxo}$ preclude the accumulation and observation of such an intermediate. Appendix A describes studies utilizing tris(bipyridyl)ruthenium(II) complexes tethered to MMOB as a method of photoreducing the diiron cluster in MMOH in the presence of dioxygen to search for spectroscopic evidence for early events of dioxygen activation.

Efficient ET from reduced ToMOC to the oxidized hydroxylase requires ToMOH and ToMOD to be mixed prior to the reduction event. Moreover, this reaction only yields ~ 50% of oxidized ToMOC as determined by the change in optical absorbance. Two- or three-exponential functions were required to model the kinetic traces obtained, suggesting that two or more processes are involved in the ET reaction. One possible explanation for this observation is that the electrons can be distributed statistically upon reacting with $ToMOH_{ox}$ to yield mixtures of reduced, mixed-valent, and oxidized diiron sites. To address this question, the species formed after reaction of varying equivalents of $ToMOC_{red}$ with $ToMOH_{ox}$ were determined by EPR spectroscopy. We observed formation of reduced diiron(II) centers at substoichiometric ratios of $ToMOC_{red}$ to $ToMOH_{ox}$, suggesting that reduction favors formation of a two-electron reduced active site as opposed to mixed-valent centers. These results, together with our dioxygen activation studies, lead us to propose that a half-sites reactivity mechanism governs both the oxidative and reductive phases of the catalytic cycle in ToMO.

REFERENCES

1. Merkx, M.; Kopp, D. A.; Sazinsky, M. H.; Blazyk, J. L.; Müller, J.; Lippard, S. J., *Angew. Chem., Int. Ed.* **2001,** *40* (15), 2782-2807, and references cited therein.

2. Kurtz, D. J., Jr., *J. Biol. Inorg. Chem.* **1997,** *2* (2), 159-167.

3. Whittington, D. A.; Lippard, S. J., *J. Am. Chem. Soc.* **2001,** *123* (5), 827-838.

4. McCormick, M. S.; Sazinsky, M. H.; Condon, K. L.; Lippard, S. J., *J. Am. Chem. Soc.* **2006,** *128* (47), 15108-15110.

5. Valentine, A. M.; Stahl, S. S.; Lippard, S. J., *J. Am. Chem. Soc.* **1999,** *121* (16), 3876-3887.

6. Nam, W.; Ryu, Y. O.; Song, W. J., *J. Biol. Inorg. Chem.* **2004,** *9* (6), 654-660.

7. Decker, H.; Dillinger, R.; Tuczek, F., *Angew. Chem., Int. Ed.* **2000,** *39* (9), 1591-1595 and references cited therein.

8. Notomista, E.; Lahm, A.; DiDonato, A.; Tramontano, A., *J. Mol. Evol.* **2003,** *56* (4), 435-445.

9. Fox, B. G.; Liu, Y.; Dege, J. E.; Lipscomb, J. D., *J. Biol. Chem.* **1991,** *266* (1), 540-550.

10. Gassner, G. T.; Lippard, S. J., *Biochemistry* **1999,** *38* (39), 12768-12785.

11. Dalton, H., *Philos. Trans. R. Soc. B* **2005,** *360* (1458), 1207-1222.

12. Sazinsky, M. H.; Dunten, P. W.; McCormick, M. S.; DiDonato, A.; Lippard, S. J., *Biochemistry* **2006,** *45* (51), 15392-15404.

13. Sazinsky, M. H.; Lippard, S. J., *Acc. Chem. Res.* **2006,** *39* (8), 558-566, and references cited therein.

14. Sazinsky, M. H.; Bard, J.; DiDonato, A.; Lippard, S. J., *J. Biol. Chem.* **2004,** *279* (29), 30600-30610, and references cited therein.

15. Whittington, D. A.; Rosenzweig, A. C.; Frederick, C. A.; Lippard, S. J., *Biochemistry* **2001,** *40* (12), 3476-3482.

16. Sazinsky, M. H.; Lippard, S. J., *J. Am. Chem. Soc.* **2005,** *127* (16), 5814-5825.

17. Jackson Rudd, D.; Sazinsky, M. H.; Lippard, S. J.; Hedman, B.; Hodgson, K. O., *Inorg. Chem.* **2005,** *44* (13), 4546-4554.

18. Walters, K. J.; Gassner, G. T.; Lippard, S. J.; Wagner, G., *Proc. Natl. Acad. Sci. U.S.A.* **1999,** *96* (14), 7877-7882.

19. Gherman, B. F.; Baik, M.-H.; Lippard, S. J.; Friesner, R. A., *J. Am. Chem. Soc.* **2004,** *126* (9), 2978-2990.

20. Zheng, H.; Lipscomb, J. D., *Biochemistry* **2006,** *45* (6), 1685-1692.

21. Balendra, S.; Lesieur, C.; Smith, T. J.; Dalton, H., *Biochemistry* **2002,** *41* (8), 2571-2579.

22. Zhang, J.; Wallar, B. J.; Popescu, C. V.; Renner, D. B.; Thomas, D. D.; Lipscomb, J. D., *Biochemistry* **2006,** *45* (9), 2913-2926.

23. Blazyk, J. L.; Gassner, G. T.; Lippard, S. J., *J. Am. Chem. Soc.* **2005,** *127* (49), 17364-17376.

24. Froland, W. A.; Andersson, K. K.; Lee, S.-K.; Liu, Y.; Lipscomb, J. D., *J. Biol. Chem.* **1992,** *267* (25), 17588-17597.

25. Liu, K. E.; Valentine, A. M.; Wang, D.; Huynh, B. H.; Edmondson, D. E.; Salifoglou, A.; Lippard, S. J., *J. Am. Chem. Soc.* **1995,** *117* (41), 10174-10185.

26. Murray, L. J.; García-Serres, R.; Naik, S.; Huynh, B. H.; Lippard, S. J., *J. Am. Chem. Soc.* **2006,** *128* (23), 7458-7459.

27. Murray, L. J.; Naik, S.; Ortillo, D. O.; García-Serres, R.; Lee, J. K.; Huynh, B. H.; Lippard, S. J., *J. Am. Chem. Soc.* **2007,** submitted.

28. Murray, L. J.; García-Serres, R.; McCormick, M. S.; Davydov, R.; Naik, S.; Hoffman, B. M.; Huynh, B. H.; Lippard, S. J., *Biochemistry* **2007,** submitted.

29. Broadwater, J. A.; Ai, J.; Loehr, T. M.; Sanders-Loehr, J.; Fox, B. G., *Biochemistry* **1998,** *37* (42), 14664-14671.

30. Sjöberg, B.-M.; Karlsson, M.; Jörnvall, H., *J. Biol. Chem.* **1987,** *262* (20), 9736-9743.

31. Baik, M.-H.; Newcomb, M.; Friesner, R. A.; Lippard, S. J., *Chem. Rev.* **2003,** *103* (6), 2385-2419.

32. Newcomb, M.; Lansakara-P., D. S. P.; Kim, H.-Y.; Chandrasena, R. E. P.; Lippard, S. J.; Beauvais, L. G.; Murray, L. J.; Izzo, V.; Hollenberg, P. F.; Coon, M. J., *J. Org. Chem.* **2007,** *72* (4), 1128-1133.

33. Moe, L. A.; Hu, Z.; Deng, D.; Austin, R. N.; Groves, J. T.; Fox, B. G., *Biochemistry* **2004,** *43* (50), 15688-15701.

34. Newcomb, M.; Chandrasena, R. E. P.; Lansakara-P., D. S. P.; Kim, H.-Y.; Lippard, S. J.; Beauvais, L. G.; Murray, L. J.; Izzo, V.; Hollenberg, P. F.; Coon, M. J., *J. Org. Chem.* **2007,** *72* (4), 1121-1127.

35. Liu, Y.; Nesheim, J. C.; Lee, S.-K.; Lipscomb, J. D., *J. Biol. Chem.* **1995,** *270* (42), 24662-24665.

36. Lipscomb, J. D., *Annu. Rev. Microbiol.* **1994,** *48* 371-399.

37. Muthusamy, M.; Ambundo, E. A.; George, S. J.; Lippard, S. J.; Thorneley, R. N. F., *J. Am. Chem. Soc.* **2003,** *125* (37), 11150-11151.

38. Colby, J.; Stirling, D. I.; Dalton, H., *Biochem. J.* **1977,** *165* 395-402.

39. Green, J.; Dalton, H., *J. Biol. Chem.* **1989,** *264* (30), 17698-17703.

40. Beauvais, L. G.; Lippard, S. J., *J. Am. Chem. Soc.* **2005,** *127* (20), 7370-7378, and references cited therein.

41. Bou-Abdallah, F.; Papaefthymiou, G. C.; Scheswohl, D. M.; Stanga, S. D.; Arosio, P.; Chasteen, N. D., *Biochem. J.* **2002,** *364* (1), 57-63.

42. Yun, D.; García-Serres, R.; Chicalese, B. M.; An, Y. H.; Huynh, B. H.; Bollinger, J. M., Jr., *Biochemistry* **2007,** *46* (7), 1925-1932.

43. Bollinger, J. M., Jr.; Edmondson, D. E.; Huynh, B. H.; Filley; Norton, J. R.; Stubbe, J., *Science* **1991,** *253* (5017), 292-298.

44. Moënne-Loccoz, P.; Baldwin, J.; Ley, B. A.; Loehr, T. M.; Bollinger, J. M., Jr., *Biochemistry* **1998,** *37* (42), 14659-14663.

45. Rinaldo, D.; Philipp, D. M.; Lippard, S. J.; Friesner, R. A., *J. Am. Chem. Soc.* **2007,** *129* (11), 3135-3147.

46. Callaghan, A. J.; Smith, T. J.; Slade, S. E.; Dalton, H., *Eur. J. Biochem.* **2002,** *269* 1835-1843.

47. Rosenzweig, A. C.; Brandstetter, H.; Whittington, D. A.; Nordlund, P.; Lippard, S. J.; Frederick, C. A., *Proteins* **1997,** *29* (2), 141-152.

48. Newcomb, M.; Shen, R.; Lu, Y.; Coon, M. J.; Hollenberg, P. F.; Kopp, D. A.; Lippard, S. J., *J. Am. Chem. Soc.* **2002,** *124* (24), 6879-6996.

49. Brazeau, B. J.; Austin, R. N.; Tarr, C.; Groves, J. T.; Lipscomb, J. D., *J. Am. Chem. Soc.* **2001,** *123* (48), 11831-11837.

CHAPTER 2

OXIDATION OF A PROXIMAL RESIDUE IN THE I100W VARIANT OF TOMOH

CONTEXT

Accessibility of buffer components or bulk solvent to active sites of diiron proteins during dioxygen activation was proposed to quench reactive intermediates, hindering observation of such species. To investigate this hypothesis, several mutations were introduced into the α-subunit of ToMOH with the aim of constricting the channel. In the I100W variant, a transient species containing a diiron(III,IV) cluster weakly coupled to neutral tryptophan radical formed during reaction of reduced diiron(II) hydroxylase with dioxygen. This species is preceeded by a diiron(III) intermediate with spectroscopic parameters that differ from those reported for dioxygen-diiron(III) species in enzyme and model systems. The mechanistic implications that reaction of this variant hydroxylase with dioxygen has on the analogous process in the wild type system are discussed.

INTRODUCTION

Metal-activated dioxygen species are capable of oxidizing a broad range of substrates.[1-4] In synthetic systems, these species are generated in a solvent that is inert to oxidation. The peptide matrix surrounding the active site protects reactive intermediates in protein systems. Enzyme are able to coordinate reduction of the active metal center and dioxygen activation to substrate binding, thereby assuring that reactive metal-oxygen units are generated only when substrate is available.[5,6] The active sites in non-heme carboxylate-bridged diiron (CBDI) proteins are buried within the protein framework as revealed by x-ray crystallography are buried within the protein framework.[7-9] Consequent, reactive intermediates such as Q, a di(μ-oxo)diiron(IV) center, in MMOH and X, a mixed-valent diiron(III,IV) cluster, in RNR-R2 can accumulate and be characterized by a number of spectroscopic methods.

The primary coordination spheres of the diiron centers in the CBDI enzyme superfamily are remarkably similar, yet the high-valent intermediates Q and X are observed only in MMOH and RNR-R2, respectively.[10] Although the capacity to form these iron(IV) species is reserved for these

two enzymes, proteins in this family activate dioxygen by analogous mechanisms. The reduced diiron(II) core reacts rapidly with O_2 to generate a peroxo-bridged diiron(III) species as the first observable intermediate. No other oxygenated intermediates are observed in Ft and Δ^9D, and the peroxodiiron(III) unit is detectable in Δ^9D only when the substrate-carrier protein conjugate is bound to the desaturase. This behavior has been ascribed to stearoyl-ACP blocking access to the active site via a large substrate channel.[11] To date, no oxygenated intermediates have been reported for the reactions of diiron(II) or diiron(III) forms of rubrerythrin with either dioxygen or hydrogen peroxide respectively. From the crystal structure, the active site of rubrerythrin is seen to be more accessible to solvent and buffer components than that of other enzymes in the family.[12] The accumulation of reactive oxygenated iron(III) and iron(IV) intermediates thus appears to be correlated with accessibility of the diiron center to potential quenching moieties in the medium.

At the outset of the present study, no transient species with UV-visible absorption bands had been detected kinetically for the reaction of reduced ToMOH with dioxygen. In the crystal structure of the native enzyme, a large channel for substrate access or product egress, extending from the protein surface to the active site pocket, was identified. As mentioned in Chapter 1, the product analogue 4-bromophenol binds within this channel, delineating its ability to serve as a pathway for substrate or product access to the diiron center.[13] Site-directed mutagenesis studies of residues within the channel of ToMOH were therefore undertaken to examine the hypothesis that reactive intermediates would accumulate if solvent or buffer components were occluded from the active site in this system. Residues I100, F198, F205, and H96 form a hydrophobic entrance to that active site from the access channel in ToMOH (Figure 2.1). Of these residues, I100 is especially noteworthy. The analogous residue in MMOH, L110, is proposed to shift to gate substrate entry to and product egress from the active site during catalysis.[7] Residue L98 in hemerythrin might perform a similar function, controlling solvent access to the diiron core.[14] We therefore wondered whether mutation of

I100 would isolate the active site pocket from the channel sufficiently to shield the dimetallic center from buffer components or solvent, allowing accumulation of reactive intermediates to observable levels. Residue F205, which is on the opposite side of the channel from I100, and L208, which is farther from the active site pocket, were also selected as targets for mutagenesis (Figure 2.2). We substituted I100 with tyrosine and tryptophan, L208 with phenylalanine, and F205 with tryptophan. Modeling structures of these variant hydroxylases using the native crystal structure suggested that they would afford maximal closure of the channel without disrupting the protein fold of the surrounding matrix. A detailed examination of dioxygen activation in ToMOH I100W by RFQ EPR, Mössbauer, and ENDOR spectroscopy, as well as stopped-flow optical spectroscopy is presented here. The reactivity of other putative channel-blocking variants, I100Y, L208F, and F205W was investigated by pre-steady-state stopped-flow optical spectroscopy and steady-state methods.

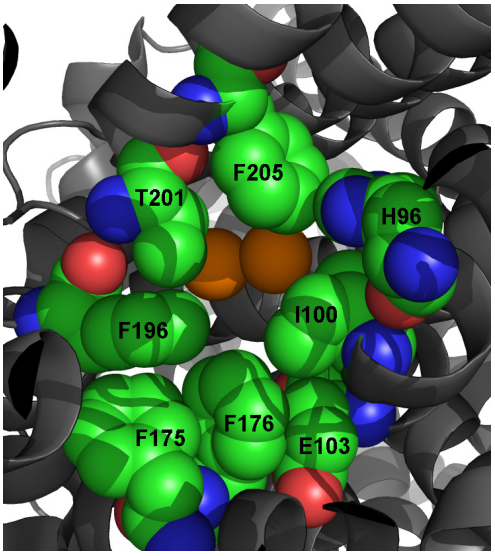

Figure 2.1. View of the active site pocket of ToMOH from the substrate access channel. The diiron atoms are depicted as orange spheres. The opening to the pocket is bordered by residues I100, T201, F205 and F196. I100 is analogous to the proposed leucine gate, L110, in MMOH.

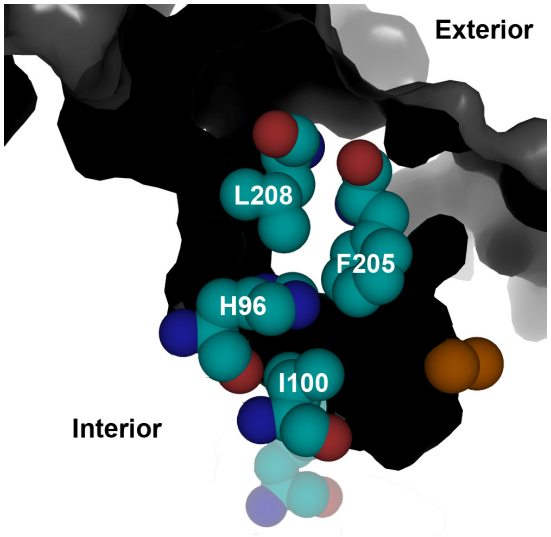

Figure 2.2. A substrate access channel (black) in ToMOH extends from the protein surface to the diiron active site. Residues H96, I100, and F205 form a hydrophobic region that joins the active site pocket to the channel. Residue L208 resides farther from the diiron active site, forming part of the channel wall. The iron atoms are depicted as orange spheres.

EXPERIMENTAL METHODS

General Considerations. Plasmids containing the genes for the ToMO components were supplied by the laboratory of Professor Alberto Di Donato, Naples, Italy. Recombinant expression and preparation of the ToMO component proteins were carried out as described elsewhere.[13] ToMOH variant proteins were prepared by the same protocol as used for the native enzyme. The iron content, measured by the ferrozine assay, ranged from 4.2 to 4.6 iron atoms per ToMOH dimer for all samples. Isotopically enriched ToMOH I100W protein for Mössbauer and ENDOR spectroscopy was obtained by expression in LeMaster's media[15] containing $^{57}FeCl_3$ or tryptophan-d_5, selectively labeled on the indole ring (Cambridge Isotope Labs, Andover, MA). The solution of $^{57}FeCl_3$ was prepared by dissolving ^{57}Fe powder (96.7% isotopic purity, Advanced Materials Technologies Ltd., Nes-Ziona, Israel) in concentrated hydrochloric acid. Deuterium oxide was purchased from Cambridge Isotope Labs and all other reagents were acquired from Aldrich Chemical Company. HPLC experiments were carried out with a Vydac protein & peptide C18 column connected to a Waters 600s controller and a Waters 2487 dual wavelength absorbance detector. Optical absorption spectra were recorded with an HP8452 diode-array spectrophotometer.

Site Directed Mutagenesis of the ToMOH α-Subunit. The mutations were introduced by site directed mutagenesis on the parent pET-22b(+)/touBEA plasmid with an MJ Research MiniCycler using DNA polymerase pfU Turbo, dNTPs, and reaction buffer (Stratagene, La Jolla, CA) according to the manufacturer's protocol. The sequences for oligonucleotides (Invitrogen, Carlsbad, CA) used as primers are given in Table 2.1. PCR products were transformed into *E. coli* XL-1 Blue supercompetent cells (Strategene, La Jolla, CA) by heat-shock as described by the manufacturer and grown overnight on LB-Agar plates containing ampicillin (300 μg/mL). Five colonies from each plate were picked and grown in 5 mL cultures (LB media, 300 μg ampicillin /mL) for 20 h. Cells were pelleted at 3500 rpm for 15 min and the plasmids were isolated with a Qiagen Mini-Prep kit.

Isolated plasmids were submitted for sequencing in the forward and reverse directions to the Biopolymers facility in the Center for Cancer Research (M.I.T.).

Table 2.1. Sequences for Mutagenic Primers for the α-Subunit of ToMOH

MUTATION	PRIMER	SEQUENCE (5' to 3')
I100W	sense	caacttcacttcggagcg**TGG**gcacttgaagaatacg
	antisense	cgtattcttcaagtgc**CCA**cgctccgaagtgaagttg
I100Y	sense	ggttagcactatgcaacttcacttcggagcg**TAT**gcacttgaagaatacg
	antisense	cgtattcttcaagtgc**ATA**cgctccgaagtgaagttgcatagtgctaacc
F205W	sense	ggcttcaccaatatgcag**TGG**ctcggtttggccg
	antisense	cggccaaaccgag**CCA**ctgcatattggtgaagcc
L208F	sense	gcagtttctcggt**TTC**cgccgctgacgctgctgaggccg
	antisense	cggcctcagcagcgtcagcggc**GAA**accgagaaactgc

Steady-State Activity Assays and Product Determinations for ToMOH Variants. A colorimetric assay was used to detect catechol that formed during steady-state hydroxylation of phenol by these variants.[16] Catechol-2,3-dioxygenase cleaves catechol to form 2-hydroxymuconic semialdehyde, which can be monitored by measuring the absorption at 410 nm ($\varepsilon = 1260\ M^{-1}cm^{-1}$). Assays were conducted at 25 ºC in 0.1 M Tris/HCl pH 7.5 in a final volume of 1 mL. Reaction mixtures contained 0.15 μM ToMOH, 10 μM ToMOD, 4 μM ToMOC, 30 nM ToMOF, and saturating amounts of catechol-2,3-dioxygenase. Steady-state hydroxylation of phenol (1 mM) was initiated with NADH to a final concentration of 1 mM.

To determine if the regiospecificity of hydroxylation was altered by these mutations, products of steady-state turnover for phenol were identified by HPLC. The ToMO protein component concentrations were 0.3 μM ToMOH, 2 μM ToMOD, 4 μM ToMOC, and 30 nM ToMOF in 0.1 M Tris/HCl pH 7.5 (150 μL). Assay solutions contained 1 mM phenol, and were initiated with NADH to a final concentration of 2 mM. Reaction mixtures were incubated at 25 ºC for 15 min, quenched with 50 μL TFA, centrifuged for 10 min at 14000 x *g*, frozen in liquid nitrogen, and stored at 20 ºC.

Samples were thawed and 100 μL of the supernatant was injected on to the Vydac column. HPLC conditions for separation of hydroxylated products from phenol were 0% buffer B for 7 min, 0% to 40% B for 1 min (linear gradient), 40% to 100% for 7 min (linear gradient), and 100% B for 3 min (A: 1% acetonitrile, 98.8% ddH2O, 0.2% TFA; B: 49.9% acetonitrile, 49.9% ddH2O, 0.2% TFA). Absorption at 280 nm was monitored with time for all samples. Retention times for catechol, resorcinol, and hydroquinone were determined under these conditions.

Stopped-Flow Optical Spectroscopy. A HiTech DX2 stopped flow instrument was made anaerobic by treatment with an anaerobic solution of sodium dithionite (> 4 mM). This solution was allowed to stand in the drive syringes and flow lines for at least 15 min to ensure complete scavenging of dioxygen. The instrument was then flushed with anaerobic 25 mM MOPS at the appropriate pH immediately prior to use. Solutions containing the hydroxylases and regulatory were made anaerobic by cycles of vacuum gas exchange with nitrogen and transferred to a Vacuum Atmospheres MO-20 anaerobic chamber, where they were reduced with excess sodium dithionite in the presence of methyl viologen. The reduced protein was dialyzed (8000 MWCO) twice against 25 mM MOPS at specific pH values. Samples were then loaded either into tonometers or Hamilton gas-tight sample-lock syringes and loaded into the anaerobic stopped-flow instrument and mixed against O_2-saturated 25 mM MOPS at a given pH. The software packages KinetAsyst 3.14 (HiTech Scientific, UK) or Kaleidagraph 3.5 (Synergy Software, Reading, PA) was used to fit the time dependence of the optical data.

Reaction of ToMOH I100W/Y, F205W, and L208F with O_2. Concentrations of the variant hydroxylases after mixing varied from 25 μM to 150 μM. Reaction mixtures contained three equivalents of ToMOD to one equivalent of ToMOH. The reduced hydroxylase pre-complexed with the regulatory protein was dialyzed against buffer, pH 7.0, and allowed to react with dioxygen-saturated buffer of the same pH. The temperature of the stopped-flow instrument was maintained at

4.0 ± 0.1 °C. Multi-wavelength data were collected between 350 and 750 nm with a xenon arc lamp and a diode array detector.

Temperature Dependence for Reaction of ToMOH I100W with O_2–Saturated Buffer. The reaction of $ToMOH_{red}$ I100W:3ToMOD with dioxygen-saturated buffer was carried out in the stopped flow instrument over the range 4.0 to 36.0 °C. The pH of the dialysis and the O_2-saturated buffer was 7.0. The concentration of ToMOH I100W:3ToMOD varied from 25 to 60 μM in the optical cell. The time-dependence of the optical signal at 500 nm was fit to an A→B→C model to determine the formation and decay rate constants. Eyring and Arrhenius plots were generated from the rate constants at different temperatures to determine $\Delta H^{\ddagger}$ and $\Delta S^{\ddagger}$ values for each processes.

Solvent Kinetic Isotope Effect (SKIE) for Formation and Decay of the ToMOH I100W Transient. Solutions of ToMOH I100W and ToMOD were prepared as described in the temperature dependence experiments. After reduction, protein mixtures were dialyzed anaerobically against either 25 mM MOPS pD 6.61 in D_2O or pH 7.0 in H_2O and allowed to react with dioxygen. The reaction was carried out over the range 4.0 and 36.0 °C. Data were collected at 500 nm, and rate constants were determined using the model described above.

Effect of pH on the Reaction of $ToMOH_{red}$ I100W with O_2. In these experiments, the pH of the reaction mixture was adjusted either by using double-mixing mode to set the pH after dialysis and prior to oxygenation in the second push, or in single-mixing mode with dialysis carried out using buffers at specific pH values. For double-mixing experiments, the concentrations of the hydroxylase and regulatory protein after mixing were 94 μM and 282 μM, respectively. The reduced protein was dialyzed against buffer with a pH value of 6.6. In the first push, the solution of the hydroxylase and regulatory protein was mixed with anaerobic buffer, pH 6.6 or 8.0, and allowed to age for 1 min. In the second push, the aged protein solution was allowed to react with oxygenated buffer, pH 6.6 or 7.2, and data were collected in multi- and single-wavelength modes. The instrument temperature was

maintained at 4.0 °C. For single-mixing experiments, the concentrations of the hydroxylase and regulatory protein in the optical cell were 18 μM and 45 μM respectively. After reduction, the first dialysis was carried out against 25 mM MOPS pH 7.0. The pH of the buffer was 6.5, 7.0, or 7.5 for the second dialysis. The reduced anaerobic samples were mixed at 4.0 °C with oxygenated 25 mM MOPS buffer at the appropriate pH values. Data were collected at 500 nm for 100 to 200 s

Effect of Substrates on the Decay Rate of the ToMOH I100W Transient. This double-mixing experiment was carried out at 4.0 ºC monitoring the absorption 500 nm. The concentration of ToMOH I100W:3ToMOD after mixing was 25 μM. Reduced ToMOH I100W:3ToMOD was dialyzed against buffer at pH 7.0, and loaded into the anaerobic stopped-flow instrument. In the first push, the reduced hydroxylase was reacted with dioxygen-saturated buffer (pH 7.0) for 3.9 s. The aged solution was subsequently mixed with 25 mM MOPS pH 7.0 containing phenol, acetylene, or propylene. The concentration of phenol after mixing ranged from 25 μM to 5.2 mM. For acetylene and propylene, an aliquot (10 mL) of buffer was sparged with the gas for 1.5 h to obtain saturated solutions of these substrates (7.7 mM or 42.4 mM, respectively).[17] Data were collected for 10 s to 200 s at 500 nm and fit to either one or two exponential functions.

RFQ Sample Preparation. Protein solutions of ToMOH I100W:3ToMOD were reduced and dialyzed against 25 mM MOPS pH 7.0 as described for stopped-flow experiments. Reduced mixtures were loaded into gas-tight syringes for an Update Instruments 1000 ram drive system connected to a model 705A computer controller. The RFQ instrumentation has been described in detail elsewhere.[18] Reduced protein was mixed with dioxygen buffer, allowed to age for reaction times between 34 ms and 600 s, and then quenched in isopentane at -140 ºC. The frozen protein solutions for this timecourse were packed into X-band EPR tubes and Mössbauer sample cups. Samples for ENDOR spectroscopy were quenched 4 s after mixing with dioxygen-saturated buffer, and packed into Q-band EPR tubes. All RFQ samples were stored in liquid nitrogen until spectra were acquired.

Mössbauer Spectroscopy. ToMOH I100W isotopically enriched with ^{57}Fe was used to generate RFQ samples for Mössbauer spectroscopy. The concentration of ToMOH I100W:3ToMOD after mixing was 290 μM. Mössbauer spectra were recorded at 4.2 K in an applied magnetic field of either 50 mT or between 1 T and 8 T applied parallel to the γ-beam on instrumentation described elsewhere.[18] The zero velocity refers to the centroid of a room temperature spectrum of an Fe foil.

X-Band EPR Spectroscopy. Samples were generated with ToMOH I100W that contained either ^{56}Fe or ^{57}Fe. The concentration of ToMOH I100W:3ToMOD in the quenched reaction mixtures was 198 μM. EPR spectra at $g = 2.00$ were recorded at 30 K with the following parameters: power = 0.02 mW; frequency = 9.65 GHz; modulation frequency = 100 kHz; modulation amplitude = 5 G; gain = 6.3×10^4. EPR spectra at $g = 16$ were recorded at 8 K with the following parameters in parallel mode: power = 20 mW; frequency = 9.39 GHz; modulation frequency = 100 kHz; modulation amplitude = 10 G; gain = 6.3×10^4.

ENDOR Spectroscopy. Samples were prepared either with 25 mM MOPS in D_2O (pD 6.6) or H_2O (pH 7.0), and the hydroxylase contained either natural abundance ^{56}Fe or was isotopically enriched with ^{57}Fe. For samples prepared with D_2O-containing buffers, the reduced protein was dialyzed against deuterated buffers. The concentration of ToMOH I100W:3ToMOD in ENDOR samples ranged from 250 μM to 350 μM. ^1H- and ^2H-Mims ENDOR spectra were recorded on instrumentation described elsewhere.[19]

Enzymatic Digestion and Mass Spectrometry of ToMOH I100W. Reduced ToMOH I100W was prepared as described above for the stopped-flow experiments. A 10-μL control aliquot of the ToMOH I100W:3ToMOD mixture was removed prior to making the protein anaerobic. The remainder of the protein was reduced with excess sodium dithionite and dialyzed under anaerobic conditions against 25 mM MOPS pH 7.0. The reduced protein was mixed with buffer oxygenated with either natural abundance $^{16}O_2$ or enriched $^{18}O_2$ (95%, Cambridge Isotope Labs, Andover, MA)

in the stopped-flow instrument. The polypeptide chains of reacted and unreacted oxidized protein solutions were separated on a 4-20% Tris/HCl SDS-PAGE gel run at 200 V for 45 min. The band corresponding to the α-subunit was excised and digested with trypsin according to the manufacturer's protocol (New England Biolabs, Ipswich, MA). Positive ion MALDI-TOF mass spectrometry of digests was carried out with a Voyager DE-STR MALDI-TOF mass spectrometer (Applied Biosystems, Foster City, CA), installed in the Biopolymers Core Facility of the M.I.T. Center for Cancer Research. The instrument was operated in reflector mode with an accelerating potential of 20 kV and mass resolution of at least 1:10000. The MALDI matrix was α-cyano-4-hydroxybenzoic acid. Protein digest samples were mixed with a 10 mg/mL matrix solution in a 1:1 ratio and were deposited on the MALDI plate. Mass spectra were obtained using a nitrogen UV laser (337 nm). Each mass spectrum is the average of 50 laser shots. The mass spectrometer was calibrated as per the manufacturer's standard operating protocols, with a mixture of peptides of known mass that were spotted on the MALDI plate adjacent to the sample. Mass spectra were processed using the Applied Biosystems Data Explorer software.

LC-MS analyses of the protein digests were carried out using a Tempo nano HPLC system (Applied Biosystems, Foster City, CA) coupled on-line to a QSTAR Elite quadrupole-time-of-flight tandem mass spectrometer (MDS Sciex/Applied Biosystems, Foster City, CA), installed in the Proteomics Core Facility of the M.I.T. Center for Cancer Research. The mass spectrometer was calibrated as per the manufacturer's standard operating protocols, with the fragment ions a peptide of known sequence. Separation of proteolytic peptides was carried out on a C18 capillary HPLC column (Michrom Bioresources, Auburn, CA) and a water-acetonitrile (with 0.1% formic acid) solvent gradient at a flow rate of 300 nL/min. Mass spectral data were acquired and processed with the Applied Biosystems Analyst QS software. Data acquisition was performed using the software "Information Dependent Acquisition" mode, with each MS scan, where peptide ion m/z values were

measured, followed by four MS/MS scans, where fragment ion spectra of the four most abundant precursor ions were acquired. A temporary exclusion list was generated by the software after each MS/MS data acquisition to minimize the generation of duplicate MS/MS spectra from the same precursor ion.

RESULTS

Steady-state Product Distribution and Activity of ToMOH Variants for Phenol. The steady-state specific activities of the ToMOH variants for phenol were lower than that observed for wild-type hydroxylase as determined by the coupled assay with catechol-2,3-dioxygenase. The I100W variant had a specific activity of 80 mU/mg compared to 1250 mU/mg for the wild-type protein. ToMOH I100Y, L208F, and F205W showed no activity under the conditions of this assay. Catechol, resorcinol, hydroquinone, and phenol are well separated by the method described in the Experimental Section, with retention times of 13, 11, 6.5, and 15 min, respectively. The peak corresponding to the enzymatic product had a retention time coincident with that of catechol (Figure 2.3). No peaks corresponding to resorcinol or hydroquinone were observed. Product analyses for the variant hydroxylases revealed catechol to be the only product formed. A trace amount of catechol was observed in assay mixtures for ToMOH I100Y, F205W, and L208F.

Stopped-Flow Optical Study of the Reaction of ToMOH Variants with O_2. No transient absorption bands between 350 and 750 nm were observed after mixing solutions of chemically reduced ToMOH variants I100Y, F205W, and L208F and ToMOD with dioxygen-saturated buffer. Reaction of reduced ToMOH I100W with dioxygen afforded an optically-active transient with an absorption maximum, λ_{max}, at 500 nm (Figure 2.4). Single-wavelength data collected at λ_{max} were fit best to a three-component sequential reaction model. Rate constants for the formation and decay rate constants and the molar extinction coefficient of this transient of the 500 nm band are $k_f = 0.804 \pm 0.001$ s^{-1}, $k_d = 0.054 \pm 0.002$ s^{-1}, and $\varepsilon = (1.5 \pm 0.2) \times 10^3$ $M^{-1}cm^{-1}$, respectively. The values for λ_{max}

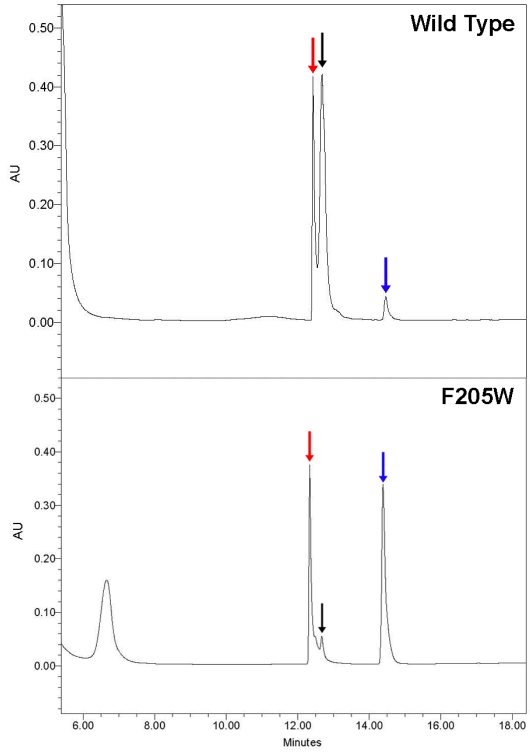

Figure 2.3. HPLC traces at 280 nm of steady-state reaction mixtures for wild-type and F205W variant of ToMOH. Catechol (black arrow) is the only observed product in reactions. The peak corresponding to phenol (blue arrow), the substrate used in these assays, was of a lower intensity in the reaction containing the F205W mutant, consistent with the reduced steady-state activity of this hydroxylase. The compound eluting at 6 min does not arise from hydroquinone, as determined by HPLC traces for samples doped with this compound. A background peak at ~ 12.5 min (red arrow) appears in all traces with equal intensity.

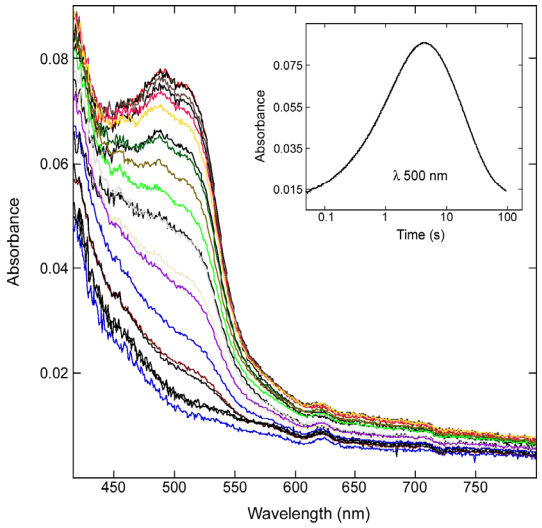

Figure 2.4. Stopped-flow UV/visible spectra for the reaction of $I100W_{red}$:3ToMOD with O_2-saturated buffer. Multi-wavelength data reveal the formation and decay of a transient species with an absorbance maximum at 500 nm. No other absorbance bands are observed during the reaction. The single wavelength data at 500 nm (inset) were fit to a three component sequential kinetic model and the calculated rate constants and the molar extinction coefficient for the intermediate are 0.804 ± 0.001 s^{-1} (formation), 0.054 ± 0.002 s^{-1} (decay), and 1.5 ± 0.2 x 10^3 $M^{-1}cm^{-1}$ respectively.

and ε are similar to those reported for deprotonated tryptophanyl radicals in small peptides and proteins.[20,21] The regulatory protein was required in the reaction mixture for formation of the transient species. The requirement for the regulatory protein to facilitate dioxygen activation in the hydroxylase has been previously reported for MMO.

Time-Dependent Mössbauer Spectra for the Reaction of $ToMOH_{red}$ I100W with O_2. The Mössbauer spectrum of the reduced protein contains only diiron(II) clusters, which are modeled as two distinct diiron(II) sites (Figure 2.5A). After mixing with dioxygen-saturated buffer, approximately 40% of the diiron(II) sites reacted rapidly to form a diiron(III) intermediate (Figure 2.5B, C). This intermediate was simulated as a single quadrupole doublet with values for the isomer shift, δ, and quadrupole splitting, ΔE_Q, of 0.54 and 0.67 mm/s, respectively (red line). These parameters differ from those of other non-heme diiron(III) intermediates characterized because $\delta <$ 0.6 mm/s and $\Delta E_Q < 1.0$ mm/s. This transient species subsequently evolves to form a mixed-valent diiron(III,IV) cluster, a process that maximizes at ~ 4 s (Figure 2.5D). A paramagnetic spectral component with features (arrows) similar to those of intermediate X was observed (Figure 2.6A).[22,23] The signals corresponding to unreacted diiron(II) and oxygenated diiron(III) precursors are omitted from this spectrum for clarity. Analysis of the spectrum indicates that this paramagnetic component accounts for 15 ± 2% of the total Fe absorption. The spectrum of this sample recorded with a strong applied field of 8 T (Figure 2.6B) showed a two-fold increase in the intensity of the paramagnetic component to 30 ± 3% of total Fe absorption. This field-dependent increase of the paramagnetic absorption indicates that the $S = ½$ diiron(III,IV) cluster is weakly spin-coupled to a nearby $S = ½$ paramagnet. For a weakly coupled system ($J < 1$ cm^{-1}) in a weak applied field of 50 mT, the energy separations of the four electronic levels are small, whereas in a strong applied field of 8 T, the Zeeman interaction increases the energy separations between these levels. At 4.2 K and 50 mT, all four levels are nearly equally populated, and the spectrum contains two equal-intensity components:

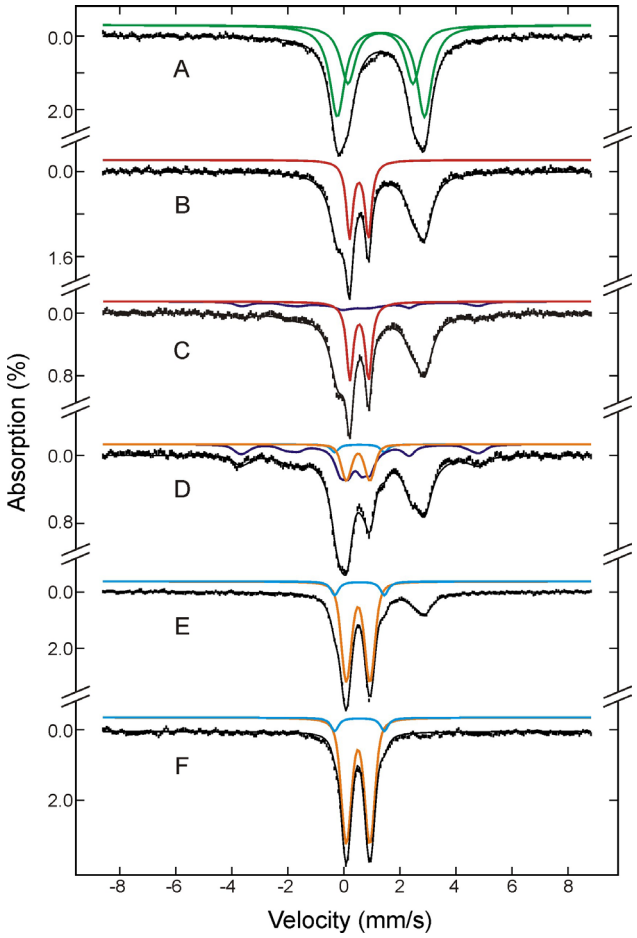

Figure 2.5. Mössbauer spectra of freeze-quenched samples from the reaction of ToMOH$_{red}$ I100W:3ToMOD with O_2. The samples were frozen before mixing (A) and 0.07 s (B), 0.44 s (C), 3.5 s (D), 37 s (E) and 900 s (F) after mixing. The spectra (vertical bars) are collected at 4.2 K in a 50 mT field applied parallel to the γ-beam. The diiron(II) spectrum (A) was simulated as a superposition of two unresolved quadrupole doublets (green lines in A) with an intensity ratio of 1.6:1 for doublet 1:doublet 2. The parameters are δ = 1.32 mm/s, ΔE_Q = 3.11 mm/s, and line width = 0.65 mm/s for doublet 1, and δ = 1.31 mm/s, ΔE_Q = 2.32 mm/s, and line width = 0.65 mm/s for doublet 2. In B-F, the red, blue, orange and cyan lines are simulated spectra of the diiron(III) transient, diiron(III,IV)-W$^{\bullet}$ intermediate, major diion(III) and minor diiron(III) products, respectively. The spectrum of the major diiron(III) product (—) is modeled with a single quadrupole doublet with δ = 0.51 mm/s, ΔE_Q = 0.84 mm/s, and line width = 0.35 mm/s. The spectrum of the minor diiron(III) product (—) is simulated with δ = 0.56 mm/s, ΔE_Q = 1.77 mm/s, and line width = 0.33 mm/s. For clarity, the diiron(II) spectral component is not shown specifically in B-F. The simulated spectra are plotted at the following absorption intensity: red, 29% and 27% in B and C, respectively; blue, 16% and 34% in C and D, respectively; orange, 14%, 60% and 65% in D, E, and F, respectively; cyan, 3%, 8% and 8% in D, E, and F, respectively. The black lines overlaid with the experimental spectra are composite spectra including the diiron(II) and all other species mentioned above.

a paramagnetic component (two $M_S = \pm 1$ sublevels of the triplet state) superposed on a diamagnetic component (the singlet state and the $M_S = 0$ sublevel of the triplet state). In contrast, at 4.2 K and 8 T, only the lowest $M_S = -1$ sublevel is populated and the diamagnetic component disappears, doubling the intensity of the paramagnetic component. We compared a simulated spectrum of the X-Y$^{\bullet}$

species in RNR-R2 W48F[23] to the spectrum of the 3.5 s sample, and the agreement was remarkable and consistent with a weakly-coupled diiron(III,IV)–W• pair (Figure 2.6B). Values for δ and ΔE_Q (Fe^{III}/Fe^{IV}) for this species are 0.47/0.22 and 0.70/0.64 mm/s, respectively.

Percentages of Fe-absorption corresponding to species generated at different time points, including others not depicted here, were thereby obtained. On the basis of the Fe/protein ratio determined for the freeze-quenched samples, 3.88 Fe atoms/ToMOH dimer, these relative percentages were converted to accumulation amounts of diiron cluster/protomer for the diiron species at various time points. The results (diamonds) are presented in Figure 2.7, which shows clearly the formation and decay of the various diiron species. Before mixing with O_2, the reduced protein sample contains mainly diiron(II) clusters, 0.96 diiron clusters/ToMOH protomer, the spectrum of which can be modeled as two unresolved quadrupole doublets (Figure 2.5A, green lines) with parameters given

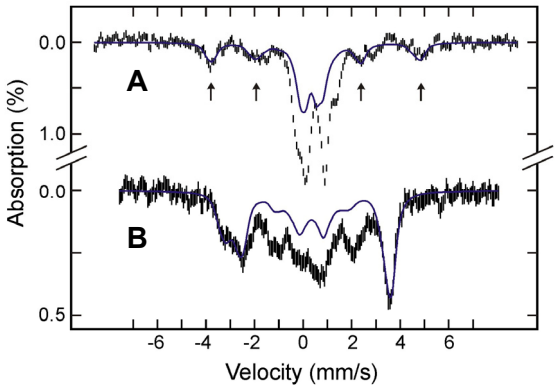

Figure 2.6. Mössbauer spectra of the sample quenched after 3.5 s recorded with an applied field of 50 mT (A) and 8 T (B) show intensity changes expected for a weakly spin-coupled system. The diiron(II) contributions (50% of the total Fe absorption) were removed from the raw data for clarity. Spectra are simulated with parameters used for X-Y• from RNR-R2 W48F (blue lines).

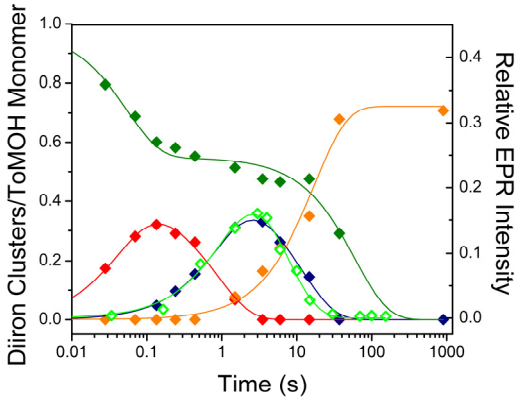

Figure 2.7. Speciation plot for the reaction of $ToMOH_{red}$ I100W:3ToMOD with dioxygen. The diiron(II) starting material (♦) rapidly converts to a diiron(III) intermediate (♦) at ~ 18 s^{-1}. The diiron(III) transient evolves to the mixed-valent species (♦) at ~ 1 s^{-1}. The formation and decay rates of the g = 2.0 signal (◇) from RFQ EPR experiments are within error of the rates for mixed-valent species determined by Mössbauer. The diiron(III) resting state (♦) is reformed as the mixed-valent species decays at ~ 0.08 s^{-1}. The diiron(II) starting material (–), the diiron(III) intermediate (–), mixed-valent diiron(III,IV) transient (–), g = 2.0 EPR signal (–), and the diiron(III) product (–) were fit to two-exponential functions.

in the figure caption. After mixing with O_2-saturated buffer, approximately 40% of the diiron(II) sites react rapidly to form the diiron(III) intermediate (Figure 2.5, red lines) with a rate constant of ~ 18 s^{-1}. Accumulation of the diiron(III) intermediate reaches a maximum of 0.32 clusters/protomer at 0.14 s and then decays at a rate of ~ 1.1 s^{-1} (Figure 2.7, red line and diamonds). The decay of the diiron(III) intermediate parallels the formation of the diiron(III,IV)–$W^{\bullet}$ species (Figure 2.7, blue line and diamonds), while the unreacted diiron(II) sites stay relatively stable (Figure 2.7, olive green line and diamonds) during this decay phase of the diiron(III) intermediate. This result establishes unambiguously that the diiron(III) transient is a true precursor to diiron(III,IV)–$W^{\bullet}$. The data also reveal that the diiron(III,IV)–$W^{\bullet}$ species reaches a maximum accumulation of 0.33 clusters/protomer at 3.5 s and decays with a rate constant of ~ 0.08 s^{-1} to generate the diiron(III) product (Figure 2.7, orange line). The formation and decay rates of the optically silent diiron(III,IV) cluster are linked to that of the optically active $W^{\bullet}$, because the rates of the former, determined from Mössbauer spectroscopy, agree with those of the latter, determined from optical studies (*17*, also, see Table 2.2). Slow oxidation (~ 0.01 s^{-1}) of residual unreacted diiron(II) species accompanies the second phase formation of the diiron(III) product and the generation of other minor, unidentified ferric species. A previously unreported, minor oxidation product (Figure 2.5, cyan lines) can detected as forming around 1 to 2 s after mixing with O_2, after 5 s its accumulation reaches a constant value of ~ 8% of the total iron in the samples. Its Mössbauer parameters (δ = 0.56 mm/s and ΔE_Q = 1.77 mm/s) and diamagnetism, revealed by high-field Mössbauer measurements, indicate a diiron(III) cluster. Its kinetic profile suggests that it is a final product. A definitive identification cannot be made, however, due to the small amount of material that accumulates.

Time-Dependent EPR Spectra for the Reaction of $ToMOH_{red}$ I100W with O_2. The intensity of two EPR signals changed during the reaction of the reduced variant hydroxylase with dioxygen. A signal at g = 16, which corresponds to diiron(II) centers, decays in a biphasic manner. The first phase

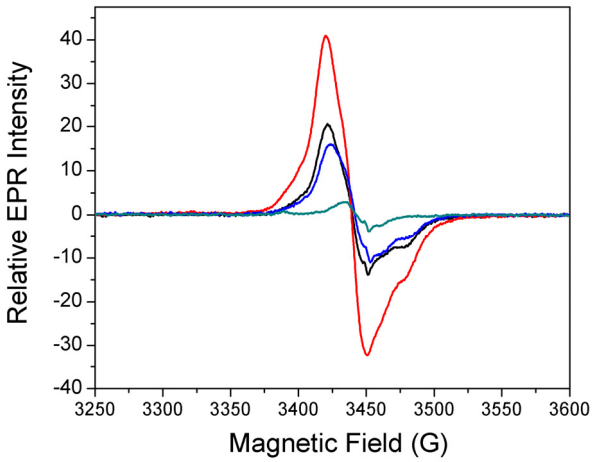

Figure 2.8. Time-dependent EPR spectra for the transient formed during the reaction of $ToMOH_{red}$ I100W:3ToMOD with O_2. The intensity of the signal at g = 2.0 maximizes 4 s (—) after mixing reduced protein with dioxygen-saturated buffer. Spectra for samples that were allowed to react for 520 ms (—), 10 s (—), and 100 s (—) are also shown.

Table 2.2. Formation and Decay Rate Constants of the Mixed-Valent Diiron(III,IV)-W• Species Measured by Optical, Mössbauer, and EPR Spectroscopy

Rate Constant	Optical	Mössbauer	EPR
k_f (s^{-1})	0.804(1)	1.1	0.77
k_d (s^{-1})	0.054(2)	0.08	0.15

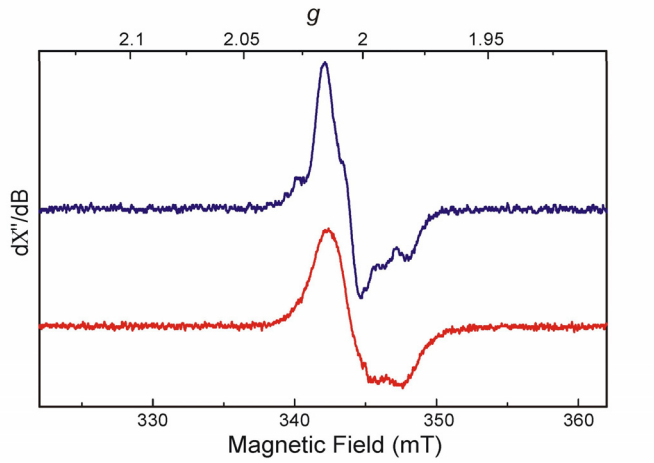

Figure 2.9. EPR spectra of the mixed-valent diiron(III,IV)–W• transient generated during reaction of reduced ToMOH I100W with dioxygen. The reaction was quenched after either 4 s for natural abundant diiron(II) protein (blue) or at 3.5 s for ^{57}Fe-enriched protein (red). Line broadening from hyperfine interactions with ^{57}Fe nuclei is evident, confirming that EPR-active species is at or near the dimetallic cluster.

is rapid and could not be simulated accurately with the data collected. This initial decay is complete by ~ 0.17 s, which is consistent with the decay kinetics of the rapidly interacting diiron(II) sites observed in the Mössbauer measurements (*vide supra*). The second phase was slower and incomplete by 150 s. Figure 2.8 displays EPR spectra of selected freeze-quenched samples in the $g = 2.0$ region, showing the rise and fall of the transient EPR signal. Line broadening of this signal was observed for samples prepared with ^{57}Fe-enriched ToMOH I100W, confirming that the unpaired electron interacts with the diiron center (Figure 2.9). This signal and the observed hyperfine interaction with the iron nuclei are similar to that reported for X–W$^{\bullet+}$ and X–Y$^{\bullet}$ in RNR-R2.[22-24] The intensity of this transient signal appeared and decayed with rate constants of 0.77 s^{-1} and 0.15 s^{-1}, maximizing at approximately 4 s (Figure 2.7, ◇ and –). The rate constants for formation and decay agree with those reported from the stopped-flow optical and Mössbauer experiments, confirming that this EPR active species corresponds to the spin coupled mixed-valent diiron(III,IV)–W$^{\bullet}$ intermediate (Table 2.2). The time-dependent EPR data indicate that the fast-reacting diiron(II) protein and the mixed-valent species are not kinetically linked because the rate of decay of the former is much faster than the rate of formation of the latter. This result indicates the presence of an intervening EPR-silent species, namely, the diiron(III) intermediate observed in the Mössbauer spectra of RFQ samples quenched between 0.03 s and 4 s, described above.

Prior to ^{1}H and ^{2}H-Mims ENDOR measurements, X-band EPR spectra were recorded on samples quenched 4 s after mixing solutions of ToMOH$_{red}$ I100W:3ToMOD with dioxygen-saturated buffer. The $g = 2.0$ signal has two contributions as previously mentioned, one from the diiron(III,IV) cluster and the other from the tryptophan radical. The radical signal is visible at temperatures up to ~ 77 K, whereas the diiron signal is visible only below ~ 40 K (Figure 2.10). The peak width of the mixed-valent diiron(III,IV)–W$^{\bullet}$ transient is smaller than that reported elsewhere for tryptophan cation and neutral radicals.[25]

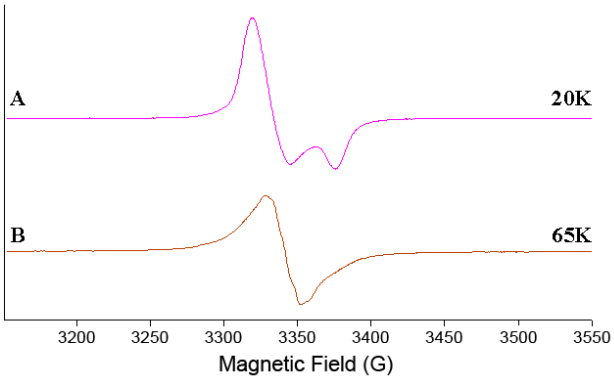

Figure 2.10. X-band EPR spectra of the diiron(III,IV)–W$^{\bullet}$ at (**A**) 20 K and (**B**) 65 K. (**A**) The spectrum at 20 K contains the anisotropic features associated with the diiron center with the radical signal saturated. (**B**) Spectrum at 65 K of the intermediate is predominantly from the W radical. The diiron center is not saturated below 60 K

Kinetic Activation Parameters and Kinetic Isotope Effects for Formation and Decay of the Diiron(III,IV)–W$^{\bullet}$ Species. The rate constants k_f and k_d vary with temperature to give linear Eyring plots (Figure 2.11). The values of $\Delta H^{\ddagger}$ and $\Delta S^{\ddagger}$ for formation of this species are similar to those reported for decay of Q to $MMOH_{ox}$ (Table 2.3).[26] Both k_f and k_d were sensitive to the hydrogen isotope concentration with normal isotope effects, $k_H > k_D$, observed over the examined temperature range (Table 2.4). The ratio of k_H/k_D decreased with increasing temperature from 2.51 to 1.97 for k_f and 3.2 to 1.72 for k_d. From Arrhenius plots, the formation activation energy is greater in deuterated

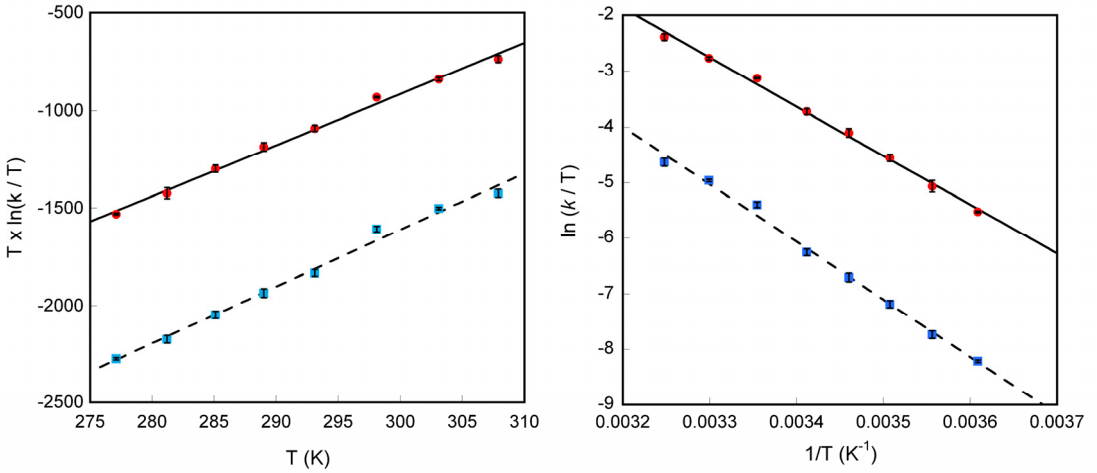

Figure 2.11. Eyring Plots for formation and decay of the tryptophanyl radical generated during reaction of reduced ToMOH I100W with oxygenated buffer. Values for $\Delta H^{\ddagger}$ and $\Delta S^{\ddagger}$ were determined from linear fits to data for k_f (●) and k_d (■) and are reported in Table 2.2.

Table 2.3. Activation Parameters for Formation and Decay of Species Observed in the Reaction of ToMOH I100W:3ToMOD and MMOH:2MMOB with Dioxygen

	Rate Constants	$\Delta H^{\ddagger}$ (kcal/mol)	$\Delta S^{\ddagger}$ (cal/mol·K)
ToMOH I100W	k_f	12.7 ± 0.5	-13 ± 2
	k_d	17.0 ± 0.4	-3 ± 2
MMOH (*M. caps*)*	k_1 ($H_{red} \rightarrow H_{peroxo}$)	27.9 ± 0.1	43 ± 2
	k_2 ($H_{peroxo} \rightarrow Q$)	28.7 ± 0.3	43.9 ± 0.5
	k_3 ($Q \rightarrow H_{ox}$)	13.7 ± 0.7	-18 ± 2

* Reference 26

Table 2.4. Formation and Decay Rate Constants for I100W Transient in H_2O and D_2O Buffers

Temp (± 0.1 °C)	H_2O		D_2O		Formation	Decay
	k_f (s^{-1})	k_d (s^{-1})	k_f (s^{-1})	k_d (s^{-1})	k_H / k_D	k_H / k_D
4.0	0.90 ± 0.01	0.093 ± 0.009	0.358 ± 0.002	0.029 ± 0.001	2.51 ± 0.04	3.2 ± 0.3
10.0	1.39 ± 0.02	0.143 ± 0.002	0.567 ± 0.003	0.060 ± 0.001	2.46 ± 0.03	2.36 ± 0.05
15.0	2.09 ± 0.03	0.218 ± 0.002	0.93 ± 0.04	0.111 ± 0.001	2.24 ± 0.08	1.97 ± 0.02
20.0	3.25 ± 0.05	0.359 ± 0.008	1.50 ± 0.06	0.195 ± 0.001	2.17 ± 0.09	1.84 ± 0.04
25.0	4.9 ± 0.1	0.59 ± 0.01	2.50 ± 0.07	0.342 ± 0.001	1.97 ± 0.07	1.72 ± 0.02

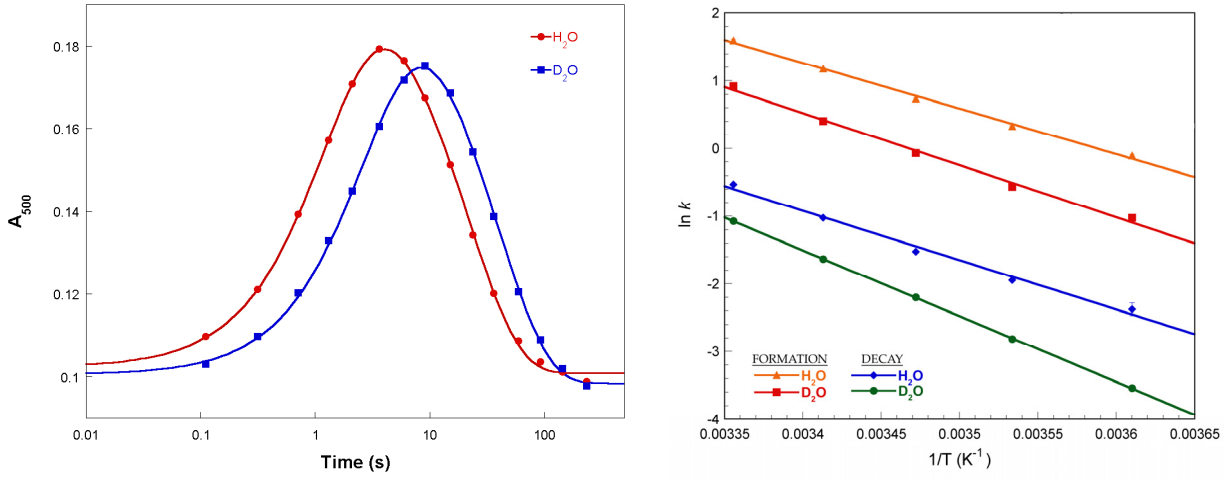

Figure 2.12. SKIE for k_f and k_d of the ToMOH I100W transient. Stopped-flow optical data acquired at 500 nm and 4.0 °C show the formation and decay of the mixed-valent diiron(III,IV)–W$^{\bullet}$ are slower in deuterated than in protic buffers (left). The difference in activation energy for both phases in protic versus deuterated buffers is non-zero as determined from the Arrhenius plots (right). The temperature dependence of k_H/k_D is therefore non-zero for both processes with the decay exhibiting a stronger dependence than formation. This data imply that hydrogen atom transfer or tunneling from W100 to the diiron(III) intermediate does not occur during formation.

solvent, 15.6 ± 0.5 kcal/mol, than in protic, 13.5 ± 0.1 kcal/mol, as expected from the ratio of k_H/k_D (Figure 2.12). The solvent kinetic isotope effect (SKIE) for the formation process is weakly dependent on temperature and contrasts with the stronger, non-linear dependence for the decay process. The magnitude and sensitivity to temperature of the SKIEs indicate that hydrogen atom transfer or tunneling does not occur in the transition state during the reaction of the diiron(III) intermediate with W100, or for subsequent decay of the mixed-valent diiron(III,IV)–W$^\bullet$ species.

Effect of pH on the Reaction of ToMOH I100W with O_2-Saturated Buffer. As the pH increased from 6.5 and 7.5, the rates of oxidation of W100 by the diiron(III) intermediate and decay of the diiron(III,IV)–W$^\bullet$ species increased (Table 2.5). From data collected in diode array mode, the absorption maximum of the tryptophanyl radical was unchanged over the examined pH range. To explain the pH dependence, we propose a model in which a rate-limiting deprotonation precedes a fast oxidation reaction. The pH dependence data agree reasonably well with this model to give a calculated proton-independent electron transfer rate of 1.22 s^{-1} (Figure 2.13). The decay rate of the transient is also sensitive to pH, following a similar trend as observed for the formation rate. Values

Table 2.5. Formation and Decay Rate Constants at Varying pH Values

pH	k_f (s^{-1})	k_d (s^{-1})
6.5	0.66 ± 0.01	0.0417 ± 0.0006
6.6	0.71 ± 0.01	0.052 ± 0.005
7.0	0.86 ± 0.04	0.070 ± 0.003
7.2	1.05 ± 0.02	0.095 ± 0.001
7.5	1.13 ± 0.02	0.091 ± 0.001

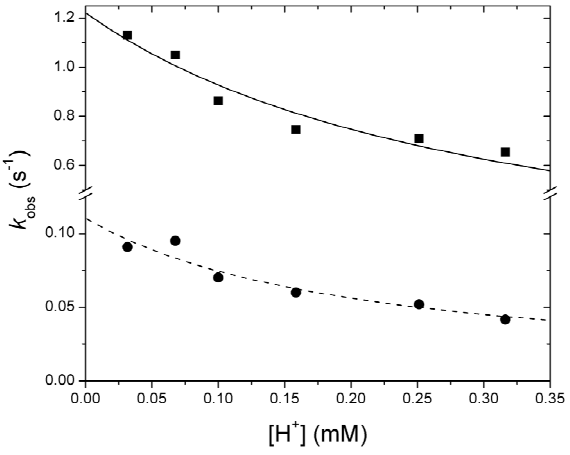

Figure 2.13. Effect of proton concentration on formation and decay of the diiron(III,IV)–W$^\bullet$ species . Increasing pH increases k_f and k_d of the ToMOH I100W transient. The rate constants both increase with decreasing [H$^+$], with k_f (■) and k_d (●) increasing ~ 2-fold between pH 6.5 and 7.5. The y-axis scales differ above and below the break.

of k_d increase almost two-fold with an order of magnitude decrease in proton concentration. The data were adequately fit with the model applied to the formation rate, rate-limiting deprotonation followed by oxidation, yielding a rate constant of 0.12 s^{-1} for the rapid second step of the reaction (Figure 2.13).

Effect of Substrates on the Decay Rate of the ToMOH I100W Transient. The presence of phenol increased the decay rate constant of the tryptophanyl radical from 0.054 s^{-1} to 13.7 ± 0.4 s^{-1}. The concentration dependence of k_d was modeled with a saturation binding model applied to the reaction of oxygenated intermediates in MMOH with alternative substrates, where a substrate-enzyme complex forms prior to reaction (eq 2.1).[27] From this analysis, the rate constant for reaction with phenol, k_{rxn}, and the substrate-enzyme dissociation constant, K_d, are 20 ± 2 s^{-1} and 2.3 ± 0.5 mM, respectively (Figure 2.14). In double-mixing experiments employing phenol, the absorbance over all wavelengths increased after decay of the transient. This growth in absorption was modeled as an independent exponential function in all data for which phenol was the substrate.

$$k_{obs} = \frac{k_{rxn}[S]}{K_d + [S]} \qquad \textbf{(2.1)}$$

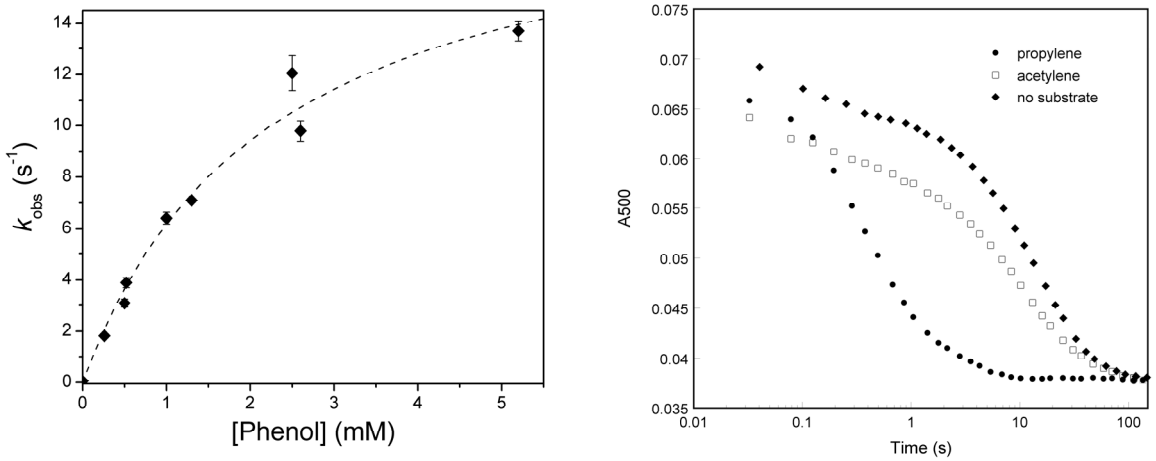

Figure 2.14. Effect of substrates on the decay rate of the tryptophanyl radical. The decay rate increases the in presence of phenol, a substrate for the native enzyme system (left). The dependence of the observed rate on phenol concentration is well modeled by saturation kinetics. The determined reaction rate of the intermediate, k_{rxn}, with phenol and the substrate binding constant, K_d, are 20 ± 2 s^{-1} and 2.3 ± 0.5 mM respectively. Propylene, a substrate for $MMOH_{peroxo}$, also accelerates k_d by more than 50-fold to 2.8 s^{-1} whereas acetylene has only a minor effect (right).

The decay rate of $W^{\bullet}$ is also accelerated in the presence of propylene. The observed decay rate constants are 0.239 ± 0.003 s^{-1} and 2.8 ± 0.1 s^{-1} for propylene concentrations of 19 μM and 3.8 mM, respectively. Addition of acetylene to the tryptophanyl radical had little influence on the decay process, increasing the rate constant from 0.079 ± 0.002 s^{-1} to 0.114 ± 0.006 s^{-1} (Figure 2.14).

^{1}H- and ^{2}H-ENDOR Spectra of the Mixed Valent Diiron(III,IV)–$W^{\bullet}$ Couple. To confirm that the protein-based radical resides on a tryptophan residue, ^{1,2}H-ENDOR spectra were recorded of this transient in H_2O/D_2O buffers using enzymes that contained either natural abundance tryptophan or the tryptophan selectively deuterated on the indole ring. Although the radical EPR signal overlaps that of the diiron center, the spectrum of the latter is substantially broader. Signals from the two can therefore be distinguished by their field dependence as well as by their different relaxation properties.

The ^{1}H–CW ENDOR spectra collected at fields associated with the radical for samples containing natural abundance tryptophan residues are dominated by signals from the C_β protons of the residue, with strong hyperfine couplings of ~ 20 MHz, and by those from the indole ring, with smaller couplings (Figure 2.15). Additional features near ν_H have been assigned to protein matrix protons in

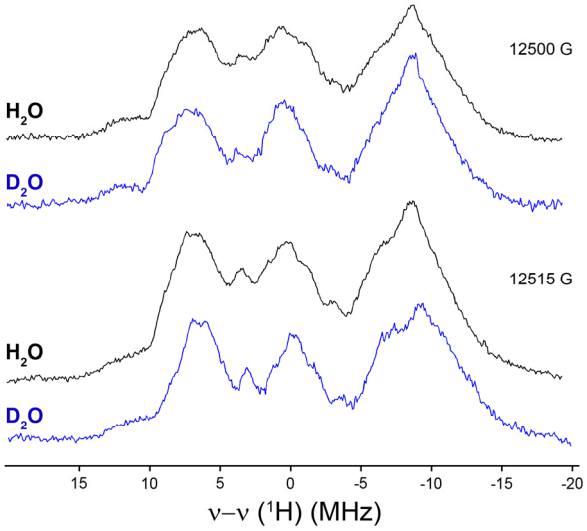

Figure 2.15. ^{1}H-Mims ENDOR spectra of the tryptophan radical in buffers containing H_2O (black) and D_2O (blue). The two spectra are superimposable indicating that there are no exchangeable protons on the radical. The spectra, as for the ^{2}H-Mims spectra, are dominated by signals from the indole protons.

other systems.[28] To determine that the radical is centered at tryptophan, we collected ^{2}H-Mims ENDOR spectra from natural-abundance and selectively deuterated, tryptophan(d_5-indole), hydroxylase.

The sample prepared with isotopically enriched tryptophan shows ^{2}H-Mims ENDOR signals with hyperfine couplings corresponding to $A_H > 10$ MHz when the field of observation is where the radical signal is strongest (Figure 2.16). These signals arise from the aromatic protons of the indole ring because they are absent at fields outside the EPR envelope of the radical signal in the natural-abundance sample. The signals unequivocally confirm that the protein-based radical resides on a tryptophan residue.

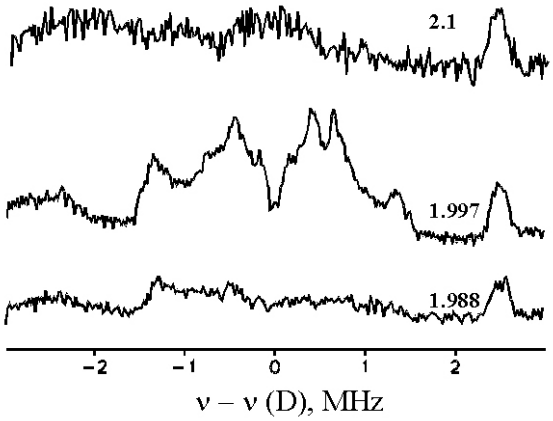

Figure 2.16. ^{2}H-Mims ENDOR spectra of the tryptophanyl radical. Protein in this sample was expressed in media containing isotopically enriched tryptophan(d_5-indole). Saturation of the transition corresponding to the radical signal at $g \sim 2.00$ (middle) yields ^{2}H signals from the labeled indole ring. These peaks disappear upon saturation at higher (top) or lower (bottom) g-values. Magnetic fields scanned are reported as g-values in the figure.

^{1}H–CW ENDOR spectra collected at the field corresponding to the maximum intensity of the radical are similar for the diiron(III,IV)–W$^\bullet$ transient generated with unlabelled protein in deuterated and protic buffers, but such comparisons are difficult because of strong signals from non-exchangeable protons (Figure 2.15). As a result, the presence of potentially exchangeable protons was investigated by ^{2}H Mims ENDOR measurements. ^{2}H-Mims ENDOR signals corresponding to ^{1}H coupling of $A_H \sim 4$-8 MHz were observed in samples generated in deuterated buffer (Figure 2.17).

Because these signals are observed at fields across the EPR envelope of the diiron center, and outside that of the tryptophanyl radical, they can be assigned to the diiron center (compare Figures 2.16 and 2.17). By analogy to the diiron centers of intermediate X and $MMOH_{mv}$, for which ENDOR signals from terminal water molecules on the iron(III) ion correspond to species with A_H ~ 7-9 MHz, the signals observed in the diiron(III,IV)–$W^{\bullet}$ transient can be assigned to a terminal water molecule or hydroxide ion on the ferric ion.[28,29]

If the tryptophanyl radical were protonated at the indole nitrogen atom, one would expect an additional ^2H signal, with A_H > 10 MHz, at fields associated with this radical.[30-34] No such ^2H signals are observed, however (Figure 2.17). The absence of an exchangeable proton associated with the

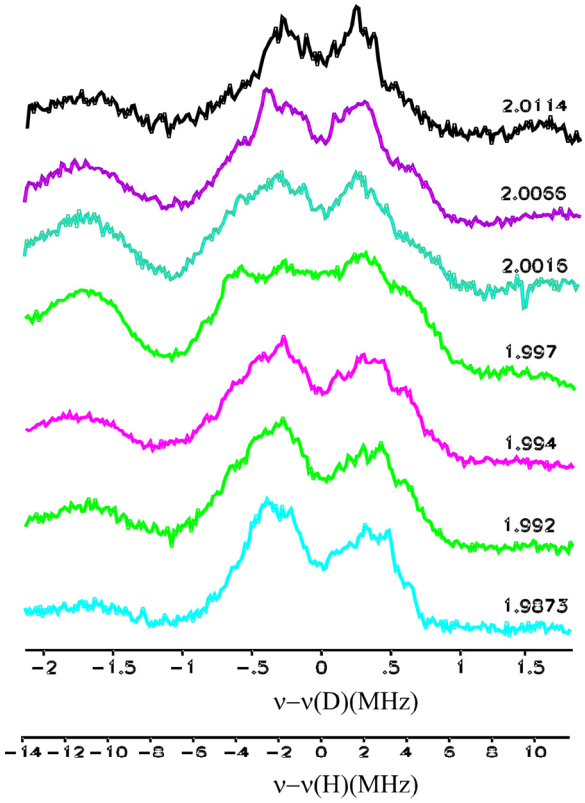

Figure 2.17. ^2H-Mims ENDOR spectra of the diiron(III,IV)–$W^{\bullet}$ species generated in deuterated buffers. Signals arising from protonated species are observed over the swept magnetic fields. The signal shows minor changes upon saturation at g = 1.9875 to 2.0 and does not correlate with the tryptophan radical. The corresponding proton scale is shown for comparison.

protein radical is consistent with our interpretation of the stopped-flow optical data, where a band with λ_{max} of 500 nm indicated a deprotonated tryptophanyl radical.

Tryptic Digestion and Mass Spectrometry Analyses of ToMOH I100W and its Oxidation Product. The most ion intense peaks in the MALDI-TOF(+) spectra are between 700 and 2500 m/z for the in-gel tryptic digested α-subunit of as-isolated and O_2-reacted $ToMOH_{red}$ I100W. The expected tryptic peptide containing W100, $_{85}$ADPGWVSTMQLHFGAWALEEYAASTAEAR$_{113}$, has a predicted monoisotopic mass of 3165.5 Da for the $[M+H]^+$ parent ion. The ion envelope at m/z = 3166 in the protein sample as-isolated after expression is well separated from other ions in the spectrum. This fragment is assigned as the 29mer peptide containing W100. Two additional envelopes of lower intensity are present at m/z values of 3182 and 3198 (Figure 2.18). The relative

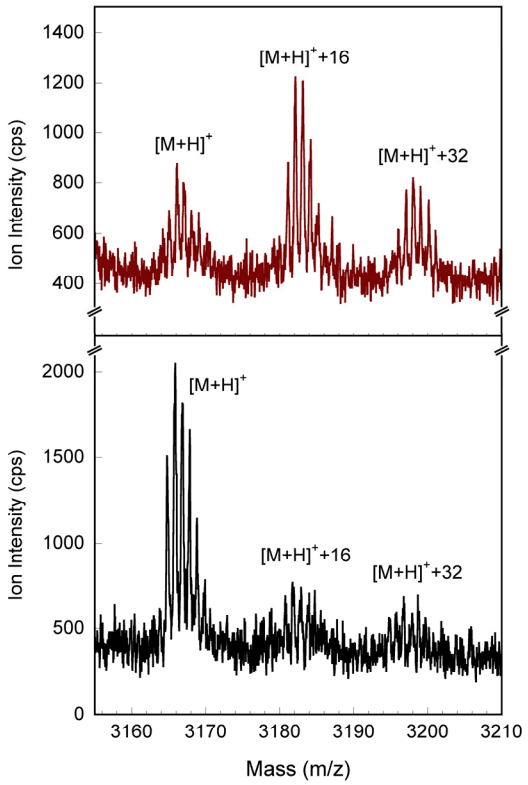

Figure 2.18. MALDI-TOF spectra of tryptic peptides for the α-subunit of O_2-reacted (top) and as-isolated (bottom) ToMOH I100W. The mass of the $[M+H]^+$ ion at 3166 m/z agrees with the predicted mass for the 29mer peptide. Two additional envelopes of 16 and 32 Da higher mass are also present. The relative intensity of these three envelopes changes in the reacted sample, with $[M+H]^+$ less abundant than $[M+H]^+$+16.

intensities of these latter two envelopes in the reacted sample increase markedly, with that at m/z = 3182 becoming the most intense. The envelopes at m/z = 3182 and 3198 were unchanged in MALDI-TOF spectra of digestion products of reduced ToMOH I100W reacted with $^{18}O_2$-saturated buffer.

The tryptic peptide of interest also contains other residues sensitive to oxidation, such as methionine and histidine. To determine the decay pathway chemistry for the $W^{\bullet}$ species, we attempted to identify the specific residue that is oxidized. Fragmention of the tryptic peptide was carried out by ESI(+)-MS/MS. Ions resulting from the $[M+H]^{3+}$ ion were assigned to respective b and y peptides[35] by considering the fragment ion mass and the peak-to-peak separation within the ion envelope. We could not identify the ions corresponding to every possible fragment because the peak intensities were below our detection threshold. From the ions that were isolated, the b ions limit the site of modification to lie between S91 and E104, a region that includes two other possible sites of oxidation, M93 and H96. The y fragment ions further narrowed the possible region of oxidation, excluding M93. Probable sites of oxidation are therefore limited to H96 and W100 (Figure 2.19).

DISCUSSION

Mixed-Valent Diiron(III,IV)–$W^{\bullet}$ Species as an Entry to Identifying ToMOH Intermediates. Dioxygen reacts rapidly, $k_{obs} \sim 18\ s^{-1}$, with reduced diiron(II) ToMOH I100W preincubated with ToMOD to yield a diiron(III) intermediate that was only disclosed because it generated the tryptophan radical. One-electron reduction of this diiron(III) transient gives rise to a mixed-valent diiron(III,IV) center. The peroxodiiron(III) species in RNR-R2 reacts in a similar manner. Oxidation of W48 and protonation of one of the oxygen atoms in the peroxo-adduct of RNR-R2 facilitates O–O bond cleavage to form X.[23,24] The proposed mechanism for dioxygen activation in cytochrome P450 enzymes requires protonation of the distal oxygen atoms in the peroxoiron(III) intermediate by a conserved threonine-aspartic acid pair.[6,19] Residue T201 in the

Ion	Mass (m/z)	Charge
b4	341.2	+1
b5	527.2	+1
b6	626.3	+1
b6	313.2	+2
b7	713.3	+1
b20	*1122.5*	*+2*
b22	*1239.6*	*+2*

Ion	Mass (m/z)	Charge
y1	175.1	+1
y2	246.2	+1
y3	375.2	+1
y4	446.3	+1
y5	547.3	+1
y6	634.3	+1
y7	705.4	+1
y8	776.4	+1
y9	939.5	+1
y12	1320.6	+1
y19	*1055.8*	*+2*
y23	*1278.6*	*+2*
y27	*1328.2*	*+2*
y27	*999.1*	*+3*

Figure 2.19. ESI-MS/MS fragment ions arising from the tryptic peptide containing W100. The fragment peptide ions of the tryptic peptide of interest are labeled using the b and y ion nomenclature (top). W100 is in red font. The $[M+H]^{3+}$ parent ion was fragmented. The fragment peptide ions were assigned based on mass and isotopic spacing of the individual envelopes. The fragment ions containing the modified residue are shown in italics. This analysis revealed that the 16 Da increase observed for the reacted sample results from modification of a residue situated between H96 and E104.

active site cavity of ToMOH, which is strongly conserved among the BMMs, could function in a proton shuttle pathway to the diiron core. In MMOH, this threonine is proposed either to deliver protons to the peroxodiiron(III) species directly,[36] or more plausibly, by strategically holding a hydronium ion for proton transfer during reduction of the oxidized diiron(III) center.[37] Conversion of the diiron(III) intermediate in ToMOH to the mixed-valent center could proceed by an analogous pathway as that in the heme systems and RNR-R2. In the I100W variant, T201 could help to provide a crucial proton to facilitate cleavage of the O–O bond to form the mixed-valent transient. Protons

would be consumed during the oxidative phase of the ToMOH catalytic cycle, which would contrast MMOH where protons are proposed to be required during reduction of the oxidized diiron(III) core. In the native system, T201 may be important for steady-state catalysis if substrate radical generation is a pathway for arene hydroxylation. Pre-steady-state studies of a series of variants at this position would be valuable in discerning its possible role in the mechanism of substrate oxidation.

An investigation of T201 variants of T4MOH demonstrated that this residue does not affect steady-state catalysis.[38] For an observable effect under steady-state conditions however, T201 must be involved in the rate-determining step. Product release is believed to be rate-limiting for hydroxylation by MMOH.[39] The products catechol and phenol can bind to the diiron center in $ToMOH_{ox}$, isolated after purification or following single-turnover experiments (Chapter 3). Lack of knowledge of the rate-determining step under steady-state catalysis prevents us from making a meaningful comparison between the earlier steady-state and current pre-steady-state analyses.

Values of δ and ΔE_Q for the mixed-valent diiron(III,IV) transient in ToMOH I100W are comparable those of the Fe(III)Fe(IV) centers of intermediate X and Q_X.[23,40] In addition, the ^{2}H-Mims ENDOR spectra of the ToMOH diiron(III,IV) species prepared in deuterated buffer suggest that an exchangeable proton-containing species is coordinated to the iron(III) ion. The observed hyperfine couplings for this protonated ligand are within the range of those reported for terminal water molecules on the ferric centers in $MMOH_{mv}$ and intermediate X.[24,29] This terminal hydroxide ion or water molecule may arise by a mechanism similar to that proposed for RNR-R2.[24] Protonation-aided cleavage of the O–O bond in the diiron(III) species would yield a water molecule that coordinates to the ferric ion. Despite the differences between the diiron(III) intermediate in ToMOH and those of other CBDI enzymes, the ability to form high-valent transients with similar spectroscopic parameters might arise from the homologous primary coordination spheres that these enzymes share.

Our preliminary assignment of the protein-based radical as W• was based on stopped-flow optical experiments. In these studies, a λ_{max} was measured to be 500 nm, within the previously reported range for tryptophanyl radicals.[20,21,41] Since the species (λ_{max} 500 nm) was observed only in the tryptophan variant, this specific residue seemed to be critical for transient formation. ^{1}H- and ^{2}H-Mims ENDOR spectra of this species containing unlabeled and selectively deuterated tryptophan residues firmly establish the presence of a tryptophanyl radical. Samples made in protic and deuterated buffers had similar ^{1}H-Mims ENDOR spectra, providing evidence that the tryptophanyl radical was deprotonated, confirming unequivocally our initial assignment that the optically active intermedate observed in stopped-flow studies was a neutral tryptophanyl radical.

The redox potentials of the aromatic side chains of tyrosine and tryptophan are pH dependent with lower proton concentrations favoring oxidation.[20,41] In the present study, we observed the deprotonated form of the radical, the λ_{max} value of which was invariant across the examined pH range of 6.5 to 7.5. We were unable to access pH values near the reported pK_a values for the indole ring[42] and the cationic indolyl radical[41] because of protein instability. Nonetheless, deprotonation of the indole nitrogen is tightly coupled to electron abstraction as the tryptophan cation radical is not observed. We exclude mechanisms such as hydrogen atom transfer from W100 to the diiron center or a proton tunneling event during the rate-determing step for formation and decay of the diiron(III,IV)–W• transient because of the magnitude and temperature dependence of the kinetic isotope effects. In enzymes where hydrogen-atom transfer or proton tunneling are proposed to occur, the isotope effect ranges from 3 to in excess of 100 and are temperature independent.[43,44] The isotope effects observed here are less than 3.2 for either rate constant and were temperature dependent, both of which are atypical of hydrogen-atom transfer or tunneling.

Disruption of electron transfer pathways from W48 and Y122 to oxygenated diiron intermediates in RNR-R2 results in the oxidation of phenylalanine and tyrosine residues near the

dimetallic center.[45-47] Models of the I100Y mutation estimate the distance between the diiron center and this tyrosine at 7 to 10 Å, positioning this residue for possible oxidation.[48] Absorption bands corresponding to tyrosyl radicals or iron-catecholate species were not observed during or after the reaction of $ToMOH_{red}$ I100Y with dioxygen. Absence of these bands suggests that, if oxidation of the tyrosine residue occurs, a stable radical species is not formed and the L-dopa product is unable to coordinate to the diiron center. Alternatively, the diiron(III) intermediate may not be a strong enough oxidant to abstract an electron from Y100. This limitation may arise from the redox potential of tyrosine or from other parameters that affect the ET, such as the distance.

As mentioned in the Results Section, a model whereby a slow reversible equilibrium precedes the fast oxidation provides the most satisfacory fit to the pH dependence data. Deprotonation of the tryptophan residue, of the diiron(III) intermediate, or of an amino acid sidechain required to accept the proton from the tryptophan residue could limit the oxidation rate. The tryptophan cation radical is not observed in our optical studies, implying that proton loss must occur either before or after oxidation of this residue. Deprotonation of the indole nitrogen before electron abstraction by the diiron(III) intermediate is expected to be unfavorable because the pK_a of this proton is estimated to be 17.[42] Oxidation of W100 prior to proton loss would yield a transient tryptophan cation radical, the pK_a of which is 3.7.[41] Deprotonation of the radical cation is therefore predicted to be facile and rapid within the examined pH range. Proton loss from the indole ring could limit the oxidation rate if it is required to occur prior to this reaction. Alternatively, if loss occurs after oxidation, the rate limiting deprotonation event might involve either the diiron(III) intermediate or other amino acid residues involved in this oxidation event.

Implications for Catalysis in Native ToMOH. The mechanism for arene hydroxylation by the native hydroxylase could proceed by either one- or two-electron oxidation pathways. If this reaction occurs by initial electron abstraction from substrate, the hydroxylation mechanism could involve

generation of a species similar to mixed-valent diiron(III,IV)–$W^{\bullet}$ center in ToMOH I100W. However, oxidation of the aromatic substrate by an electrophilic attack on the π-system would be comparable to the reactions of $MMOH_{peroxo}$ with electron-rich substrates[26] and bypass stable radical intermediates.

Both radical- and cation-derived products were observed for oxidation of RCS probes by T4MO, implying that one- and two-electron oxidation mechanisms might occur in this system.[49] Formation of both of these products could reflect two competing mechanisms for substrate oxidation arising from ease of approach of these unnatural substrates to the diiron site. If substrate is bound close to the reactive intermediate, then oxidation proceeds by hydride abstraction to generate a substrate cation. Ring-opening of the substrate gives rise to the observed cation-derived product. On the other hand, if the hydrocarbon is not in close proximity to the oxidizing intermediate, electron abstraction may predominate to generate substrate-radical intermediates. If the diiron(III) species is the only iron-based transient formed during dioxygen activation in the native hydrooxylase, the preference for electron-rich substrates, such as the indole ring of W100 or aromatic compounds, by this transient in ToMOH is similar to the observed reactivity of $MMOH_{peroxo}$ and the peroxodiiron(III) species in RNR-R2. The formation of both radical- and cation-derived RCS products could arise from two distinct intermediates that react with these substrates. In MMOH, Q is proposed to carry out one-electron oxidations whereas $MMOH_{peroxo}$ reacts by hydride abstraction and epoxidation mechanisms.[26] The diiron(III) intermediate observed in ToMOH I100W is the only observed precursor to the mixed-valent diiron(III,IV) center, yet we cannot exclude formation of a short-lived di(μ-oxo)diiron(IV) intermediate. Formation of a Q-type intermediate would facilitate electron abstraction pathways and the diiron(III) intermediate would allow for two-electron oxidation mechanisms. Investigation of the diiron(III) transient in the wild type hydroxylase is important for probing further whether one- or two-electron oxidation pathways and high-valent diiron

intermediates can form during dioxygen activation and substrate hydroxylation and is discussed in greater detail in Chapter 3.

The Mössbauer parameters and lack of optical absorption features in the near-IR region for the diiron(III) transient species are unique among intermediates at this oxidation level in the CBDI enzyme family.[4] Specifically, values for λ_{max} near 700 nm, $\delta > 0.6$ mm/s, and $\Delta E_Q > 1$ mm/s are characteristic parameters of μ-1,2-peroxodiiron(III) clusters in synthetic and enzyme systems.[10] This intermediate is EPR–silent like other peroxo-bridged diiron(III) clusters. We tentatively assign this intermediate as a peroxodiiron(III) species based on the similarities of the proposed reactivity to other peroxo-intermediates and by analogy to the mechanism of dioxygen activation at synthetic and enzymatic CBDI centers.

The differences between the Mössbauer parameters for this intermediate and those of other peroxodiiron(III) species might arise from an alternate binding geometry of the peroxide moiety to the diiron core. Binding modes, such as μ-η^1:η^2- and μ-1,1-, of peroxide fragments at diiron(III) centers are proposed to occur during formation of $MMOH_{peroxo}$[50] and X.[51,52] The peroxide fragment here might adopt such a conformation. The protonation state of the peroxide bridge may also differ. Hydroperoxoiron(III) intermediates reported in heme systems are proposed to be electrophilic oxidants,[6,53] similar to the observed reactivity of peroxodiiron(III) centers. Detailed structural investigations of this intermediate in the native system by ENDOR and XAS would provide insight into the structure of this species.

The redox potential of the diiron(III) intermediate can be estimated by Marcus Theory (eq 2.2). The variable k_{ET} is the electron transfer rate, k_0 is the characteristic frequency of the nuclei, usually assigned a value of 10^{13}, R is the gas constant, and T is the temperature in K.[54] The term β, fixed at 1.1 $Å^{-1}$, is related to the nature of the intervening medium between the redox partners. The distance

$$k_{ET} = k_0 e^{-\beta(r-r_0)} e^{\left[\frac{-(\Delta G+\lambda)^2}{4\lambda RT}\right]} \qquad \textbf{(2.2)}$$

between the tryptophan residue and the diiron center, r, was determined from the crystal structure to be 6.5 Å,[48] and r_0 is the contact distance, which is generally set to 3 Å. Reorganization energies, λ, of 1 and 0.1V were used to calculate a range for the reduction potential of the diiron(III) intermediate. The driving force, ΔG, is the sum of the reduction potentials for the forward reaction. Since we did not observe a transient tyrosyl radical in the I100Y variant, the reduction potential of the diiron(III) intermediate might lie between that of Y and W. Depending on whether deprotonation of the indole ring occurs before or after electron abstraction, the potential may be further limited to between those of the $W^{\bullet}/W^{-}$ and the $W^{\bullet+}/W$ half reactions. To obtain a conservative estimate of the oxidizing power of the diiron(III) intermediate, we assumed that proton loss must occur prior to electron transfer as the energetic cost is less for oxidation of the deprotonated versus neutral indole ring. The foregoing analysis was used to estimate the potential for the $Fe_2^{III}/Fe_2^{III,IV}$ half reaction, assuming that the $W^{\bullet}/W^{-}$ couple was 0.73 V which corresponds to deprotonation of 50% of the tryptophan residues.[41] To negate the inhibitory effect of protons on the oxidation rate, the calculated proton-independent oxidation rate of 1.22 s^{-1} determined from the variable pH data was used for k_{ET}. With these assumptions, we estimate the reduction potential of the intermediate is between 1.1 and 1.3 V versus NHE. This range is close to the reduction potentials of oxidants such as hydrogen peroxide (0.878 V), manganese dioxide (1.224 V), and chromate (1.35 V). The latter two oxidants, MnO_2 and CrO_4^-, are commonly employed for the conversion of hydroxyl groups to either carbonyl or carboxylate functionalities. The peroxodiiron(III) intermediate in MMOH is proposed to carry out similar oxidation reactions albeit via hydride abstraction.[26]

Mechanism of Dioxygen Activation and W100 Oxidation. Scheme 2.1 depicts our proposed mechanism of formation for the mixed-valent diiron(III,IV)–$W^{\bullet}$ transient. Dioxygen binding to the reduced diiron(II) enzyme would yield a peroxodiiron(III) intermediate, two possible geometries for which are depicted. Electron abstraction from W100 by the diiron(III) center is accompanied by

protonation-aided cleavage of the O–O bond to form the mixed-valent diiron(III,IV)–W• transient. The structure of the mixed-valent diiron core is similar to that proposed for intermediate X, where the oxygen atoms derived from dioxygen (filled circles in Scheme 2.1) become an oxo-bridge and a terminal hydroxide or water molecule.

Scheme 2.1. Proposed Mechanism for Formation of the Diiron(III,IV)–W• Transient.

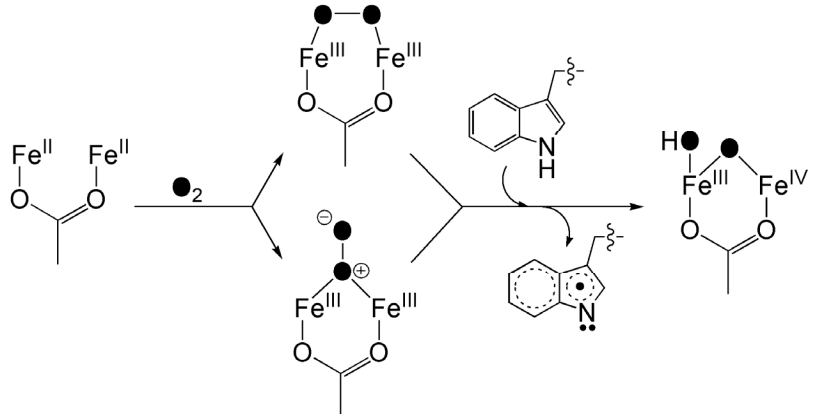

The diiron(III,IV) cluster and W• radical decay at the same rate as measured by Mössbauer, EPR, and optical spectroscopy. The two $S = ½$ centers are therefore likely to share a common mechanism to restore the oxidized diiron(III) cluster and quench the protein radical. In reacted ToMOH I100W, the installed tryptophan appears to be oxidized, as evidence by the 16 Da increase in mass of the tryptic peptide containing W100 and the fragmentation peptides thereof. In the crystal structure of ToMOH I100W, the indole ring adopts conformations in which the C4–C7 vector is oriented either away from or toward the active site.[48] We predict that C5 or C6 is the site of oxidation, based on the distances between these two carbon atoms and the diiron core in the oxidized crystal structure. Oxidation of W• arising from attack by dioxygen is unlikely, as the mass of the predicted products would be 32 Da greater than the parent $[M+H]^+$ ion of the unmodified peptide, disagreeing with experimental results.[55] The peak at m/z = 3198 in the MALDI-TOF spectra (Figure 2.19) is of weak intensity and is attributed to further oxidation of the W100 from multiple turnovers of the hydroxylase, instead of oxidation of the indolyl radical by O_2. In addition, such a pathway

would not explain the simultaneous decay of the mixed-valent diiron(III,IV) center. Instead, we propose a radical recombination mechanism, where an oxygen atom species on the diiron(III,IV) cluster is transferred to the indolyl radical (Scheme 2.2).

Scheme 2.2. Proposed Mechanism for Decay of the Diiron(III,IV)–W• Transient.

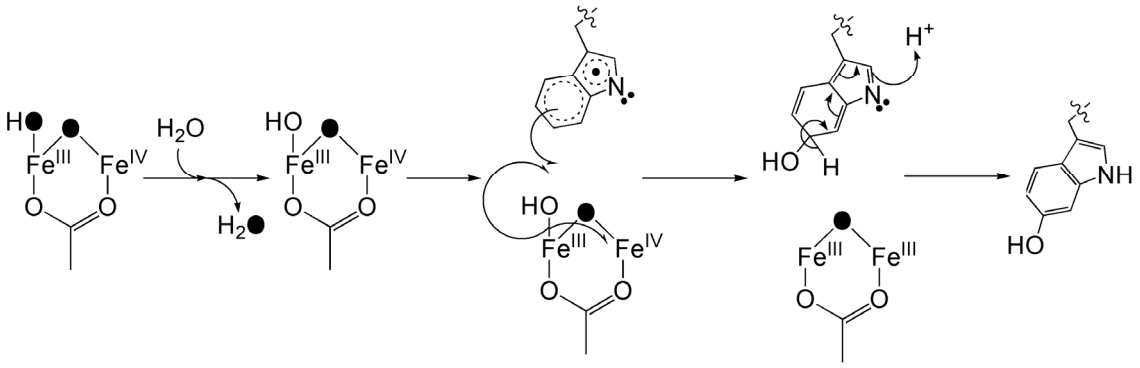

The terminal hydroxide or water molecule must be exchangeable to explain the insensitivity of the mass of the tryptic peptide and its fragments containing W100 to the isotopic content of the dioxygen source. ^{2}H-ENDOR spectra of the transient in deuterated buffers identified an exchangeable species with hyperfine coupling constants similar to those reported for terminal water ligands on the ferric ion in X and $MMOH_{mv}$.[28,29] The exchange rate of this labile species must be significantly faster than that of the decay of the transient species to prevent incorporation of ^{18}O-atoms into the tryptic peptide. Rapid exchange of oxygen atom ligands at high-valent iron centers has been reported for bridging and terminal ligands in intermediate X[24] and terminal oxo-groups at mononuclear iron centers.[56,57] Hydroxyl radical transfer from the diiron center to W• followed by rearomatization of the indole ring gives rise to an oxo-bridged diiron(III) cluster and a hydroxyindole side chain at W100. Addition of water to the diiron core reforms the di(μ-hydroxo)diiron(III) resting state.

The decay reaction is sensitive to proton concentration. The active site of ToMOH is charge neutral, and depending on the ligand type and binding geometries in the intermediate, the terminal

ligand could be either a bound water or hydroxide. If the terminal species is a bound water molecule, deprotonation might be required prior to hydroxyl radical transfer. Alternatively, the protonation state of residues within the active site cavity or channel near W100 may be important for stabilizing the diiron(III,IV) or W$^{\bullet}$. Deprotonation of these residues could favor decay of these transient species. More detailed structural information on the transient species formed during dioxygen activation in the native and I100W variant of the hydroxylase will be required to determine the source of this proton dependence.

Potential substrates for BMMs, such as propylene and phenol, accelerate decay of the tryptophanyl radical in stopped-flow optical studies. In the steady state, the activity of ToMOH I100W is more than an order of magnitude lower than that of the wild type enzyme, possibly due to retardation of substrate access or product egress in the variant hydroxylase. The ability of phenol and propylene to accelerate the decay rate is interesting. Phenol could quench the tryptophanyl radical by hydrogen atom transfer from the O–H group to form a phenoxyl radical. Similar reactivity is observed in small molecule chemistry where analogues of phenol are used as radical scavengers. Neutral and cationic tryptophanyl radicals reportedly abstract hydrogen atoms from the hydroxyl group of *p*-methoxyphenol at rates exceeding 10^5 s^{-1}.[58] No absorption bands were observed at 410 nm during our double-mixing optical experiments, which indicates that any phenoxyl radical formed by hydrogen-atom abstraction must be short-lived. To explain the sensitivity of the decay rate on propylene and acetylene, we consider the bond dissociation energies of the weakest C–H bonds in these molecules. The BDE of the phenolic O–H bond is similar to that of the methyl sp^3 C–H bond in propylene, ~ 87 kcal/mol.[59,60] Acetylene, by comparison, has a C–H BDE almost 50 kcal/mol greater than that of phenol or propylene. The tryptophanyl radical is capable of abstracting a hydrogen atom from the weak O–H bond in phenol and C–H bond in propylene, accelerating the decay of this transient.

Because the same reaction with acetylene requires more energy, the decay rate is not appreciably perturbed upon mixing the radical with this substrate.

The reaction of phenol with the neutral tryptophan radical is a pathway distinct from hydroxylation of to yield catechol under steady state conditions where the diiron centers are distributed into populations of reduced, diiron(III) intermediate, diiron(III,IV)–W$^{\bullet}$ transient, and diiron(III) product species. The presence of W100 effectively out-competes the phenolic substrate for the diiron(III) intermediate, if substrate binding occurs after dioxygen activation. Substrate could conceivably bind to the active site in either the reduced state, prior to dioxygen binding and activation, or in the oxidized state after oxidation of W100 or phenol. The reduced capacity of the I100W hydroxylase to oxidize phenol reflects the retarded access of substrate into the active site pocket afforded by the mutation. Considering the location of residue 100 in the ToMOH α-subunit, separating the active site pocket from the rest of the channel and cavity 2, it is reasonable to propose that it may serve to gate substrate entry, product egress, or solvent access to the diiron center as proposed for L110 in MMOH and L98 in hemerythrin [14,61]. Evidence supporting this proposal is illustrated by the two conformations of the indole side chain in the crystal structure of I100W, which allow different levels of access to the diiron center of ToMOH.

CONCLUSIONS

The reaction of diiron(II) ToMOH I100W with dioxygen yields a diiron(III) intermediate, which subsequently abstracts an electron from W100 to form a chromophoric mixed-valent diiron(III,IV)–W$^{\bullet}$ species. This coupled species could decay by transfer of an O-atom from the diiron core to the protein-based radical. The one-electron redox chemistry afforded by the diiron(III) intermediate resembles that of the peroxodiiron(III) intermediate in RNR-R2. No other high-valent diiron species were observed, suggesting that oxidation of hydrocarbons in this system occurs at the diiron(III) level. This diiron(III) intermediate is spectroscopically different to μ-1,2-peroxodiiron(III) clusters in

CBDI enzymes and model compounds. These differences suggest that this intermediate in ToMOH may have an alternate binding geometry or protonation state of the dioxygen-derived fragment. The oxidation of W100 to form deprotonated tryptophanyl radical has allowed for an estimation of the reduction potential of the diiron(III) intermediate at 1.1 – 1.3 V. The mixed-valent diiron(III,IV) center has spectroscopic parameters similar to those of intermediates X and Q_X, although the diiron(III) precursors differ spectroscopically.

REFERENCES

1. Song, W. J.; Seo, M. S.; George, S. D.; Ohta, T.; Song, R.; Kang, M.-J.; Tosha, T.; Kitagawa, T.; Solomon, E. I.; Nam, W., *J. Am. Chem. Soc.* **2007,** *129* (19), 1268-1277.

2. Nam, W., *Acc. Chem. Res.* **2007,** *40* (7), 522-531.

3. Mirica, L. M.; Vance, M.; Jackson Rudd, D.; Hedman, B.; Hodgson, K. O.; Solomon, E. I.; Stack, D. P., *Science* **2005,** *308* (5730), 1890-1892.

4. Lippard, S. J., *Philos. Trans. R. Soc. A* **2005,** *363* (1829), 861-877.

5. Sinnecker, S.; Svensen, N.; Barr, E. W.; Ye, S.; Bollinger, J. M., Jr.; Neese, F.; Krebs, C., *J. Am. Chem. Soc.* **2007,** *129* (19), 6168-6179.

6. Denisov, I. G.; Makris, T. M.; Sligar, S. G.; Schlichting, I., *Chem. Rev.* **2005,** *105* (6), 2253-2277.

7. Rosenzweig, A. C.; Brandstetter, H.; Whittington, D. A.; Nordlund, P.; Lippard, S. J.; Frederick, C. A., *Proteins* **1997,** *29* (2), 141-152.

8. Logan, D. T.; Su, X.-D.; Åberg, A.; Regnström, K.; Hajdu, J.; Eklund, H.; Nordlund, P., *Structure* **1996,** *4* (9), 1053-1064.

9. Lindqvist, Y.; Huang, W.; Schneider, G.; Shanklin, J., *EMBO J.* **1996,** *15* (16), 4081-4092.

10. Merkx, M.; Kopp, D. A.; Sazinsky, M. H.; Blazyk, J. L.; Müller, J.; Lippard, S. J., *Angew. Chem., Int. Ed.* **2001,** *40* (15), 2782-2807.

11. Broadwater, J. A.; Ai, J.; Loehr, T. M.; Sanders-Loehr, J.; Fox, B. G., *Biochemistry* **1998,** *37* (42), 14664-14671.

12. Jin, S.; Kurtz, D. J., Jr.; Liu, Z.-J.; Rose, J.; Wang, B.-C., *J. Am. Chem. Soc.* **2002,** *124* (33), 9845-9855.

13. Sazinsky, M. H.; Bard, J.; DiDonato, A.; Lippard, S. J., *J. Biol. Chem.* **2004,** *279* (29), 30600-30610.

14. Farmer, C. S.; Kurtz, D. J., Jr.; Phillips, R. S.; Ai, J.; Sanders-Loehr, J., *J. Biol. Chem.* **2000,** *275* (2), 17043-17050.

15. LeMaster, D. M.; Richards, F. M., *Biochemistry* **1985,** *24* (25), 7263-7268.

16. Cafaro, V.; Scognamiglio, R.; Viggiani, A.; Izzo, V.; Passaro, I.; Notomista, E.; Dal Piaz, F.; Amoresano, A.; Casbarra, A.; Pucci, P.; DiDonato, A., *Eur. J. Biochem.* **2002,** *269* (22), 5689-5699.

17. Wilhelm, E.; Battino, R.; Wilcock, R. J., *Chem. Rev.* **1977,** *77* (2), 219-262.

18. Ravi, N.; Bollinger, J. M., Jr.; Huynh, B. H.; Edmondson, D. E.; Stubbe, J., *J. Am. Chem. Soc.* **1994,** *116* (18), 8007-8014.

19. Davydov, R.; Perera, R.; Jin, S.; Yang, T.-C.; Bryson, T. A.; Sono, M.; Dawson, J. H.; Hoffman, B. M., *J. Am. Chem. Soc.* **2005,** *127* (5), 1403-1413.

20. Reece, S. Y.; Stubbe, J.; Nocera, D. G., *Biochim. Biophys. Acta* **2005,** *1706* (3), 232-238.

21. Aubert, C.; Vos, M. H.; Mathis, P.; Eker, A. P. M.; Brettel, K., *Nature* **2000,** *405* (6786), 586-590.

22. Baldwin, J.; Krebs, C.; Ley, B. A.; Edmondson, D. E.; Huynh, B. H.; Bollinger, J. M., Jr., *J. Am. Chem. Soc.* **2000,** *122* (49), 12195-12206.

23. Krebs, C.; Chen, S.; Baldwin, J.; Ley, B. A.; Patel, U.; Edmondson, D. E.; Huynh, B. H.; Bollinger, J. M., Jr., *J. Am. Chem. Soc.* **2000,** *122* (49), 12207-12219.

24. Burdi, D.; Willems, J.-P.; Riggs-Gelasco, P.; Antholine, W. E.; Stubbe, J.; Hoffman, B. M., *J. Am. Chem. Soc.* **1998,** *120* (49), 12910-12919.

25. Lendzian, F., *Biochim. Biophys. Acta* **2005,** *1707* (1), 67-90.

26. Beauvais, L. G.; Lippard, S. J., *J. Am. Chem. Soc.* **2005,** *127* (20), 7370-7378.

27. Ambundo, E. A.; Friesner, R. A.; Lippard, S. J., *J. Am. Chem. Soc.* **2002,** *124* (30), 8770-8771.

28. Willems, J.-P.; Lee, H.-I.; Burdi, D.; Doan, P. E.; Stubbe, J.; Hoffman, B. M., *J. Am. Chem. Soc.* **1997,** *119* (41), 9816-9824.

29. Smoukov, S. K.; Kopp, D. A.; Valentine, A. M.; Davydov, R.; Lippard, S. J.; Hoffman, B. M., *J. Am. Chem. Soc.* **2002,** *124* (11), 2657-2663.

30. Himo, F.; Eriksson, L. A., *J. Phys. Chem. B* **1997,** *101* (47), 9811-9819.

31. Huyett, J. E.; Doan, P. E.; Gurbiel, R.; Houseman, A. L. P.; Sivaraja, M.; Goodin, D. B.; Hoffman, B. M., *J. Am. Chem. Soc.* **1995,** *117* (35), 9033-9041.

32. Walden, S. E.; Wheeler, R. A., *J. Phys. Chem.* **1996,** *100* (5), 1530-1535.

33. Rigby, S. E. J.; Jünemann, S.; Rich, P. R.; Heathcote, P., *Biochemistry* **2000,** *39* (20), 5921-5928.

34. O'Malley, P. J.; Ellson, D. A., *Chem. Phys. Lett.* **1996,** *260* 492-498.

35. Papayannopoulos, I. A., *Mass Spectrom. Rev.* **1995,** *14* 49-73.

36. Lee, S.-K.; Lipscomb, J. D., *Biochemistry* **1999,** *38* (14), 4423-4432.

37. Lovell, T.; Li, J.; Noodleman, L., *Inorg. Chem.* **2001,** *40* (20), 5267-5278.

38. Pikus, J. D.; Mitchell, K. H.; Studts, J. M.; McClay, K.; Steffan, R. J.; Fox, B. G., *Biochemistry* **2000,** *39* (4), 791-799.

39. Lipscomb, J. D., *Annu. Rev. Microbiol.* **1994,** *48* 371-399.

40. Valentine, A. M.; Tavares, P.; Pereira, A. S.; Davydov, R.; Krebs, C.; Hoffman, B. M.; Huynh, B. H.; Lippard, S. J., *J. Am. Chem. Soc.* **1998,** *120* (9), 2190-2191.

41. Tommos, C.; Skalicky, J. J.; L.Pilloud, D.; Wand, A. J.; Dutton, P. L., *Biochemistry* **1999,** *38* (29), 9495-9507.

42. Yagil, G., *Tetrahedron* **1967,** *23* (6), 2855-2861.

43. Aikens, J.; Sligar, S. G., *J. Am. Chem. Soc.* **1994,** *116* (3), 1143-1144.

44. Kohen, A., *Prog. React. Kinet. Mech.* **2003,** *28* 119–156.

45. Baldwin, J.; Voegtli, W. C.; Khidekel, N.; Moënne-Loccoz, P.; Krebs, C.; Pereira, A. S.; Ley, B. A.; Huynh, B. H.; Loehr, T. M.; Riggs-Gelasco, P. J.; Rosenzweig, A. C.; Bollinger, J. M., Jr., *J. Am. Chem. Soc.* **2001,** *123* (29), 7017-7030.

46. Parkin, S. E.; Chen, S.; Ley, B. A.; Mangravite, L.; Edmondson, D. E.; Huynh, B. H.; Bollinger, J. M., Jr., *Biochemistry* **1998,** *37* (4), 1124-1130.

47. Ormö, M.; deMaré, F.; Regnström, K.; Åberg, A.; Sahlin, M.; Ling, J.; Loehr, T. M.; Sanders-Loehr, J.; Sjöberg, B.-M., *J. Biol. Chem.* **1992,** *267* (13), 8711-8714.

48. McCormick, M. S.; Lippard, S. J., unpublished results.

49. Moe, L. A.; Hu, Z.; Deng, D.; Austin, R. N.; Groves, J. T.; Fox, B. G., *Biochemistry* **2004,** *43* (50), 15688-15701.

50. Gherman, B. F.; Baik, M.-H.; Lippard, S. J.; Friesner, R. A., *J. Am. Chem. Soc.* **2004,** *126* (9), 2978-2990.

51. Baldwin, J.; Krebs, C.; Saleh, L.; Stelling, M.; Huynh, B. H.; Bollinger, J. M., Jr.; Riggs-Gelasco, P. J., *Biochemistry* **2003,** *42* (45), 13269-13279.

52. Brunold, T. C.; Tamura, N.; Kitajima, N.; Moro-oka, Y.; Solomon, E. I., *J. Am. Chem. Soc.* **1998,** *120* (23), 5674-5690.

53. Nam, W.; Ryu, Y. O.; Song, W. J., *J. Biol. Inorg. Chem.* **2004,** *9* (6), 654-660.

54. Blazyk, J. L.; Gassner, G. T.; Lippard, S. J., *J. Am. Chem. Soc.* **2005,** *127* (49), 17364-17376.

55. Candeias, L. P.; Wardman, P.; Mason, R. P., *Biophys. Chem.* **1997,** *67* (1-3), 229-237 and references cited therein.

56. Dorovska-Taran, V.; Posthumus, M. A.; Boeren, S.; Boersma, M. G.; Teunis, C. J.; Rietjens, I. M. C. M.; Veeger, C., *Eur. J. Biochem.* **1998,** *253* (3), 659-668.

57. Seo, M. S.; In, J.-H.; Kim, S. O.; Oh, N. Y.; Hong, J.; Kim, J.; Que, L., Jr.; Nam, W., *Angew. Chem., Int. Ed.* **2004,** *43* (18), 2417-2420.

58. Jovanovic, S. V.; Steenken, S.; Simic, M. G., *J. Phys. Chem.* **1991,** *95* (2), 684-687.

59. Blanksby, S. J.; Ellison, G. B., *Acc. Chem. Res.* **2003,** *36* (4), 255-263.

60. Silva, G.; Chen, C.-C.; Bozzelli, J. W., *Chem. Phys. Lett.* **2006,** *424* (1-3), 42-45.

61. Whittington, D. A.; Sazinsky, M. H.; Lippard, S. J., *J. Am. Chem. Soc.* **2001,** *123* (8), 1794-1795.

CHAPTER 3

CHARACTERIZATION OF THE ARENE-OXIDIZING INTERMEDIATE IN ToMOH AS A DIIRON(III) SPECIES

CONTEXT

The observation of a diiron(III) intermediate during oxygenation of $ToMOH_{red}$ I100W with optical and Mössbauer parameters that differ from transients with the same oxidation state in other CBDI systems led to a reinvestigation of the wild-type hydroxylase. This same diiron(III) intermediate was observed in RFQ Mössbauer samples generated during reaction of the wild-type diiron(II) hydroxylase and ToMOD with dioxygen-saturated buffer. The decay rate of this species was slower than observed in ToMOH I100W and sensitive to phenol, reacting quantitatively with this substrate to produce catechol. Under steady-state conditions, hydrogen peroxide is generated if substrate is not present, and consumed in the absence of reducing equivalents. The Hammett relationship determined from the specific activities for hydroxylation of a variety of *p*-substituted phenols yielded values of $\rho < 0$, indicative of an electrophile attacking the substrate. The oxidation state and reactivity of the intermediate, and the evolution of hydrogen peroxide suggest that this species is a peroxo-bridged diiron(III) center where the binding geometry or protonation state of the $\{O_2^{2-}\}$ fragment differs from those previously characterized.

INTRODUCTION

Dioxygen activation at structurally homologous active sites in metalloproteins often leads to transient species having similar spectroscopic properties. For example, heme prosthetic groups bind dioxygen in their ferrous forms to generate η^1-peroxoiron(III) intermediates.[1,2] Protonation of the distal oxygen atom in this transient species facilitates O–O bond cleavage and formation of an (oxo)iron(IV)–porphyrin cation radical (Scheme 3.1). The reactivity of the heme iron unit is modulated by the proximal ligand trans to the O_2-binding site on the metal center and by the surrounding protein matrix, dictating dioxygen binding or activation depending on the requisite enzyme function. Similar phenomena occur for the non-heme carboxylate-bridged diiron (CBDI) protein superfamily, in which a reduced, diiron(II), form reacts with dioxygen (Scheme 3.1).[3,4] The

choice of non-bridging ligands at the dimetallic center, histidine versus aspartate or glutamate, and the availability of an open coordination site determine whether O_2 will bind reversibly or be activated for substrate oxidation. For dioxygen activation, the diiron(II) form of the protein typically reacts with dioxygen to form a peroxodiiron(III) center. In the hydroxylase component of methane monooxygenase, either homolytic[5] or heterolytic[6] cleavage of the O–O bond in this species occurs to yield a high-valent di(μ-oxo)diiron(IV) core, designated Q. In the R2 subunit of ribonucleotide reductase, the peroxo intermediate carries out a one-electron oxidation of W48 to form a mixed-valent diiron(III,IV) species, designated X.[7] The peroxodiiron(III) units in MMOH and RNR-R2 are the only ones in the CBDI enzyme superfamily that evolve to form iron(IV) intermediates.

Scheme 3.1. Dioxygen Activation at Iron-Heme and CBDI Centers

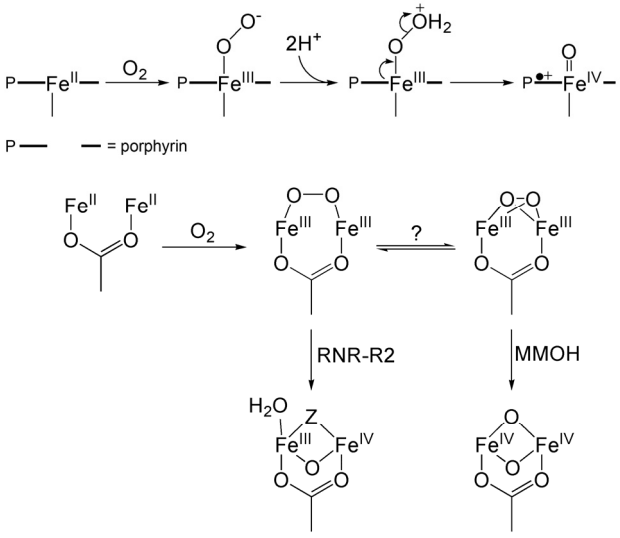

As noted in Chapters 1 and 2, the primary coordination spheres of stearyol-ACP Δ^9D desaturase,[8] rubrerythrin,[9] and ToMOH[10,11] bear a strong resemblance to those of MMOH and RNR-R2. No intermediates have previously been reported for reaction of the reduced forms of these enzymes with dioxygen. Addition of the substrate-carrier protein conjugate to reduced Δ^9D prior to reaction with dioxygen allowed such an intermediate to be generated, however, the Mössbauer, rR, and optical spectroscopic parameters of which are indicative of a μ-1,2-peroxodiiron(III) species.[12,13]

In Chapter 2, we described how the access of solvent or buffer components to the diiron center in ToMOH during dioxygen activation might be modified by occluding the substrate access channel in various variants. Reaction of $ToMOH_{red}$ I100W with O_2 led to formation of a transient mixed-valent diiron(III,IV)–$W^{\bullet}$ chromophore in this system that was characterized by various spectroscopic methods. Of particular interest was a diiron(III) intermediate, formed prior to the diiron(III,IV)–$W^{\bullet}$ species, having Mössbauer parameters and optical absorption features different from those of other peroxodiiron(III) transients.[4,14] Its isomer shift lies within the range of known peroxide-bridged synthetic diiron(III) complexes, but the quadrupole splitting differs by more than 0.3 mm/s.[14-16] No transient optical absorption band, other than that of the deprotonated tryptophanyl radical signal at 500 nm, were apparent during reaction of reduced ToMOH I100W and ToMOD with dioxygen.

We describe in the present chapter the results of experiments, including single- and double-mixing rapid-freeze quench Mössbauer studies, to determine whether this same diiron(III) species forms in native ToMOH. As will be demonstrated, such an intermediate does indeed accumulate over a relatively long time scale of 1 to 2 s, and reacts with substrate as examined by double-mixing methods in which the oxygenated species was first generated and then exposed to buffer containing phenol. To gain further insight into the nature of this intermediate, steady-state experiments were conducted to determine (i) whether hydrogen peroxide evolves during catalytic turnover; (ii) whether a peroxide shunt pathway to this species is accessible in this system; and (iii) the reactivity profile of the diiron(III) center in comparison to those of other CBDI enzymes and synthetic complexes. The results suggest that this intermediate contains a $\{O_2^{2-}\}$ fragment bound to a diiron(III) center, but with a previously unknown coordination geometry and/or protonation state.

EXPERIMENTAL METHODS

General Considerations. Plasmids containing the genes for the *Pseudomonas* sp. OX1 ToMO component proteins were kindly supplied by the laboratory of Professor Alberto Di Donato, Naples,

Italy. Expression and preparation of ToMOH and ToMOD were carried out as described elsewhere[10] with the following changes. For ^{57}Fe enrichment, ToMOH was expressed in media (10 g tryptone, 10 g NaCl, and 2 g Cassamino acids per liter of ddH_2O) supplemented with 40 μM $^{57}FeCl_3$. The solution of $^{57}FeCl_3$ was prepared by dissolving enriched metal powder (96.7% isotopic purity, Advanced Materials Technologies Ltd., Nes-Ziona, Israel) in concentrated hydrochloric acid. Ion exchange buffers contained $^{57}FeCl_3$ (150 μM) instead of Mohr's salt. Specific activities for phenol for the isolated components were greater than 1200 mU/mg. The iron content of the hydroxylase was 4.2 ± 0.3 Fe:H dimer as measured by the ferrozine assay.[17] HPLC experiments were performed with a Vydac protein & peptide C18 column connected to an Agilent 1200 series instrument equipped with a multi-wavelength detector. Instrumentation for optical and Mössbauer spectroscopy are as reported elsewhere.[18,19] All other reagents were purchased from Aldrich Chemical Company and used as received.

Rapid-Freeze Quench Sample Preparation for Mössbauer Spectroscopy. Samples of ^{57}Fe-enriched ToMOH and ToMOD were reduced and dialyzed as described in Chapter 2 and elsewhere.[18] For single-mixing rapid-freeze quench (RFQ) experiments, a solution of ToMOH:2ToMOD (690 μM) in 25 mM MOPS buffer, pH 7.0, was rapidly combined with an equal volume of O_2-saturated buffer at 4.0 °C. The oxygenated protein was allowed to react for a specific period of time, ranging from 34 ms to 15 min, after which the protein mixtures were quenched in isopentane at –140 °C. Samples were packed into Mössbauer sample cups and stored in liquid nitrogen. For double-mixing experiments, oxygenated buffer and the reduced protein solution (510 μM ToMOH, 1.02 mM ToMOD) were first mixed with an equal volume of O_2 saturated buffer and allowed to react for ~ 170 ms. This oxygenated protein solution was then mixed with a half volume of buffer containing phenol (4.6 mM in 25 mM MOPS buffer, pH 7.0), aged for times varying from 25 ms to 30 min, and quenched in isopentane at -140 °C. A sample of the 0.17-s aged oxygenated

protein without phenol was collected as a reference. The dilution factors for single- and double-mixing samples were two and three, respectively. The product of phenol oxidation was determined and quantified in double-mixing RFQ Mössbauer samples, for which the oxygenated protein was allowed to react with substrate for at least 5 s in the following manner. Ascorbic acid (20 μL, 22 mM in ddH_2O) was added to an aliquot (50 μL) of a thawed Mössbauer sample. This mixture was allowed to stand for 5 min, after which TFA (30 μL, 50% in ddH_2O) was added. Samples were centrifuged and the supernatant was loaded onto a Vydac column. HPLC conditions for separation of hydroxylated products from phenol were 0% buffer B for 7 min, 0% to 40% B for 1 min (linear gradient), 40% to 100% for 7 min (linear gradient), and 100% B for 3 min (A: 1% acetonitrile, 98.8% ddH2O, 0.2% TFA; B: 49.9% acetonitrile, 49.9% ddH2O, 0.2% TFA). Absorption at 280 nm was monitored with time for all samples. Retention times for catechol, resorcinol, and hydroquinone were determined under these conditions. Mössbauer measurements were carried out at 4.2 K with an applied magnetic field parallel to the γ-irradiation using spectrometers described previously.[19] Analysis of the Mössbauer spectra were performed with the program WMOSS (WEB Research). The zero velocity refers to the centroid of a room-temperature spectrum of a metallic Fe foil.

Assay for Hydrogen Peroxide Release in the Steady-State. A colorimetric assay employing potassium thiocyanate and ferrous ammonium sulfate was used to detect hydrogen peroxide.[20] Each reaction solution contained 1 μM ToMOH, 2 μM ToMOC, 4 μM ToMOD, 0.1 μM ToMOF, and 1 mM NADH in 500 μL of Tris/HCl buffer, pH 7.5, at 25 °C. In samples containing phenol as a substrate, the concentration was 4 mM. Reactions were initiated by addition of NADH, quenched after a specified reaction time with 100 μL of 0.4 M trichloroacetic acid, and centrifuged at 13,500 × *g* for 5 min. After centrifugation, aliquots of solutions of potassium thiocyanate (100 μL, 2.5 M) and ferrous ammonium sulfate (200 μL, 10 mM) in ddH_2O were added to the supernatant (500 μL). The mixture was shaken vigorously and allowed to stand for 5 min before the absorbance at 480 nm was

measured. Solutions of hydrogen peroxide were standardized by measuring the absorbance at 240 nm.[21] These solutions were treated as described for the enzyme reaction mixtures to generate a standard curve. The consumption of NADH to liberate hydrogen peroxide was determined by monitoring the absorbance decrease at 340 nm, which corresponds to the depletion of NADH (ε_{340} = 6220 $M^{-1}cm^{-1}$), for 5 min, quenching the reaction, and measuring the concentration of hydrogen peroxide present. To monitor the absorbance change at 340 nm, the initial NADH concentration in the assay solution was reduced from 1 mM to 0.2 mM.

An Attempt to Initiate Catalysis by a Peroxide Shunt Pathway. HPLC analysis of reaction mixtures was conducted following steady-state experiments as above in which NADH and ToMOF were omitted and hydrogen peroxide was added as a reduced dioxygen source. Assay mixtures (0.5 mL) contained 15 μM ToMOH, 30 μM ToMOC, 40 μM ToMOD, 20 mM hydrogen peroxide, and 2 mM phenol in 0.1 M Tris/HCl buffer, pH 7.5. ToMOH was the last component added to each mixture. These solutions were stirred and allowed to react at 25 °C for specified times ranging from 30 s to 12 min. Samples were quenched with 100 μL of 0.4 M trichloroacetic acid, centrifuged, and loaded onto the HPLC column as described above. A series of experiments was also performed in which the concentrations of hydrogen peroxide produced were assayed as outlined above except that, prior to measuring the absorbance, the sample was diluted 15-fold with ddH_2O. Solutions of hydrogen peroxide, which were standardized by measuring the absorbance at 240 nm, were used to calibrate HPLC peak integrals. Dioxygen release from reaction mixtures containing ToMOH and ToMOD was assayed by the alkaline pyrogallol method.[22] Anaerobic assay mixtures for O_2 generation contained 100 μM ToMOH and 400 μM ToMOD in 200 μL of 25 mM MOPS, pH 7.5, to which hydrogen peroxide (0.6 mL, 30% solution) was added. Control samples were also prepared in which the protein solution or hydrogen peroxide was substituted with buffer.

Hammett Studies. The steady-state activity of ToMOH using as substrates the following *para*-substituted phenols, cresol, phenol, fluorophenol, chlorophenol, and nitrophenol, were determined by

directly quantifying the catechol products by the HPLC protocol described above. Assay mixtures comprising 0.3 μM ToMOH, 15 μM ToMOD, 2 μM ToMOC, 40 nM ToMOF, and 1 mM substrate in 0.1 M Tris/HCl, pH 7.5, were incubated at 25 °C. Steady-state turnover was initiated by addition of NADH to a final concentration of 1 mM. Aliquots (100 μL) were removed at 10-s intervals, quenched with TFA (10 μL), vortexed for 5 s, and centrifuged at 5000 rpm for 5 min to pellet the denatured protein. Each aliquot was then frozen in liquid nitrogen and stored at -78 °C. For *p*-chloro and *p*-nitrophenol, samples were taken at 30-s instead of 10-s intervals. The supernatant was analyzed by HPLC as mentioned previously. The absorbance was monitored at 280 nm for all substrates except for nitrophenol, the samples of which were monitored at 465 nm. Standard curves were generated for catechol products with the appropriate substituent in the 4-position. 4-Fluorocatechol was synthesized according to a literature procedure[23] and characterized by ^{1}H-NMR spectroscopy. The solid catechols were vacuum-sublimed and stored in the dark prior to use.

RESULTS

Formation of a Diiron(III) Intermediate by Oxygenation of ToMOH$_{red}$. Because the diiron(III) intermediate identified in the ToMOH I100W variant is diamagnetic and exhibits no apparent optical absorption bands (Chapter 2), Mössbauer spectroscopy was used to seek spectroscopic evidence for the possible accumulation of this same diiron(III) intermediate in the reaction of reduced wild-type ToMOH with dioxygen. The reaction was freeze-quenched at various reaction times (0.07 s, 0.14 s, 0.44 s, 2 s, and 32 s) by the RFQ method (Experimental Methods) and the resulting samples were characterized by Mössbauer spectroscopy. Figure 3.1 displays the 4.2-K Mössbauer spectrum of the diiron(II) ToMOH before reaction with O_2 (A). Also presented are spectra of several freeze-quenched samples (B-D) that clearly reveal the sequence of events that occur during the reaction. By comparison with the spectrum of the reduced ToMOH reactant (A), the

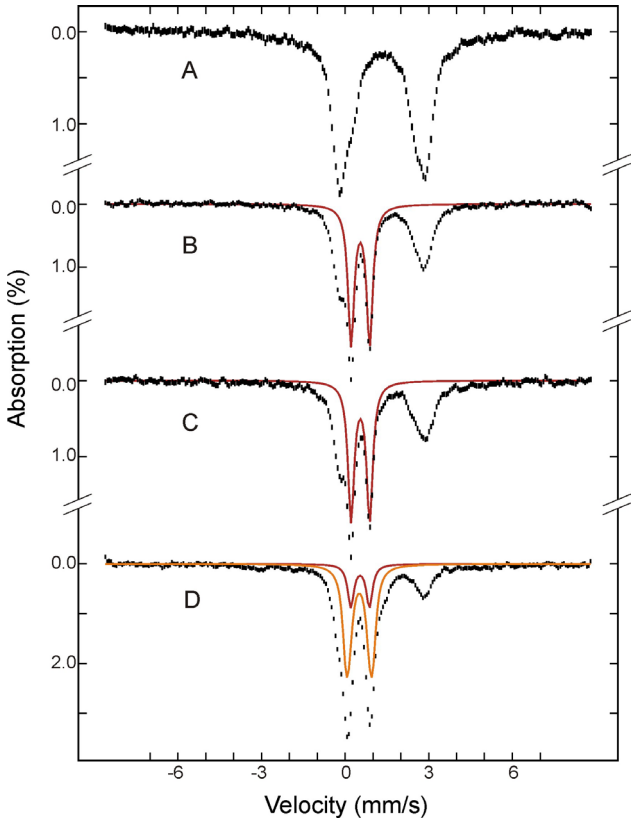

Figure 3.1. Mössbauer spectra of freeze-quenched samples from the reaction of reduced ToMOH:2ToMOD mixtures with O_2. The samples were frozen before mixing (A) and 0.14 s (B), 2 s (C), and 32 s (D) after mixing. The spectra (vertical bars) are collected at 4.2 K in a 50 mT field applied parallel to the γ-ray beam. The red and orange lines are simulated spectra of the diiron(III) intermediate and diiron(III) product, respectively. The spectrum of the diiron(III) intermediate (red) was modeled with a single quadrupole doublet with $\delta = 0.55$ mm/s, $\Delta E_Q = 0.67$ mm/s and line width = 0.27 mm/s. The spectrum of the diiron(III) product (orange) was simulated as a superposition of two equal intensity quadrupole doublets with parameters $\delta = 0.52$ mm/s, $\Delta E_Q = 0.73$ mm/s and line width = 0.32 for doublet 1 and $\delta = 0.52$ mm/s, $\Delta E_Q = 0.97$ mm/s and line width = 0.28 mm/s for doublet 2. They are plotted at the following absorption intensities: red, 44%, 41% and 13% in B, C, and D; orange, 41% in D. Unreacted diiron(II) protein accounts for ~ 56% of total Fe absorption at maximal accumulation of the intermediate (B). These parameters and intensities are the results of a global analysis of the entire set of the Mössbauer spectra including those that are not depicted here.

spectrum of a sample freeze-quenched at 0.14 s reaction time (B) shows ~ 45% reduction in intensity of the quadrupole doublet arising from the reduced, diiron(II) ToMOH and the appearance of a sharp quadrupole doublet (red line in B) with parameters ($\delta = 0.55 \pm 0.02$ mm/s, $\Delta E_Q = 0.67 \pm 0.03$ mm/s, and line width = 0.27 mm/s) that are identical to those of the diiron(III) intermediate observed in ToMOH I100W. A high-field experiment confirms that this doublet arises from a diamagnetic system (Figure 3.2). These observations establish that the diiron(II) sites in wild-type ToMOH indeed react rapidly with O_2 to generate a diiron(III) intermediate that reported in Chapter 2.

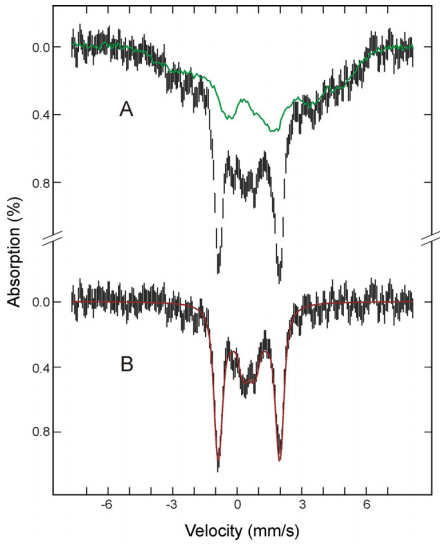

Figure 3.2 High-field Mössbauer spectrum (vertical bars in A) of a freeze-quench sample from the reaction of reduced ToMOH:2ToMOD with O_2 frozen at 0.14 s after mixing the reduced protein with O_2. The spectrum was collected at 4.2 K in an applied field of 8 T parallel to the □-beam. The green line in A is the spectrum of the diiron(II) protein before mixing recorded under the same experimental conditions, and is plotted at 56% of the total Fe absorption of the freeze-quenched sample. Removal of the diiron(II) contribution from spectrum A yields spectrum B (vertical bars). The red line in B is a theoretical spectrum of the diiron(III) intermediate simulated with parameters determined at low field (see caption of Figure 1) and assuming diamagnetism. The excellent agreement between theory and experiment indicate the ground state of the diiron(III) intermediate is diamagnetic, revealing antiferromagnetic coupling between the two ferric ions.

Accumulation of this intermediate reaches a maximum corresponding to 44% of the total Fe absorption and remains unchanged for several seconds (compare spectra B and C) before decaying directly to the diiron(III) product (orange line in D). No other intermediates were detected.

Kinetics of the Reaction of $ToMOH_{red}$ with O_2. To obtain a quantitative estimate of the time evolution of Fe species generated during the oxidation of reduced ToMOH, it is necessary to deconvolute the Mössbauer spectra into various spectral components corresponding to the different Fe species. Although δ values for the diiron(III) intermediate (0.55 mm/s) and product (0.52 mm/s) are similar, different ΔE_Q values for the intermediate (0.67 mm/s) and product (0.85 mm/s) allow the spectra of these two species to be readily deconvoluted (Figure 3.3). A global analysis of the entire set of the Mössbauer spectra, including those for time points not depicted, yields the characteristic

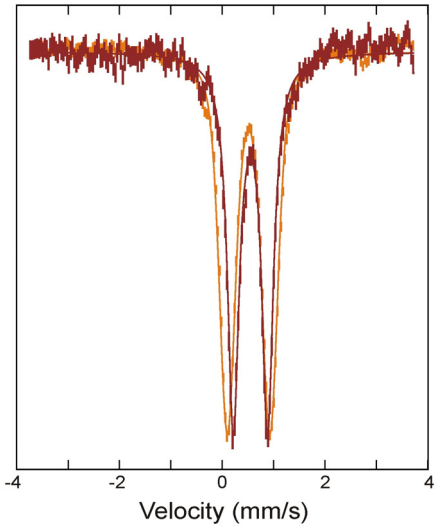

Figure 3.3. Overlay of Mössbauer spectra of the diiron(III) intermediate (red) and product (orange). The spectrum for the intermediate (red vertical bars) was prepared by removing the 56% diiron(II) contribution from the raw spectrum of the 0.14 s freeze-quenched sample (Figure 3.1B), and the product spectrum (orange vertical bars) was the spectrum of as-purified oxidized ToMOH. For comparison the two spectra are scaled to matching intensities. The solid lines are theoretical spectra simulated with parameters of the Fe species reported in the caption of Figure 3.1.

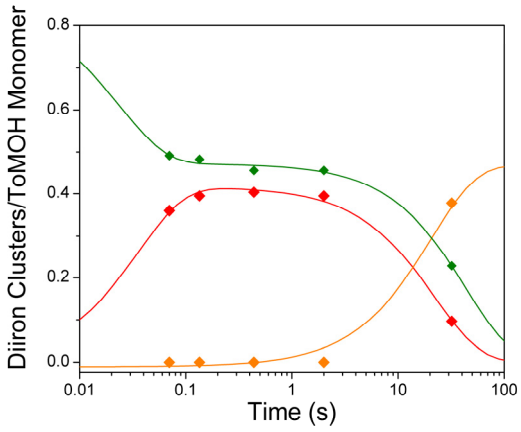

Figure 3.4. Speciation plot for reaction of diiron(II) ToMOH:2ToMOD with dioxygen. Reduced diiron(II) protein (♦) reacts with dioxygen at ~ 26 s^{-1} to form a diiron(III) transient species (♦). Only ~45% of diiron(II) clusters give rise to this intermediate. The diiron(III) transient subsequently decays to the oxidized resting state (♦) at ~ 0.045 s^{-1}. The unreacted diiron(II) centers decay slowly at 0.02 s^{-1}. Solid lines are one- or two-exponential fits to the data.

parameters reported above as well as percentages of Fe absorption for the species detected in the freeze-quenched samples. On the bases of the Fe and protein contents determined for the freeze-quenched samples, 3.5 Fe atoms/ToMOH dimer, these percentages can be converted into amounts of diiron clusters per ToMOH monomer. The results are presented in Figure 3.4 (diamonds). Analysis of these data indicate that the diiron(III) intermediate (red diamonds) forms rapidly with a rate constant of ~ 26 s^{-1} and accumulates to a maximum of 0.4 clusters/ToMOH monomer (or 0.8 clusters/dimer). It decays slowly at a rate of 0.045 s^{-1} to generate the diiron(III) product (orange diamonds). Data for the reduced ToMOH (green diamonds) reveal two populations for the diiron(II) sites that are differentiable by their rates of reaction with dioxygen. One population (0.4 clusters/ToMOH monomer) reacts rapidly (26 s^{-1}) to form the diiron(III) intermediate, while the remaining diiron(II) sites react slowly at a rate of ~ 0.02 s^{-1}.

Effect of Phenol on Decay of the Diiron(III) Intermediate. The reactivity of the diiron(III) intermediate with phenol as a substrate was probed by using the double-mixing RFQ technique and Mössbauer spectroscopy. Reduced ToMOH was allowed to react with O_2 for 0.17 s to afford a maximum accumulation of the diiron(III) intermediate prior to the introduction of the substrate phenol. The oxygenated protein mixture was then mixed with a buffer solution containing phenol. The reaction was allowed to proceed for various times and then quenched at -140 °C (Experimental Methods). Samples were collected for Mössbauer investigations. The resulting Mössbauer spectra for a few of these time points are presented in Figure 3.5. As in the single-mixing experiments, the spectrum of the 0.17-s aged oxygenated protein shows that ~ 40% of the diiron(II) sites evolve to the diiron(III) intermediate (Figure 3.5, spectrum A, red line). After mixing with phenol, the quadrupole doublet corresponding to this species decreases its intensity almost immediately and becomes nearly undetectable at 5 s (Figure 3.5, B-D, red lines). This behavior is in stark contrast to the relatively stable accumulation of this species observed in the absence of phenol. In addition, the diiron(III) product is detected almost immediately after mixing with phenol and grows into a dominant species at 5 s (Figure 3.5, B-D, orange lines). The unreacted diiron(II) protein, however, remains relatively stable (compare the absorption peak at 3 mm/s in spectra A to D) and starts to decay several seconds after mixing with phenol, behavior similar to that observed in the absence of phenol. As in the single mixing study, a global analysis to deconvolute the entire set of spectra into spectral components was performed and kinetic data for the Fe species generated after mixing with phenol were thereby obtained. The data are depicted in Figure 3.6 (diamonds) together with results of kinetic modeling of the formation and decay of the diiron species (color lines). The decay rate of the diiron(III) intermediate increases by more than 40-fold, from 0.045 s^{-1} to 2.0 s^{-1}, in the presence of phenol. Because the amount of unreacted diiron(II) sites remains constant during the decay phase of this transient, the decay of the diiron(III) intermediate (Figure 3.6, red line) parallels the early formation of the diiron(III) product (Figure 3.6, orange line), both in rate constant (2.0 s^{-1}) and in the extent of

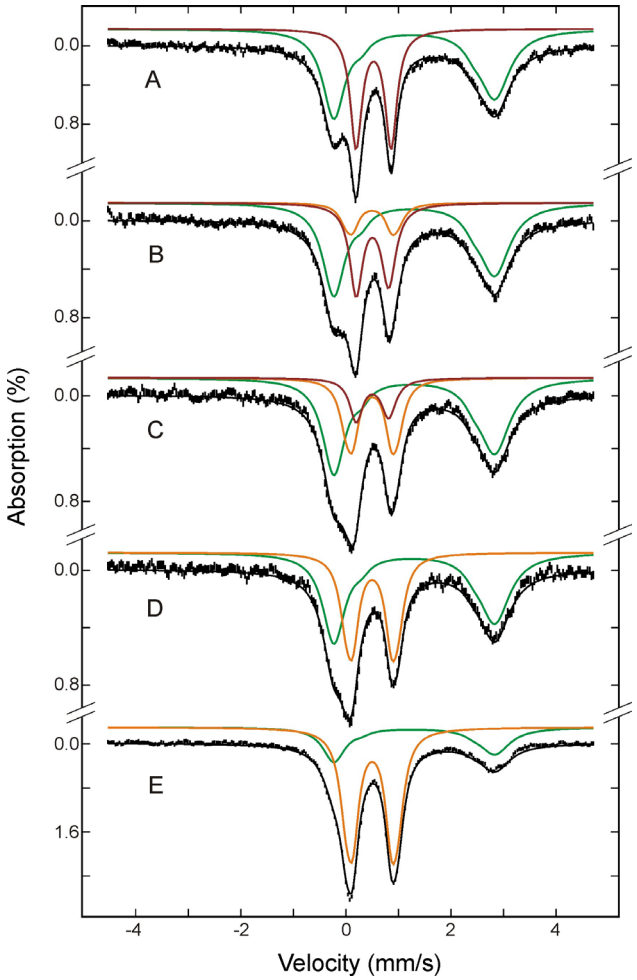

Figure 3.5. Mössbauer spectra of double-mixing RFQ samples for reaction of the diiron(III) intermediate with buffer containing phenol. Reduced protein was allowed to react with O_2 for 0.17 s to generate the intermediate before mixing with phenol (A). After mixing with phenol, the reaction mixture was freeze-quenched at 0.14 s (B), 0.67 s (C), 5 s (D) and 100 s (E). The spectra (vertical bars) are collected at 4.2 K in a 50 mT applied field parallel to the γ-ray beam. The green, red and orange lines are simulated spectra, respectively, of the unreacted diiron(II) protein, diiron(III) intermediate and diiron(III) product. The spectra of the diiron(III) intermediate in the absence of phenol (red in A) and diiron(III) product (orange) were simulated using the parameters reported in the caption of Figure 3.1. The spectrum of the diiron(III) intermediate was perturbed slightly by the presence of phenol (see the following Figure 3.6) and was simulated with the altered parameters reported in text (red lines in B-E). The spectrum of the unreacted diiron(II) was modeled as a superposition of two quadrupole doublets with an intensity ratio of 10 to 1, and the following parameters: δ = 1.32 mm/s, ΔE_Q = 3.06 mm/s for the intense doublet, and δ = 1.39 mm/s and ΔE_Q = 2.13 mm/s for the minor doublet. The simulated spectra are plotted at the following absorption intensities: green, 61%, 60%, 58%, 57% and 29%; red, 39%, 30%, 14%, 0% and 0%; orange, 0%, 12%, 28%, 43% and 71% in A, B, C, D and E, respectively. The black lines overlaid with the spectra are composite spectra including all the Fe species mentioned above.

accumulation (0.4 clusters/ToMOH monomer). Decay of the unreacted diiron(II) species, with a rate constant of ~0.01 s^{-1}, accounts for the second phase of production of the diiron(III) product. No other intermediate was detected. Mössbauer parameters of the diiron(III) intermediate differ in the

presence and absence of phenol (Figure 3.7); in the presence of phenol, this species was modeled by a quadrupole doublet with parameters (δ = 0.52 ± 0.02 mm/s and ΔE_Q = 0.62 ± 0.03 mm/s) that are slightly different from those (δ = 0.55 mm/s and ΔE_Q = 0.67 mm/s) observed in the absence of this substrate. Also, the absorption lines of this doublet are broader by 0.03 mm/s and 0.06 mm/s for the low-energy and high-energy line, respectively, in samples containing phenol (Figure 3.7). These differences, although minor, suggest that phenol perturbs the diiron center of the intermediate prior to reacting with it.

The acceleration of the decay rate of the diiron(III) transient by phenol provides strong evidence that this species is responsible for the substrate oxidation. Indeed, catechol was detected and determined by HPLC analyses to be the only observed aromatic product in the double-mixing samples at reaction times equal to and longer than 5 s. The concentration of this hydroxylation product in the samples was 145 ± 1 μM, in good agreement with the estimated intermediate

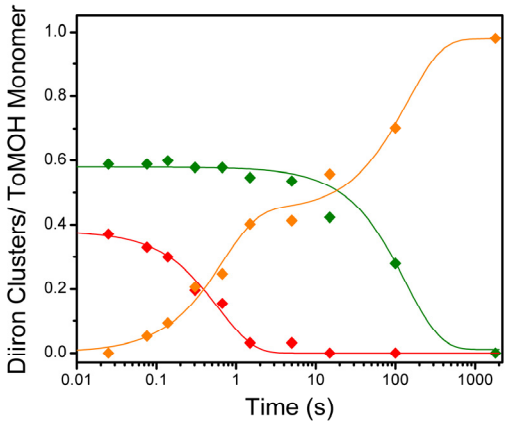

Figure 3.6. Speciation plot for reaction of the diiron(III) intermediate with phenol. The intermediate (♦) decays at 2 s^{-1} to give rise to the early formation phase of diiron(III) product (♦). Diiron(II) clusters (♦) that do not traverse the intermediate oxidize more slowly, with a rate constant of ~ 0.01 s^{-1} to product. Solid lines represent one- or two-exponential fits to the data.

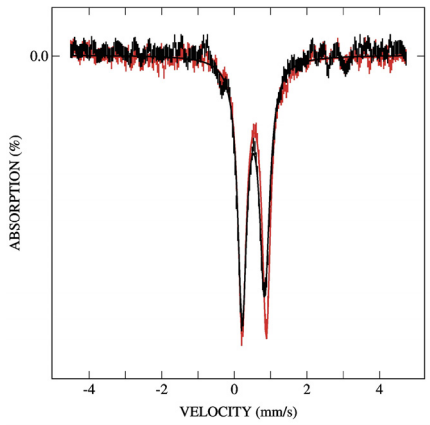

Figure 3.7. Overlay of Mössbauer spectra of the diiron(III) intermediate in the absence (red) and presence (black) of phenol. These spectra were prepared by removing the unreacted diiron(II) contributions from the spectrum shown in Figure 3.5A and spectrum of a sample freeze-quenched at 70 ms after mixing with phenol. Addition of phenol results in smaller values for δ and ΔE_Q as compared to the intermediate generated in the absence of substrate (see text for parameters). Absorption lines also broaden in the presence of phenol by 0.03 and 0.06 mm/s, for low- and high-energy lines, respectively.

concentration, ~ 135 μM, accumulated before mixing with phenol. The intermediate concentration was estimated from the result of the Mössbauer analysis (40% Fe absorption for the intermediate before mixing with phenol) and protein and Fe contents determined for the double mixing samples (170 μM protein and 3.92 Fe/ToMOH dimer). A broad optical absorption band centered at 580 nm, consistent with that of an iron-catecholate charge transfer transition, was observed in optical spectra of samples prepared by double-mixing (Figure 3.8). Coordination of catechol to the diiron center, however, appears to cause only minor perturbations to the diiron site, since the Mössbauer spectrum of the final product, the oxidized protein (Figure 3.5E, orange line), could be simulated with quadrupole doublets identical to those used to model the Mössbauer absorption of the as-purified diiron(III) ToMOH (Figure 3.3, orange spectrum).

Release of Hydrogen Peroxide by ToMO under Steady-State Conditions. Under steady-state conditions, hydrogen peroxide was evolved in the absence of phenol (Figure 3.9). Its rate of formation could be modeled with a hyperbolic function, suggesting that the enzyme system may be inactivated in the presence of hydrogen peroxide, as reported for phenol hydroxylase from *Pseudomonas* sp. CF600.[24] The efficiency of the NADH oxidase reaction, defined as the ratio of the decrease in NADH concentration to the increase in hydrogen peroxide concentration, was 51(4)%.

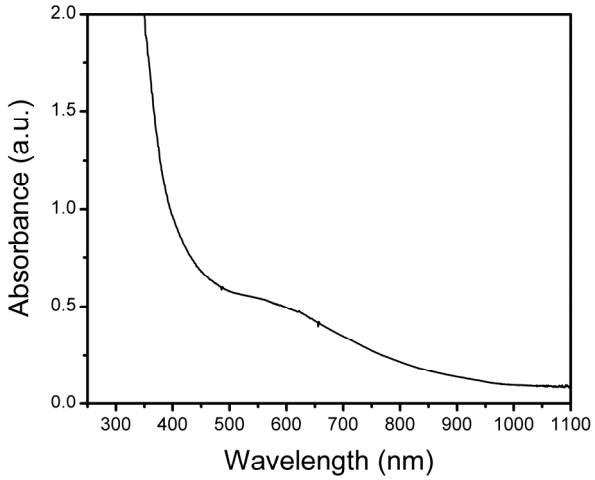

Figure 3.8. Optical spectrum of a sample following an RFQ double-mixing Mössbauer experiment. The broad absorption band is centered at ~ 580 nm.

Addition of substrate to the reaction mixture retarded peroxide formation, implying that phenol reacts either with a peroxodiiron(III) center or a precursor of such a transient.

Peroxide Shunt Pathway and Catalase Activity of ToMOH$_{ox}$. Hydroxylation products were not detected in samples containing hydrogen peroxide, ToMOH$_{ox}$, ToMOD, and ToMOC. Inclusion of ToMOC in the reaction mixtures was to assure that protein component interactions would not affect our inability to access a peroxide shunt pathway. We noticed during the course of the experiments that hydrogen peroxide was rapidly consumed. Its concentration was monitored in acid-quenched samples by integrating the peak eluting at ~ 3.3 min in HPLC traces recorded at 240 nm (Figure 3.10) and by the colorimetric method used to assay for hydrogen peroxide release. Samples in which the hydroxylase was omitted showed no appreciable decrease in H_2O_2 concentration.

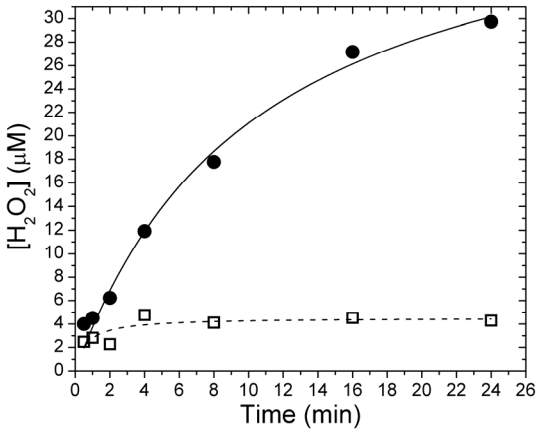

Figure 3.9. Concentration of hydrogen peroxide evolved under steady-state conditions with (□) and without (•) phenol. Hydrogen peroxide is formed slowly as NADH is consumed by the enzyme system. The addition of substrate inhibits peroxide formation. Data were fit with hyperbolic functions.

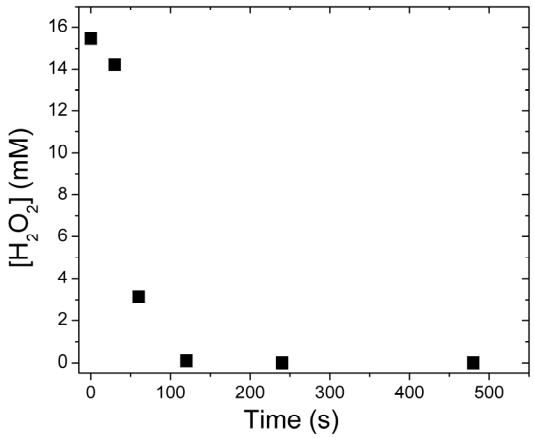

Figure 3.10. Change in the concentration of hydrogen peroxide with time after mixing with ToMOH–ToMOD mixtures. Hydrogen peroxide is rapidly consumed and evolved dioxygen in a manner independent of the presence of substrate. A peroxide shunt pathway was not accessed because catechol was not observed in assay solutions that contained phenol.

Experiments utilizing only ToMOH$_{ox}$ and ToMOD revealed that dioxygen was rapidly evolved upon addition of aliquots of hydrogen peroxide. The evolved gas from these reaction mixtures oxidized the pale pink solution of alkaline pyrogallol to a brown color. Addition of hydrogen peroxide to vials containing buffer, or addition of buffer to protein solutions, did not result in

oxidation of pyrogallol.

Hammett Relationship for Substrate Oxidation by ToMO. Initial reaction rates were used to generate Hammett plots for the oxidation of phenolic substrates by ToMO (Figure 3.11). Plots of the substituent constants σ_m and σ_p^+ against the logarithm of the ratio of the initial rates for the substituted phenols and phenol were fit with a linear equation. Reaction constants, ρ, of -1.3 and -1.7 for σ_m and σ_p^+ were determined for this system, consistent with electrophilic attack on the aromatic substrate. The rate data were plotted against two substituent constants because of the hydroxylation mechanism proposed for the homologous T4MO system. In that system, NIH shift experiments suggested that the substrate is attacked either at the site of oxidation (σ_m), to yield a substrate cation,

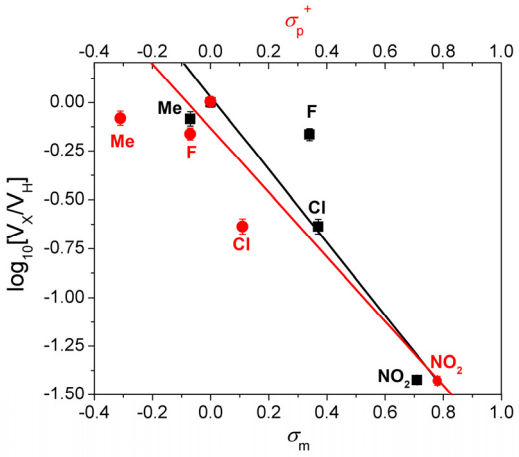

Figure 3.11. Hammett plots for oxidation of *p*-substituted phenols by ToMO. The values of ρ were -1.3 and -1.7 for σ_m (■) and σ^+ (●) respectively. A negative reaction constant is indicative of electrophilic reactions. The goodness of fit as measured by R^2 for either σ value is 0.81.

Scheme 3.2. Proposed Pathways for Substrate Hydroxylation

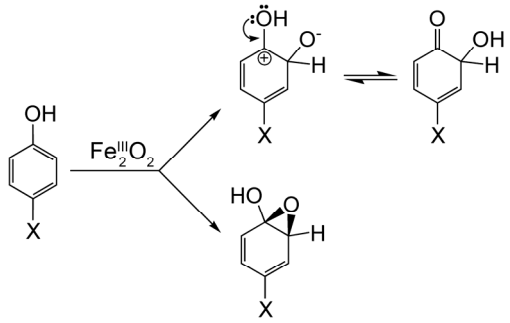

or at the *para* and *meta* positions (σ_p^+), to form a transient arene epoxide (Scheme 3.2). There is appreciable scatter in the plots, however, with $R^2 \sim 0.81$ in both cases. Scaling the initial reaction velocities to account for the percentage of deprotonated substrate does not significantly improve the quality of the fit.

DISCUSSION

Mechanism of Dioxygen Activation by ToMOH. The reduced diiron(II) forms of the CBDI enzymes are reactive toward dioxygen, activating the molecule to yield intermediates with Fe–O bonds that react with substrates.[3,12,25-28] The first intermediate observed spectroscopically in the systems characterized thus far is a peroxodiiron(III) adduct, with well-defined spectroscopic parameters, including a near-IR optical absorption band.[4] Despite the structural homology of the active sites of ToMOH and MMOH,[10] the first intermediate observed upon oxygenation of $ToMOH_{red}$ is a diiron(III) transient for which no such absorption feature could be detected. The Mössbauer spectroscopic parameters, δ and ΔE_Q, for this intermediate are 0.55 and 0.67 mm/s, respectively, which are both lower than those of peroxodiiron(III) centers in related enzymes and model complexes. Despite the spectroscopic differences, we tentatively assign the diiron(III) transient formed after oxygenation of reduced ToMOH as a peroxodiiron(III) center. This assignment is based on the following observations: (i) the reactivity of the transient is similar to that reported for peroxodiiron(III) intermediates in other systems and requires that the regulatory protein ToMOD be present in order to form; (ii) hydrogen peroxide is liberated during steady-state turnover in the absence of substrate; and (iii) by analogy to dioxygen activation in other CBDI systems, in which the diiron(III) intermediates are all peroxo species. The observed spectroscopic differences from peroxo intermediates in other systems may arise from a weak or red-shifted absorption band in the optical spectrum, photodecomposition, additional ligands coordinated to the diiron center, or an alternative geometry or protonation state of the peroxide moiety.

The $\{O_2^{2-}\}$ fragments in the peroxodiiron(III) intermediates in RNR-R2,[29,30] Δ^9D,[12] and Ft[31,32] are proposed to bind in a *cis*-μ-1,2- fashion and that in MMOH has alternatively been given the same assignment[33-35] or that of a μ–η^2,η^2 side-on peroxide.[5,27,36] In the former geometry, the out-of-plane and in-plane π^* dioxygen orbitals interact with d_{yz} and d_z^2 orbitals, respectively, on the iron atoms. The out-of-plane orbitals form π–bonds and the in-plane orbital gives rise to σ–bonds between peroxide and the dimetallic unit. In the case of iron(III), π-bonding dominates the interaction because the metal orbitals are half-filled.[37] The characteristic low energy absorption feature centered at ~700 nm in μ-1,2-peroxodiiron(III) species arises from π_π* to d_{yz} transitions, according to one formalism.[37] The strength of this π–bonding interaction dictates therefore the energy and intensity of this transition as well as the O–O bond strength. In systems where high-valent oxygenated diiron species are observed, π–bonding is proposed to dominate the interaction between the $\{O_2^{2-}\}$ fragment and the diiron center because cleavage of the consequent weaker O–O is more facile. The extinction coefficients for the peroxodiiron(III) intermediate in MMOH, RNR-R2, Δ^9D, and Ft follow the expected trend therefore, with those reported for this transient in RNR-R2 and MMOH being greater than those for the same species in Δ^9D and Ft. If π-bonding in the ToMOH intermediate is weak, the energy and intensity of this charge transfer are predicted to decrease. The absorption maximum will therefore be red-shifted, with a smaller extinction coefficient than that of similar diiron(III) species. Weaker π-bonding would favor peroxide release, disfavor formation of high-valent intermediates, and reduce the electron density on the iron atoms. The Mössbauer parameters are indicators of the symmetry of the electric field gradient around (ΔE_Q), and effective charge or oxidation state (δ) of, the iron atoms. Reducing the electron density therefore should lower δ relative to systems with stronger π-bonds. Longer Fe–O bonds may increase the symmetry, translating into a smaller ΔE_Q values. The Fe–O–O bond angle, which determines in part the Fe–Fe distance, strongly influences the π-bonding contribution from the peroxide fragment, with smaller angles favoring σ-only

bonding. If the absorption band is therefore weak and low in energy in $ToMOH_{peroxo}$, we predict that the Fe–Fe distance in this intermediate will be shorter than that observed in peroxo-adducts of other CBDI systems.

Another possibility is that the peroxodiiron(III) species might decompose upon irradiation, as reported previously for a *cis*-μ-1,2-peroxodiiron(III) complex[37] and for the superoxodiiron(III) intermediate in *myo*-inositol oxygenase.[25] Reaction of reduced ToMOH I100W and ToMOD with dioxygen quantitatively converts the diiron(III) intermediate to the mixed-valent diiron(III,IV)–$W^{\bullet}$ couple (Chapter 2). The calculated extinction coefficient at 500 nm of the radical agrees with the accumulation of $ToMOH_{peroxo}$, judging by Mössbauer spectroscopy. The photodecomposition rate of the diiron(III) transient, therefore, must slower than ~ 1 s^{-1} to permit quantitative formation of the diiron(III,IV)–$W^{\bullet}$ species. Given an estimated formation rate constant of 25 s^{-1} for this intermediate from Mössbauer studies, we predict that this transient should accumulate to adequate levels to permit detection of any optical features. We can therefore exclude photodecomposition as an explanation for the lack of an optical absorption band.

The nature, number, and protonation state of the bridging ligands in dioxygen adducts of CBDI model complexes influence the spectroscopic features of the characterized *cis*-μ-1,2-peroxodiiron(III) intermediates. Model compounds with oxo,[38,39] hydroxo,[39] or alkoxo[15,16,40,41] bridges opposite the bound peroxide have absorption maxima, extinction coefficients, and Mössbauer parameters that cover a broad range of values (Table 1).[14-16,39,42] A number of these compounds have values for δ within range of the present 0.52 mm/s value, although all the ΔE_Q parameters are ~ 1.0 mm/s. Amino acid side chains in the active site pocket of ToMOH, such as E243, which shifts between the Mn(II)-reconstituted and diiron(III) forms,[10,11] could be incorporated as additional oxygen atom bridges, thereby modulating the absorption and Mössbauer spectra of $ToMOH_{peroxo}$. Any absorption band arising from this intermediate would either have to be obscured by end absorption from the protein optical band at 280 nm or lie in the near-IR region, beyond the range of

our diode array instrument detector.

Table 3.1. Mössbauer and Optical Spectroscopic Parameters for μ-1,2-Peroxodiiron(III) Complexes

Donor Set	Bridging Ligands	λ_{max} [nm]	ε [$M^{-1}cm^{-1}$]	δ [mm/s]	ΔE_Q [mm/s]	Ref.
N_3O_3	hydroxo	644	3000	0.50	1.31	39
N_3O_3	oxo	577	1500	0.50	1.46	39
N_3O_3[a]	alkoxo carboxylato	665	2300	0.57	1.44	15
N_3O_3[a]	alkoxo carboxylato	710	1500	0.58	1.17	15
N_3O_3	alkoxo carboxylato	500 – 800	1700	0.65 0.58	1.70 0.70	14
N_3O_3	dicarboxylato	694	2650	0.66	1.40	16
N_4O_2*	oxo	494, 648, 846	1100, 1200, 230	0.54	1.68	42

[a]These compounds were characterized by Mössbauer and optical spectroscopy only.

Finally, the geometry or protonation state of the peroxide fragment in $ToMOH_{peroxo}$ may differ from those of other μ-1,2-peroxodiiron(III) intermediates. Diiron(III) centers containing 1,1-peroxo-, 1,1-hydroperoxo-, or $\eta^1:\eta^2$-peroxo bridges have all been proposed for transition states linking the reduced diiron(II) forms to diiron(III) and high-valent intermediates in MMOH and RNR-R2.[5,36,37,43] If the intermediate is protonated, such proton transfers could not be rate-determining within the limits of RFQ methods because we find no solvent kinetic isotope effect for either its formation or decay in single-mixing Mössbauer studies.[44] Hydroperoxy intermediates in cytochromes P450 and heme iron synthetic complexes are proposed to be electrophilic oxidants, reacting with electron-rich substrates.[45] $MMOH_{peroxo}$ and the peroxo intermediate in RNR-R2 are also capable of oxidizing electron-rich substrates, such as aromatic side chain residues,[26,46] alkenes,[28] and ethers.[27] The reactivity profile of the intermediate reported here is similar to those of hydroperoxoiron(III) species in heme systems, $MMOH_{peroxo}$, and the peroxo intermediate in RNR-R2. ToMOH can epoxidize or hydroxylate halogenated alkenes and a number of aromatic compounds, preferring electron-rich substrates over poorer ones.[47,48] A preliminary cryoreduction study of the ToMOH intermediate gives

rise to an EPR-active species, which will allow us to probe its structure by ^{17}O-ENDOR spectroscopy in future work.[49]

ToMOH is unique among BMMs studied to date because it can serve as a catalase in the absence of reducing equivalents and as an NADH oxidase in conjunction with the other components of the enzyme system. The catalase activity of $ToMOH_{ox}$ suggests that dioxygen activation by $ToMOH_{red}$ may be reversible, if protons are lost prior to ET. Dioxygen binds reversibly to diiron(II) clusters in respiratory proteins, such as hemerythrin, but has not been reported for CBDI enzymes that catalyze substrate oxidation. RFQ Mössbauer spectra of samples from reaction of dioxygen with $ToMOH_{red}$ and ToMOD demonstrate that $ToMOH_{peroxo}$ decays to form only the oxidized diiron(III) center. The catalase reaction was conducted with more than a 20-fold excess of hydrogen peroxide, which could drive the reaction in the reverse direction. Hydrogen peroxide could react with $ToMOH_{ox}$, liberating two water molecules and generating $ToMOH_{peroxo}$ (Scheme 3.3). Oxidation of the peroxide fragment by the diiron(III) center evolves dioxygen with formation of $ToMOH_{red}$. Binding of a second molecule of hydrogen peroxide, possibly in a μ-1,1 fashion, to the diiron(II) center would allow for protonation of the distal oxygen atom followed by cleavage of the O–O bond. This binding mode for a peroxide fragment to a diiron(II) center has been previously proposed during reaction of synthetic peroxodiiron(III) complexes with the diiron(II) starting compound.[41] The oxo-bridged diiron(III) center formed after O–O bond cleavage can react with water to form $ToMOH_{ox}$ or

Scheme 3.3. Reaction of $ToMOH_{ox}$ with Hydrogen Peroxide

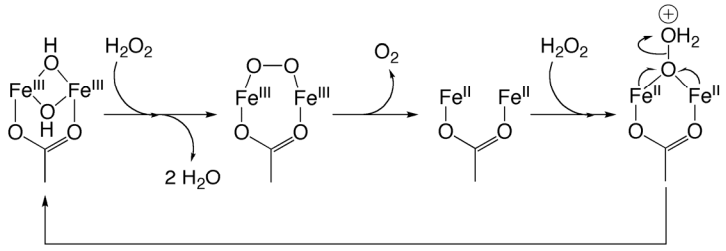

with hydrogen peroxide to generate $ToMOH_{peroxo}$.

The ToMO enzyme system catalyses the two-electron reduction of dioxygen to hydrogen

peroxide with an efficiency of 51%. Reductive quenching of the diiron(III) intermediate in the absence of substrate could explain this poor efficiency. Electron transfer from reduced ToMOC to $ToMOH_{peroxo}$ prior to dissociation of peroxide may allow for complete reduction of dioxygen to water, as occurs in MMOH.[17] The combined rate for dissociation of ToMOD, and binding and ET from reduced ToMOC to $ToMOH_{peroxo}$, would have to exceed the decay rate of the transient, for which the rate constant is 0.05 s^{-1}. The catalytic rate of phenol hydroxylation is 20-fold greater than the decay rate of $ToMOH_{peroxo}$.[50] The rate of protein complex formation and ET is faster therefore than that of $ToMOH_{peroxo}$ decay, suggesting that reductive quenching of $ToMOH_{peroxo}$ is kinetically feasible. The reduction of $ToMOH_{peroxo}$ could give rise to a peroxodiiron(II) species, similar to that proposed in Scheme 3.3.

Substrate Hydroxylation by ToMOH. The rate constant for decay of the ToMOH diiron(III) intermediate is sensitive to phenol, increasing by more than thirty-fold, from 0.05 s^{-1} to 2 s^{-1}, in its excess. The reaction is quantitative and forms catechol. The Mössbauer spectrum of $ToMOH_{peroxo}$ differs with phenol present, in contrast to that of the diiron(III) end product in double-mixing samples, which can be modeled with parameters identical to those in the absence of catechol (Figures 2 and 4). Presumably, phenol accesses the CBDI active site via the channel and binds to the diiron center before undergoing oxidation. Coordination of phenol to a CBDI center in this manner would direct hydroxylation at the *ortho* position. The high regioselectivity of phenol hydroxylation by ToMO parallels that of model complexes in which the substrates are tethered to ligands bound to iron and where oxidation occurs regiospecifically at the closest accessible position.[16,51,52]

Substrate coordination might potentiate reaction pathways that are otherwise unavailable in its absence. The choice of phenol as substrate for our experiments was determined because of the weak regioselectivity exhibited by the enzyme system for toluene. ToMO oxidizes phenol exclusively to catechol, but oxidation of toluene yields a mixture of cresols.[50] To ensure that the Mössbauer spectrum of the diiron(III) product could be readily distinguished from that of the diiron(III)

intermediate, phenol was therefore chosen as substrate.

A possible detailed mechanism for phenol hydroxylation is shown in Scheme 3.4. Dioxygen activation involves formation a peroxodiiron(III) intermediate, which we arbitrarily depict with a μ-1,2- geometry. Phenol next coordinates to one iron(III) center atom, after which there is an electrophilic attack of the $\{O_2^{2-}\}$ fragment on the arene π-system. The resulting arene epoxide ring opens, and rearomatization leads to oxidized diiron(III) center with bound product. In the absence of substrate, the intermediate slowly liberates hydrogen peroxide to return the resting diiron(III) state, $ToMOH_{ox}$. For reaction with toluene, a similar mechanism is expected but with substrate orientation

Scheme 3.4. Substrate Hydroxylation and Dioxygen Activation by ToMOH

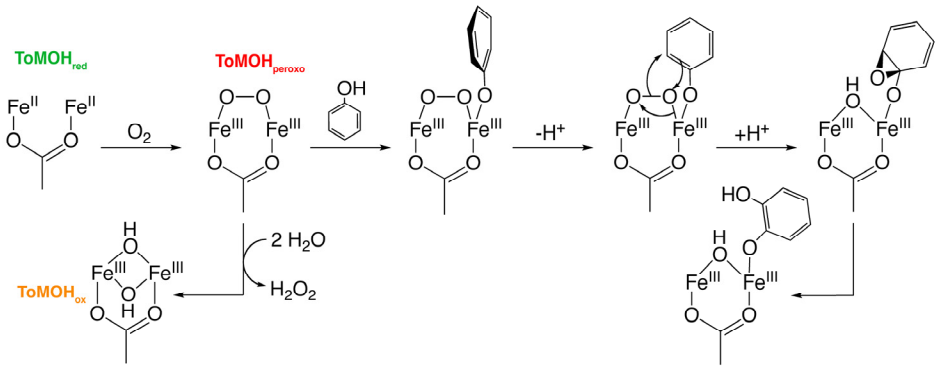

being affected by residues within the active site pocket rather than by coordination to the diiron center. No EPR active species were observed in samples from the double-mixing studies. We previously reported the reaction of the diiron(III) intermediate to produce a neutral tryptophanyl radical centered at the mutagenic site (I100W, Chapter 2). Oxidation of phenol to catechol did not produce a similar substrate-based radical with an appreciable lifetime. Substrate proximity to the diiron center may direct the reaction through radical pathways at longer distances and two-electron processes at shorter distances.

Linear free energy relationships for steady-state hydroxylation of substrate by ToMO have negative slopes (Figure 11), indicative of electrophilic attack on the aryl ring with substrate oxidation being at least partially rate-limiting. Activation of an aromatic substrate by donation from a hydroxyl group predisposes the system to electrophilic attack. As such, hydroxylation could proceed by a

mechanism different from that that used for less activated arenes, such as toluene and benzene. Hammett studies of the homologous T4MO enzyme system employing substituted benzenes as substrates, however, are consistent with an electrophilic attack on the π-ring.[53] The results of NIH shift experiments using T4MO suggested that hydroxylation involves formation of a transient arene epoxide that opens reversibly, or attack at a specific carbon atom, to yield a substrate carbocation.[54] The intermediate in ToMOH is therefore electrophilic, demonstrating a preference for two-electron oxidation of electron-rich substrates, such as alkenes and arenes, or one-electron abstraction from a nearby redox active residue, as occurred in the I100W variant.

Slow binding of substrate in the active site pocket will retard the steady-state hydroxylation rate and bring about deviations from a linear Hammett relationship. Mutation of two glutamate residues, E214 and E284, on the protein surface near the channel opening and far from the active site enhance the rate of steady-state hydroxylation of 4-nitrophenol.[48] More than 60% of this substrate is deprotonated at pH 7.5. Removal of negative charge at the opening of the substrate access channel could eliminate repulsion with deprotonated carboxylate side chains of E214 and E284, increasing the ease of substrate access to the active site. Correcting the observed hydroxylation rate of substrates in the Hammett study for the fraction of substrate that is protonated at pH 7.5 did not improve the quality of the fit. Other factors, such as the energy cost in bringing a charged species into a buried, neutral active site pocket in ToMOH, may also hinder access and affect the oxidation of these electron-poor aromatic compounds.

A portion of the product remains bound to the diiron center, as evidenced by the appearance of a broad absorption band at 580 nm. Phenol, the substrate used here, is also a reaction product of benzene hydroxylation by ToMOH. Phenol, like catechol, can also bind to the diiron center and does so, as evidenced by the growth of an absorption band centered at 495 nm during titration of $ToMOH_{ox}$ with phenol (data not shown). A similar absorption band was reported in a mutant of RNR-R2 in which F208 is hydroxylated and binds to the diiron center.[26] Product release in this pre-

steady-state system may be slow because the installed hydroxyl group allows coordination to the diiron center. Dissociation and egress of products is proposed to be the rate-determining step in steady-state hydroxylation by MMOH.[55] Coordination of products to the diiron center after hydroxylation, and the effects of these events on the reaction rate, are probably common to the hydroxylation mechanisms of BMMs. In ToMOH, a linear Hammett relationship provides strong evidence that substrate hydroxylation limits the reaction rate, implying that product dissociation is at least partially rate-limiting.

Quantitation of catechol formed in double-mixing samples was possible only after treatment of the diiron(III) protein with ascorbic acid. Under steady-state conditions, reduction of product-bound $ToMOH_{ox}$ facilitates its release to restart a catalytic cycle. Reduction-facilitated product release has been proposed previously for MMOH.[17,56] Such a mechanism, whereby product release is enhanced by reduction of the diiron center would require that diffusion of product out of the active site occur more rapidly than subsequent steps involving dioxygen activation, hydrocarbon diffusion into the active site, and hydroxylation. Previously steady-state oxidation of benzene by ToMO results in the initial accumulation of phenol, and phenol is only hydroxylated to catechol at low benzene concentrations.[50] The accumulation of phenol is therefore evidence that the rate of product dissociation exceeds that of reduction of the oxidized hydroxylase and subsequent dioxygen activation.

ToMOD enhanced binding of phenol to the diiron center by a factor of two, as measured by optical titration of the oxidized hydroxylase with phenol.[44] This result suggests that hydroxylase-regulatory protein interactions perturb the diiron center, possibly by reorienting residues to increase the active site volume and allow substrate access. The flexibility of the active site to facilitate changes in the volume of the substrate-binding cavity was reported previously for other BMMs. For example, the volume is increased by partial unwinding of helix E in $MMOH_{ox}$ upon binding of 6-bromohexanol.[57] Analogous helical rearrangements were also noted in the crystal structure of the

PHH–PHM complex.[58] The regulatory protein in these systems may therefore effect structural changes to allow for dioxygen activation and substrate access to, and/or product egress from, the diiron center.

Implications for the CBDI Protein Family. Half-sites reactivity, whereby two equivalent active sites alternate in traversing opposite halves of the catalytic cycle, has been proposed in RNR-R2,[59] Δ^9D,[12] and MMOH.[17] The maximum observed accumulation of the peroxodiiron(III) intermediate in ToMOH is consistently recorded to be ~ 45%, with the remaining protein present as unreactive diiron(II) starting material. Such reproducible yields of the intermediate generated upon oxygenation of reduced wild-type and mutant I100W[18] hydroxylases suggests that dioxygen activation in this system only occurs at one active site per dimer. This conserved feature of CBDI family members may reflect allosteric changes transmitted through the protein framework as amino acid side chains shift with the transition from the reduced enzyme to intermediate and oxidized forms. The protein framework can modulate the mechanism of dioxygen activation and the reactivity of those intermediates, as evidenced by the ability of MMOH and RNR-R2 to form high-valent species, of Δ^9D and Ft to form only peroxo-bridged intermediates, and of ToMOH to form a putative peroxodiiron(III) transient with different spectroscopic characteristics. DFT methods have proposed that compression of the Fe–Fe vector by the protein matrix aids in the formation of Q.[5] Subtle changes afforded by the orientation of subunits or complex formation with other components may be responsible for tuning the different reactivities of BMMs.

CONCLUSIONS

The reactive intermediate in ToMOH that hydroxylates arenes is a diiron(III) species, which we tentatively assign as a peroxo adduct. This intermediate is an electrophile, similar to μ-1,2-peroxodiiron(III) transients in RNR-R2 and MMOH. ToMOH is distinct, however, because it generates hydrogen peroxide during steady-state turnover in the absence of substrate and acts as a

catalase, consuming hydrogen peroxide to liberate dioxygen. Our results suggest that the dioxygen activation step(s) may be reversible in this system, which has not been previously reported for any BMM. The Mössbauer parameters and optical characteristics of $ToMOH_{peroxo}$ differentiate it from other μ-1,2-peroxodiiron(III) centers in biology. Further characterization of this intermediate by ENDOR, XAS, and X-ray crystallography will provide invaluable insight into factors that govern dioxygen activation at CBDI centers in biology.

REFERENCES

1. Nam, W., *Acc. Chem. Res.* **2007,** *40* (7), 522-531.

2. Denisov, I. G.; Makris, T. M.; Sligar, S. G.; Schlichting, I., *Chem. Rev.* **2005,** *105* (6), 2253-2277.

3. Kurtz, D. J., Jr., *J. Biol. Inorg. Chem.* **1997,** *2* (2), 159-167.

4. Merkx, M.; Kopp, D. A.; Sazinsky, M. H.; Blazyk, J. L.; Müller, J.; Lippard, S. J., *Angew. Chem., Int. Ed.* **2001,** *40* (15), 2782-2807.

5. Rinaldo, D.; Philipp, D. M.; Lippard, S. J.; Friesner, R. A., *J. Am. Chem. Soc.* **2007,** *129* (11), 3135-3147.

6. Lee, S.-K.; Lipscomb, J. D., *Biochemistry* **1999,** *38* (14), 4423-4432.

7. Sturgeon, B. E.; Burdi, D.; Chen, S.; Huynh, B. H.; Edmondson, D. E.; Stubbe, J.; Hoffman, B. M., *J. Am. Chem. Soc.* **1996,** *118* (32), 7551-7557.

8. Lindqvist, Y.; Huang, W.; Schneider, G.; Shanklin, J., *EMBO J.* **1996,** *15* (16), 4081-4092.

9. Jin, S.; Kurtz, D. J., Jr.; Liu, Z.-J.; Rose, J.; Wang, B.-C., *J. Am. Chem. Soc.* **2002,** *124* (33), 9845-9855.

10. Sazinsky, M. H.; Bard, J.; Di Donato, A.; Lippard, S. J., *J. Biol. Chem.* **2004,** *279* (29), 30600-30610.

11. McCormick, M. S.; Sazinsky, M. H.; Condon, K. L.; Lippard, S. J., *J. Am. Chem. Soc.* **2006,** *128* (47), 15108-15110.

12. Broadwater, J. A.; Ai, J.; Loehr, T. M.; Sanders-Loehr, J.; Fox, B. G., *Biochemistry* **1998,** *37* (42), 14664-14671.

13. Broadwater, J. A.; Achim, C.; Münck, E.; Fox, B. G., *Biochemistry* **1999,** *38* (38), 12197-12204.

14. Kim, K.; Lippard, S. J., *J. Am. Chem. Soc.* **1996,** *118* (20), 4914-4915.

15. Ookubo, T.; Sugimoto, H.; Nagayama, T.; Masuda, H.; Sato, T.; Tanaka, K.; Maeda, Y.; Ōkawa, H.; Hayashi, Y.; Uehara, A.; Suzuki, M., *J. Am. Chem. Soc.* **1996,** *118* (3), 701-702.

16. Yamashita, M.; Furutachi, H.; Tosha, T.; Fujinami, S.; Saito, W.; Maeda, Y.; Takahashi, K.; Tanaka, K.; Kitagawa, T.; Suzuki, M., *J. Am. Chem. Soc.* **2007,** *129* (1), 2-3.

17. Gassner, G. T.; Lippard, S. J., *Biochemistry* **1999,** *38* (39), 12768-12785.

18. Murray, L. J.; García-Serres, R.; Naik, S.; Huynh, B. H.; Lippard, S. J., *J. Am. Chem. Soc.* **2006,** *128* (23), 7458-7459.

19. Ravi, N.; Bollinger, J. M., Jr.; Huynh, B. H.; Edmondson, D. E.; Stubbe, J., *J. Am. Chem. Soc.* **1994,** *116* (18), 8007-8014.

20. Hildebrandt, A. G.; Roots, I., *Arch. Biochem. Biophys.* **1975,** *171* (2), 385-397 (method b).

21. Keller, R. J.; Halmes, N. C.; Hinson, J. A.; Pumford, N. R., *Chem. Res. Toxicol.* **1993,** *6* (4), 430-433.

22. Chufán, E. E.; Verani, C. N.; Puiu, S. C.; Rentschler, E.; Schatzschneider, U.; Incarvito, C.; Rheingold, A. L.; Karlin, K. D., *Inorg. Chem.* **2007,** *46* (8), 3017-3026 and references cited therein.

23. Corse, J.; Ingraham, L. L., *J. Org. Chem.* **1951,** *16* (9), 1345-1348.

24. Cadieux, E.; Vrajmasu, V.; Achim, C.; Powlowski, J.; Münck, E., *Biochemistry* **2002,** *41* (34), 10680-10691.

25. Xing, G.; Diao, Y.; Hoffart, L. M.; Barr, E. W.; Prabhu, K. S.; Arner, R. J.; Reddy, C. C.; Krebs, C.; Bollinger, J. M., Jr., *Proc. Natl. Acad. Sci. U.S.A.* **2006,** *103* (16), 6130-6135.

26. Baldwin, J.; Voegtli, W. C.; Khidekel, N.; Moënne-Loccoz, P.; Krebs, C.; Pereira, A. S.; Ley, B. A.; Huynh, B. H.; Loehr, T. M.; Riggs-Gelasco, P. J.; Rosenzweig, A. C.; Bollinger, J. M., Jr., *J. Am. Chem. Soc.* **2001,** *123* (29), 7017-7030.

27. Beauvais, L. G.; Lippard, S. J., *J. Am. Chem. Soc.* **2005,** *127* (20), 7370-7378.

28. Valentine, A. M.; Stahl, S. S.; Lippard, S. J., *J. Am. Chem. Soc.* **1999,** *121* (16), 3876-3887.

29. Moënne-Loccoz, P.; Baldwin, J.; Ley, B. A.; Loehr, T. M.; Bollinger, J. M., Jr., *Biochemistry* **1998,** *37* (42), 14659-14663.

30. Yun, D.; García-Serres, R.; Chicalese, B. M.; An, Y. H.; Huynh, B. H.; Bollinger, J. M., Jr., *Biochemistry* **2007,** *46* (7), 1925-1932.

31. Hwang, J.; Krebs, C.; Huynh, B. H.; Edmondson, D. E.; Theil, E. C.; Penner-Hahn, J. E., *Science* **2000,** *287* (5450), 122-125.

32. Moënne-Loccoz, P.; Krebs, C.; Herlihy, K.; Edmondson, D. E.; Theil, E. C.; Huynh, B. H.; Loehr, T. M., *Biochemistry* **1999,** *38* (17), 5290-5295.

33. Que, L., Jr.; Dong, Y., *Acc. Chem. Res.* **1996,** *29* (4), 190-196.

34. Wallar, B. J.; Lipscomb, J. D., *Chem. Rev.* **1996,** *96* (7), 2625-2658.

35. Valentine, A. M.; Lippard, S. J., *J. Chem. Soc., Dalton Trans.* **1997,** *1997* (21), 3925-3931.

36. Gherman, B. F.; Baik, M.-H.; Lippard, S. J.; Friesner, R. A., *J. Am. Chem. Soc.* **2004,** *126* (9), 2978-2990.

37. Brunold, T. C.; Tamura, N.; Kitajima, N.; Moro-oka, Y.; Solomon, E. I., *J. Am. Chem. Soc.* **1998,** *120* (23), 5674-5690.

38. Shan, X.; Que, L., Jr., *Proc. Natl. Acad. Sci. U.S.A.* **2005,** *102* (15), 5340-5345.

39. Zhang, X.; Furutachi, H.; Fujinami, S.; Nagatomo, S.; Maeda, Y.; Watanabe, Y.; Kitagawa, T.; Suzuki, M., *J. Am. Chem. Soc.* **2005,** *127* (3), 826-827.

40. Feig, A. L.; Lippard, S. J., *J. Am. Chem. Soc.* **1994,** *116* (18), 8410-8411.

41. Feig, A. L.; Becker, M.; Schindler, S.; van Eldik, R.; Lippard, S. J., *Inorg. Chem.* **1996,** *35* (9), 2590-2601.

42. Dong, Y.; Zang, Y.; Shu, L.; Wilkinson, E. C.; Que, L., Jr., *J. Am. Chem. Soc.* **1997,** *119* (51), 12683-12684.

43. Bollinger, J. M., Jr.; Tong, W. H.; Ravi, N.; Huynh, B. H.; Edmondson, D. E.; Stubbe, J., *J. Am. Chem. Soc.* **1994,** *116* (18), 8015-8023.

44. Murray, L. J.; Naik, S.; Ortillo, D. O.; Huynh, B. H.; Lippard, S. J., unpublished results.

45. Nam, W.; Ryu, Y. O.; Song, W. J., *J. Biol. Inorg. Chem.* **2004,** *9* (6), 654-660.

46. Ormö, M.; deMaré, F.; Regnström, K.; Åberg, A.; Sahlin, M.; Ling, J.; Loehr, T. M.; Sanders-Loehr, J.; Sjöberg, B.-M., *J. Biol. Chem.* **1992,** *267* (13), 8711-8714.

47. Ryoo, D.; Shim, H.; Canada, K.; Barbieri, P.; Wood, T. K., *Nat. Biotechnol.* **2000,** *18* (7), 775-778.

48. Vardar, G.; Ryu, K.; Wood, T. K., *J. Biotechnol.* **2005,** *115* (2), 145-156.

49. Murray, L. J.; Davydov, R.; Naik, S.; Huynh, B. H.; Hoffman, B. M.; Lippard, S. J., unpublished results.

50. Cafaro, V.; Izzo, V.; Scognamiglio, R.; Notomista, E.; Capasso, P.; Casbarra, A.; Pucci, P.; Di Donato, A., *Appl. Environ. Microbiol.* **2004,** *70* (4), 2211-2219.

51. Carson, E. C.; Lippard, S. J., *Inorg. Chem.* **2006,** *45* (2), 828-836.

52. Carson, E. C.; Lippard, S. J., *Inorg. Chem.* **2006,** *45* (2), 837-848.

53. Mitchell, K. H.; Studts, J. M.; Fox, B. G., *Biochemistry* **2002,** *41* (9), 3176-3188.

54. Mitchell, K. H.; Rogge, C. E.; Gierahn, T.; Fox, B. G., *Proc. Natl. Acad. Sci. U.S.A.* **2003,** *100* (7), 3784-3789.

55. Lipscomb, J. D., *Annu. Rev. Microbiol.* **1994,** *48* 371-399.

56. Lee, S.-K.; Nesheim, J. C.; Lipscomb, J. D., *J. Biol. Chem.* **1993,** *268* (29), 21569-21577.

57. Sazinsky, M. H.; Lippard, S. J., *J. Am. Chem. Soc.* **2005,** *127* (16), 5814-5825.

58. Sazinsky, M. H.; Dunten, P. W.; McCormick, M. S.; Di Donato, A.; Lippard, S. J., *Biochemistry* **2006,** *45* (51), 15392-15404.

59. Sjöberg, B.-M.; Karlsson, M.; Jörnvall, H., *J. Biol. Chem.* **1987,** *262* (20), 9736-9743.

CHAPTER 4

OXIDATION OF NORCARANE BY ToMO

CONTEXT

In Chapters 2 and 3, we examined the diiron intermediates formed during the reaction of reduced hydroxylase with dioxygen. In Chapter 4, we present the steady-state hydroxylation for norcarane, a radical clock substrate that can distinguish between one- and two-electron oxidation pathways. For this substrate, opening of the cyclopropane ring after H-atom or hydride abstraction gives rise to diagnostic products. We carefully examined the enzymatic oxidation of norcarane by ToMO, paying close attention to minor products formed during the reaction. The ToMO enzyme system readily desaturates norcarane under steady-state conditions to yield a mixture of 2- and 3-norcarene. These unsaturated compounds are better substrates than the parent norcarane, giving rise to a number of secondary oxidation products. We identified 17 oxidation products in the enzyme oxidation reactions, half of which arise from norcarene oxidation. These products have similar elution times and fragmentation patterns in GC/MS analyses, preventing accurate quantification of the diagnostic radical and cationic products. We estimate the lifetime of any substrate radical intermediate formed during oxidation by ToMO to be short-lived with a lifetime no greater than 25 ps. Lifetimes calculated by using norcarane as an RCS probe are typically greater than those reported from the oxidation of a number of other probes, probably because the desaturation chemistry observed here was not considered.

INTRODUCTION

Radical clock substrate probes have been used extensively to investigate enzymatic oxidation reactions. These small organic compounds contain strained ring systems that rearrange upon radical formation to yield a diagnostic product. Recombination of the substrate radical and the enzyme intermediate to form hydroxylated products competes with substrate radical rearrangement for these probes. Armed with the known rate of rearrangement for a particular RCS probe, the lifetime of the enzyme radical species can be estimated from the ratio of radical-rearranged and unrearranged

products. A handful of RCS probes, such as norcarane (**1**), can also distinguish between one- and two-electron oxidation pathways. Upon hydride abstraction from this probe, the substrate cation ring opens to yield a product distinct from the radical-derived one. For norcarane, formation of a radical or a cation at C2 gives product alcohol **21** or **22,** respectively, as shown in Scheme 4.1. The two oxidation pathways can thus be distinguished with one probe. No information regarding transient species is directly obtained, however, as the experiment monitors only product distributions at the end of the reaction. To take advantage of the mechanistic insight offered by these substrates, accurate quantification and identification of all oxidation products are required.

Norcarane (**1**) has been applied as a probe in studies of many enzyme-catalyzed oxidation reactions.[1-7] Radical and cation-rearranged products were detected in low yield, suggesting that one- and two-electron oxidation pathways were accessible to these enzymes. The evidence for radical-derived products in norcarane studies and the consequent conclusion that radical intermediates exist disagreed, in most instances, with experimental results conducted with other RCS probes.[8,9] Moreover, results from "hypersensitive" radical probes,[10] including those that can differentiate between radical and cation pathways, indicated that no radicals with significant lifetimes were formed during oxidation reactions. Most studies employing norcarane reported yields of radical and cation rearranged products that were similar to those of a number of unidentified oxidation products of norcarane. Eight oxidation products from norcarane have been reported, but the reaction mixtures appeared to contain many more products with similar molecular weights and GC retention properties.

In this work, we studied oxidation reactions of norcarane by the ToMO system with careful

Scheme 4.1. Ring-Expansion Products Arising from Norcarane Oxidation

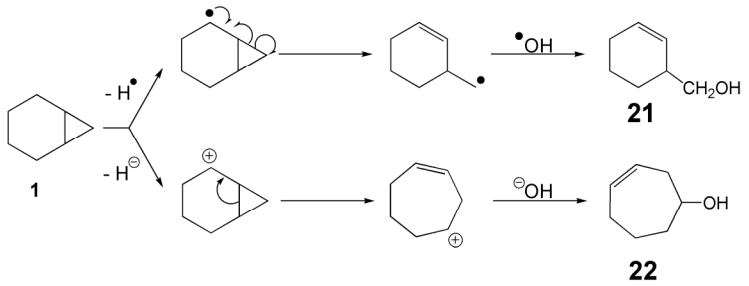

attention to the identities of minor products. Norcarane was desaturated to 2- and 3-norcarene in addition to forming primary oxidation products such as **17**. These unsaturated compounds were better substrates for this system than the parent norcarane, undergoing oxidation to yield secondary oxidation products. To understand the extent to which these secondary oxidation products might complicate product identification and quantification, enzymatic reactions were carried out employing both norcarenes as substrates. The number of characterized potential products arising from norcarane oxidation was determined to be twenty, with almost half resulting from norcarene oxidation. These compounds have similar retention times and mass spectra on GC/MS instruments equipped with a low polarity column. In particular, we found that the radical- and cation-derived rearrangement products from norcarane co-elute with norcarene oxidation products. We conclude that the already small yields attributed to these rearranged products were *overestimated* in earlier studies by an order of magnitude or more.

EXPERIMENTAL METHODS

General Considerations. Syntheses of norcarane (**1**), 2-norcarene (**2**), 3-norcarene (**3**), and oxygenated products **4**-**22** were carried out as described elsewhere (Scheme 4.2).[3,11-18] Norcarane (ca. 99% pure) was treated with mCPBA to oxidize trace olefinic materials and purified by preparative GC (¼ inch × 8 ft column, 10% SE-52 on 60/80 Chromosorb W). The isolated sample was shown to be > 99.96% homogeneous by analytical GC. The unsaturated derivatives, 2- and 3-norcarene, were purified by preparative GC (10% SE-52 on 60/80 Chromosorb W, 1/4 in × 8 ft column) at 100 ^{o}C (isothermal). Sample purities were determined by GC (DB-5, 40 °C) using flame ionization detection (FID). NMR spectra were recorded in $CDCl_3$ at 300 or 500 MHz. Proton correlation was resolved with bidimensional COSY experiments, and stereochemistry was determined by monodimensional NOE difference experiments. All yields and purities of other authentic samples were determined by GC (DB-5) using flame ionization detection and GC-MS (HP-5MS 5% phenylmethyl siloxane

Scheme 4.2. Products of Norcarane Oxidation

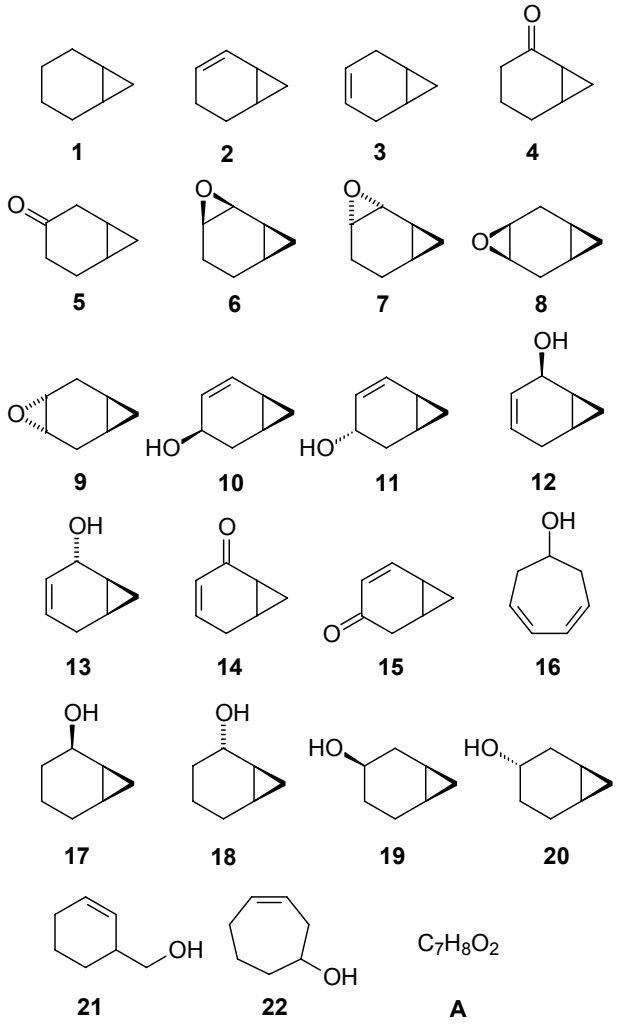

column) with electron impact (EI) ionization. Mass spectra of purified samples are reported elsewhere.[11]

Enzymatic Oxidations by ToMO. Purified ToMOF and plasmids containing the genes for ToMOH, ToMOD, and ToMOC were kindly supplied by Professor Alberto Di Donato, Naples, Italy. The proteins were expressed in *E. coli* and purified as described elsewhere.[19,20] The specific activity on phenol was $1.2(1) \times 10^3$ mU/mg of hydroxylase, and the iron content for ToMOH was 4.3 ± 0.2 as determined by previously reported methods.[19,20] In a typical reaction, a mixture of 1 nmol of ToMOH, 66.57 nmol of ToMOD, 20 nmol of ToMOC, and 0.1 nmol of ToMOF was diluted to a volume of 2 mL with 20 mM potassium phosphate buffer (pH = 7.4). The mixture was allowed to

stand in an ice bath for 10 min. Either 2-, 3-norcarene (10 μL, 2 mg norcarene/100 μL methanol), or norcarane (1.5 mmol, neat) was added as substrate. The mixture was incubated at 26 °C for 10 min while shaking. The enzymatic hydroxylation was initiated by addition of buffer solution containing NADH to give a sample concentration of 1 mM NADH. The mixture was gently shaken at 26 ºC for 30 min and then extracted with CH_2Cl_2 (3 × 2 mL). The combined organic phase was dried ($MgSO_4$) and filtered. An internal standard of 1-phenyl-1-propanol was added, and the mixture was concentrated under a stream of nitrogen. The concentrated sample was analyzed by GC/FID (0.32 mm × 30 m capillary column, 5% phenyl silicone bonded phase) and GC-MS (0.25 mm × 30 m, capillary column, 5% phenyl silicone bonded phase).

RESULTS & DISCUSSION

Desaturase Reactions of Norcarane. Small amounts of impurities including norcarenes can be detected in distilled samples of norcarane. To avoid complications from the use of slightly contaminated substrate, distilled norcarane was treated with mCPBA to oxidize traces of olefins and isolated by preparative GC. Analysis of the purified sample by analytical GC indicated that norcarane was at least 99.96% homogeneous, and no impurities of 2-norcarene or 3-norcarene could be detected to the limit of instrumental sensitivity.

Both 2- and 3-norcarene were observed in the product mixture for enzyme-catalyzed oxidation of norcarane by ToMO prior to concentrating sample and were formed in ~ 5% yield (Figure 4.1). The yield of norcarenes was 0.1% relative to initial substrate loading but was greater than that of all oxidation products of norcarane except the norcaranols. The yields of alcohols **21** and **22**, the radical- and cation-derived products respectively, were approximately six-fold lower than those of the norcarenes.

Non-heme diiron enzymes have been previously reported to perform desaturase reactions. For example, Δ^9D converts stearoyl-ACP to oleoyl-ACP, and MMO from *M. trich.* desaturates

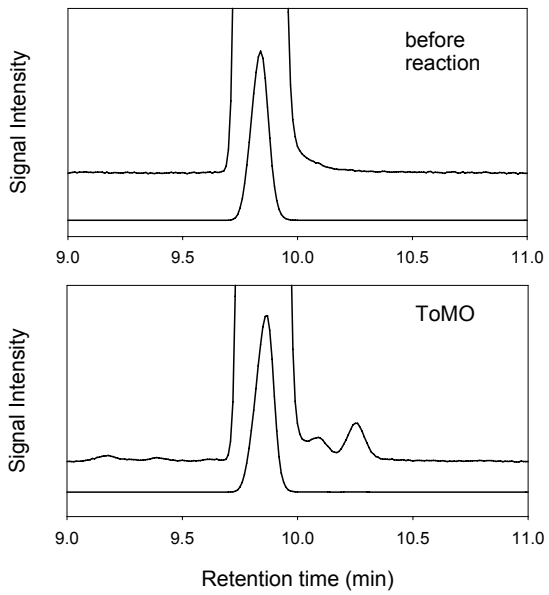

Figure 4.1. Portions of GC traces (40 °C, DB-5 column) of norcarane before (top) and after (bottom) reaction with ToMO. The expansions are 100× the amplitude of the lower traces. Under the GC conditions used for these analyses, 3-norcarene and 2-norcarene elute with retention times of 10.1 and 10.3 min, respectively.

ethylbenzene to styrene and cyclohexadienes to benzene in 9 and 40% yield, respectively.[21] Previous studies, however, did not realize that norcarane was susceptible to similar desaturation. As steady state assays proceed, the relative affinity of ToMO for norcarane and norcarenes can impact the number of oxidation products in the reaction mixture and the final ratio of norcarenes to norcarane. ToMOH oxidizes 3-norcarene more efficiently than norcarane (*vide infra*). An examination of product distributions arising from norcarane oxidation requires consideration of the enzymatic hydroxylation products of norcarene. Conditions were therefore surveyed to develop GC methods to separate products from norcarane and norcarene oxidation.

Analytical Protocol for Oxidation Products. Identification and quantification of these compounds by GC/MS with selective ion monitoring and GC/FID, respectively, is challenging because the molecular weights, fragmentation patterns, and elution times are similar for oxidation products of norcarane and norcarenes. The radical- (**21**) and cation-derived (**22**) products are of particular concern because the utility of radical clock substrates requires accurate quantification of

these products and unrearranged alcohols **17** - **20**. Product **21** presents further complications because the fragmentation pattern contains two large molecular weight ions that are found in most other mass spectra (Figure 4.2). Furthermore, its retention time on a low polarity column is similar to those of **10**, **13**, **16**, and **A**, all of which arise from norcarene oxidation. This observation supports our conclusion that the enzymatic decomposition of norcarenes must be characterized in studies employing norcarane as a diagnostic probe.

Authentic samples and a mixture containing radical-derived product 3-hydroxymethylcyclohexene (**21**), cyclohepta-3,5-dienol (**16**), and *syn*-2-norcaranol (**17**) in an approximate 1:1:50 ratio illustrate the similar elution times and difficulty separating these compounds (Table 4.1). On a low polarity 5% phenyl silicone column (DB-5), **21** and **16** eluted at coincidental times at oven temperatures of 70 °C or greater, whereas peaks corresponding to **21** and **17** overlapped at 50 °C or 60 °C. The major product formed was **17** in enzyme-catalyzed oxidations of norcarane and would obscure detection of the small amount of **21**. Compound **16** arises from oxidation of norcarenes and could result in an overestimation of the yield of **21** if higher column temperatures were used. A similar phenomenon was observed for other alcohol products, such as **10**, where the temperature effect on the retention of each alcohol product differed. As such, quantification of **21** independent of other products was not possible under any of the examined conditions. To obtain accurate yields of **21**, the combined yield of all products eluting at that retention time must be determined along with the percentage of **21** present. Overall yields were determined by GC/FID, and the identity and percentage composition were determined by GC/MS.

Product Yields from Norcarane Oxidations. GC/FID traces contained a number of overlapping peaks incompletely resolved, as expected from our discussion above, but 17 oxidation products could be identified by comparison to standards (Table 4.2). The structure of one product, **A**, could not be determined. The major oxygenated products are 2-norcaranols **17** and **18**, as reported for similar diiron enzymes.[3,5,6] Activation of this C–H bond is more facile because of the lower bond

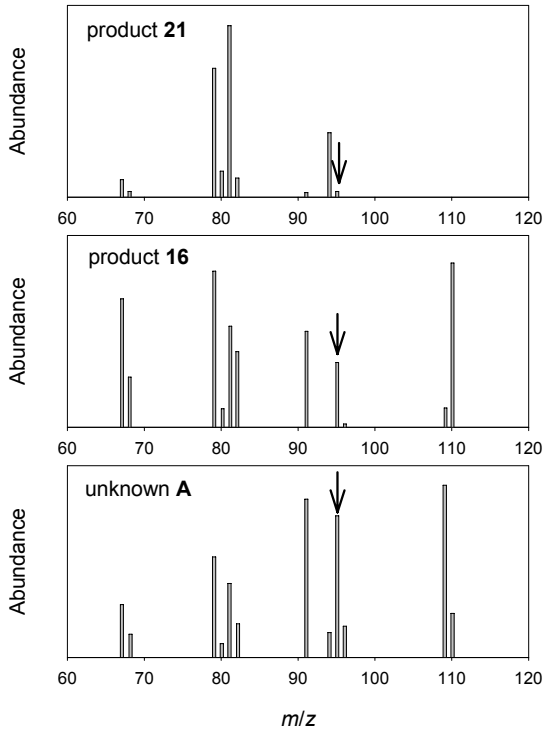

Figure 4.2. SIM mode GC spectra obtained by monitoring 12 ion channels. Spectra of **21**, **16**, and **A** at the same GC elution time have similar fragmentation patterns except for differences in the ratio of intensity of *m*/*z* = 95 to 94 and 81 to 79. In each spectrum, the *m*/*z* = 95 signal is marked with an arrow for calibration.

Table 4.1. Observed Retention Times for GC Elutions as a Function of Column Temperature[a]

T (°C)	21	16	17
100	7.0	7.0	7.1
90	8.4	8.4	8.6
80	10.7	10.7	10.9
70	14.4	14.4	14.6
60	20.7	20.5	20.8
50	31.6	30.8	31.3

[a]Reported in min on a DB-5 column. Compounds **16**, **17**, and **21** are shown in Scheme 4.1

dissociation relative to that at C3.[22] The high yield of 2- and 3-norcarene is surprising as these products were not reported previously for norcarane oxidation by *any* BMM.[3,5,6] Peaks corresponding to norcarene oxidation products were observed in previous studies with norcarane, but these products were not identified.

Although the detection of products **21** and **22** provides evidence for radical or cationic substrate-based intermediates, accurate quantification is required to estimate the lifetime of such species as well as the partitioning of the reaction between one- and two-electron processes. Yields cannot be determined as accurately as desired because of limitations in our capacity to separate these compounds from other oxidation products. From mass spectra, compound **21** is not the major component of the mixture **21** + **16** + **A**, as evidenced by the ratio of peaks with m/z = 95 to 94 and 81 to 79. If the yield of **21** is 50% of the co-eluting species, the calculated lifetime of a putative radical intermediate is at most 25 ps. This lifetime is in disagreement with that of 263 ps reported from norcarane oxidation by T4MO.[5] In that experiment, cation-rearranged products were not observed for norcarane oxidation, but cation-derived products were formed in four-fold greater yield than that of the radical-derived products for reaction mixtures using 1,1-diethyl- and 1,1-dimethylcyclopropane. The results reported here for ToMO agree with those of the latter from oxidation of cyclopropane probes by T4MO, for which radical-derived products were formed in low yield.

Enzyme-Catalyzed Oxidations of Norcarenes. For enzyme systems where unnatural substrates are not efficiently oxidized, products arising from the reaction of minor impurities with the enzyme intermediate(s) can accumulate and complicate data analysis. As for norcarane, preparative GC was used to ensure that the norcarene substrates were of the highest possible purity. Substrates **2** and **3** used in our experiments contained no detectable impurities by NMR spectroscopy and were 99.7% and 99.3% pure, respectively, by analytical GC. The distribution of ToMO oxidation products of the norcarenes is listed in Table 4.3.

Product yields were almost 15-fold higher in ToMO oxidations when 3-norcarene was the substrate instead of 2-norcarene. Two other BMMs, MMO and PH, and cytochrome P450 2B1 showed a similar preference for 3-norcarene over 2-norcarene. Compounds **16** and **A**, previously mentioned because of the similarity of their retention times to that of **21**, are observed in product mixtures of 3-norcarene oxidation by ToMO. These products were not exclusive to 3-norcarene

Table 4.2. Product Yields from ToMO, PH, and MMO Catalyzed Oxidations of Norcarane

Enzyme (nmol)	**21+16+A**	**18+19+11**	**22+12**	**17**	**4**	**20**	**5**	**7**	**10+13**	**14**	**15**	**8**	**9**
ToMO (1.0)	0.11	5.0	0.06	5.5	0.04	0.14	0.31	d	0.03	0.03	0.02	0.02	0.02
PH (1.0)	0.03	0.55	0.05	2.7	0.04	0.13	0.25	0.07	0.03	0.03	0.04	0.02	0.12
MMO (20)	0.07	9.0	0.29	14.4	0.77	1.80	0.50	d	0.06	0.20	0.05	d	d

Yields are reported in nmoles. d = not detected

Table 4.3. Product Yields from Oxidations of Norcarane Catalyzed by ToMO

Substrate	**4**	**5**	**6**	**7**	**8**	**9 + B**	**10 + 13**	**11**	**12**	**14**	**15**	**16 + A**	**total**
2-norcarene	0.03	2.20	<0.01	0.09	d	0.19	0.12	0.30	0.04	0.17	0.09	d	3.23
3-norcarene	0.04	0.55	d	0.05	1.03	41.61	1.19	0.55	0.50	0.38	0.33	0.61	46.84

Yields are reported in nmoles. d = not detected

because 2-norcarene was also oxidized to **16** and **A** by MMO, PH, and cytochrome P450 2B1. Furthermore, these products are also observed in norcarane oxidation reactions because norcarenes are generated by desaturation of norcarane (*vide supra*). Whereas the yield of **16** is 1.3% of all 3-norcarene products for ToMO, that of **16** relative to that of **21** in norcarane reactions is of greater consequence. The poor turnover for norcarane compared to norcarenes by ToMO and the short lifetime of any radical species in ToMO ensure that **16** and **A** are formed in a high enough yield to hamper an accurate estimation of lifetimes.

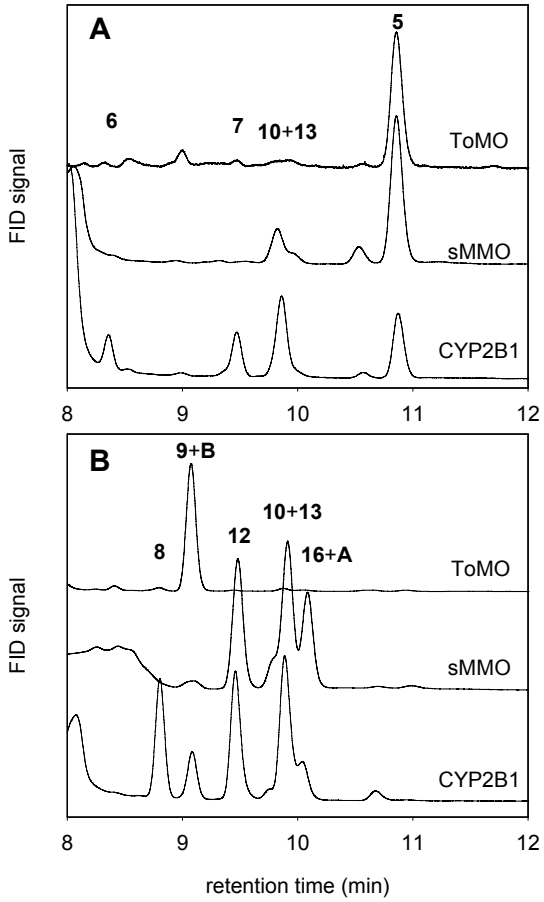

Figure 4.3. Portions of GC traces of products from oxidation of 2-norcarene (**A**) and 3-norcarene (**B**) with toluene monooxygenase from *P.* sporium OX1 (ToMO), soluble methane monooxygenase from *M. capsulatus* (Bath) (sMMO), and cytochrome P450 2B1 (CYP2B1). The identities of some of the products are indicated with the compound numbers.

The oxidation product varied depending on the position of the double bond; for 2-norcarene, the major product was ketone **5**, whereas 3-norcarene reactions contained predominantly epoxide **9**

(Figure 4.3). Oxidation of 3-norcarene by MMO or cytochrome P450 2B1 yields primarily the alcohol products rather than the epoxide. An unidentified product **B** eluted at the same retention time as **9**, but was a minor product based on a comparison of mass spectra for the peak to that of an authentic sample of **9**.

Desaturation Effects on Radical Clock Probe Oxidations. In systems where product yields are low because of inefficient enzymatic oxidation of norcarane, the contamination level with norcarenes must be as minimal as possible. Treatment of distilled samples of norcarane with mCPBA followed by preparative GC scavenged trace 2-norcarene. Even using this material, it was not possible to measure precisely the yield of **21**. Studies employing norcarane as an RCS probe must consider oxidation products of norcarane and norcarenes. The extent to which product distributions in earlier studies using norcarane were influenced by trace norcarenes cannot be evaluated because substrate purities were not reported. Any future study using norcarane as a probe should demonstrate by high performance GC that the norcarane sample is not contaminated with norcarenes. An alternative strategy that will circumvent complications arising from norcarene oxidation products is to conduct assays under single turnover rather than steady-state conditions. To accumulate norcarene oxidation products requires multiple turnovers of the enzyme system, which cannot occur in single turnover experiments. Unfortunately, many enzymes do not efficiently oxidize norcarane, and this strategy will be prohibitive in most cases because the required enzyme concentration will be high.

The efficiency of desaturation of norcarane is surprising, and one should expect that any mechanistic probe with a reactive CH functionality adjacent to the readily oxidized position would undergo desaturation. Any probe that meets this criterion is predicted to yield relatively large amounts of secondary oxidation products that complicate mechanistic studies. Included are most conceivable probes, of course, except the subset containing a methyl group adjacent to a cyclopropyl ring. Oxidation of the methyl group is not expected to result in desaturation because of the large increase in strain energy that would result from an sp^2-hybridized carbon atom in a cyclopropyl ring.

When the probe is capable of reacting in a desaturase reaction, care should be taken to identify as many products as possible, including secondary oxidation products from the dehydrogenated probe, to avoid the pitfalls outlined for norcarane.

Implications for Catalysis in ToMO. In Chapters 2 and 3, we proposed that the active oxidant is electrophilic in character, resembling the established reactivity of other peroxodiiron(III) intermediates. Prior to the radical clock studies discussed here, ToMO had not been observed to carry out hydroxylation of aliphatic compounds. The same observation was made with T4MO, where radical clock substrates, such as norcarane and 1,2-diethylcyclopropane, were the first reported saturated hydrocarbons to be oxidized by this system.[5] Only a small amount of product **21** was observed for oxidation of norcarane by ToMOH, contrasted by the greater yields of the norcaranols and norcarenes. Oxygen-atom insertion into the C–H bond of norcarane to give norcaranols may occur by a mechanism similar to that proposed for methane hydroxylation by Q or diethyl ether hydroxylation by $MMOH_{peroxo}$.[23,24] The intermediate observed in ToMOH can carry out one- and two-electron oxidation reactions, as evidenced by the ToMOH I100W results discussed in Chapter 2, and by the studies of the wild type hydroxylase in Chapter 3. Proximity and positioning of these substrates relative to the diiron center in the active site pocket could determine the reaction pathway.

In systems where more than one reactive intermediate is present, distinct reactivity profiles such as insertion across C–H bonds and epoxidation could be attributed to different species.[9] Only one intermediate is observed in ToMOH, however, requiring a mechanism that bifurcates to yield two products. Initial hydride abstraction from the substrate would form a transient carbocation. For desaturation, an amino acid side chain, such as the hydroxyl group of Thr201, could abstract a proton from the carbon atom adjacent to the positively-charged center to yield norcarenes. For substrate hydroxylation, recombination of the substrate cation with the oxygen atom on the iron center that accepted the hydride would yield the norcaranol products (Scheme 4.3). Two conditions must be satisfied for this mechanism to be valid. First, the rearrangement rate of the substrate cation must be

slower than that of either recombination or proton abstraction. Second, the rate of recombination must be greater than the rate of proton abstraction, as the yield of norcaranols is 8-fold greater than the norcarene yield.

Scheme 4.3. Hydride Abstraction Mechanism for ToMO Oxidation of Norcarane

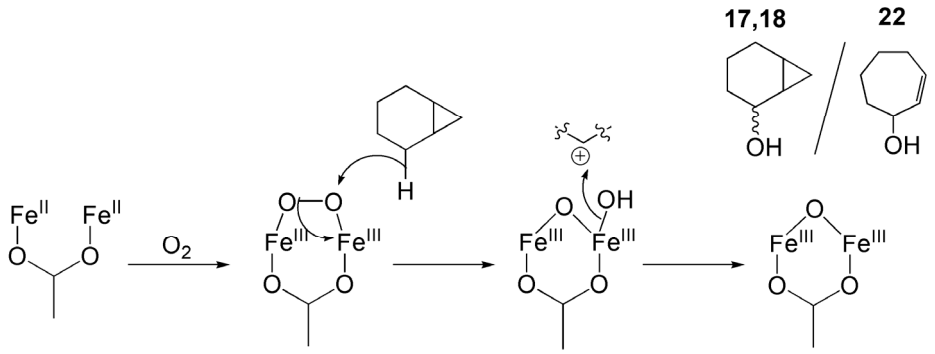

An alternate mechanism for desaturation might involve substrate hydroxylation followed by elimination of water. Similar reactivity has been reported for Δ^9D, where O-atom transfer from the diiron center to the sulfur atom in thioether substrates was observed.[25] For addition across a C–H bond, a two-electron three-centered transition state would allow for formation of the norcaranols. This mechanism is analogous to that proposed for alkene epoxidation and diethyl ether oxidation by $MMOH_{peroxo}$.

Changes in oxidation products as well as the preference of 3-norcarene most likely arise from binding of substrate within the active site. Toluene and norcarene are of comparable shape and size[5] and are therefore likely to bind in a similar manner. The enzymatic product distribution for toluene hydroxylation is biased towards the *para* position.[19] The methylene bridge of norcarene could mimic the tolyl methyl group. The double bond in 3-norcarene is therefore placed favorably to undergo epoxidation whereas the double bond in 2-norcarene is less accessible to the oxidizing intermediate. Oxidation of C3 in 2-norcarene followed by rearrangement would yield 3-norcarenol (Scheme 4.4). Subsequent dissociation and tautomerization of this product would yield **5**.

Scheme 4.4. Oxidation Pathways of 2- and 3-Norcarene by ToMO

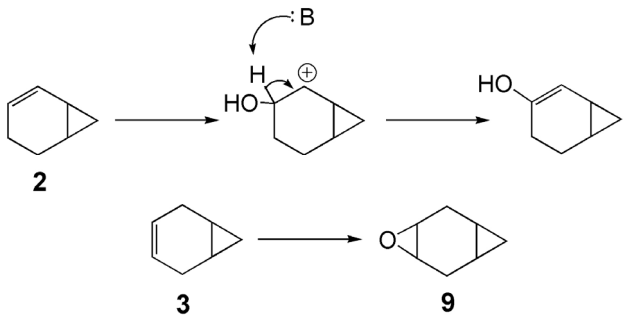

CONCLUSIONS

Radical clock substrate probes have been widely used to provide mechanistic insight into enzyme catalyzed oxidations. Desaturation of these substrates was not been considered previously. For norcarane, desaturation is a significant pathway during oxidation of this probe by ToMO. Of greater concern, the oxidation of the norcarenes is favored over that of norcarane, leading to an accumulation of over 20 products. By considering the rich uncharacterized chemistry of these probes upon reaction with ToMO, we have ascertained that a radical pathway does not predominate the hydroxylation of this substrate, contrary to previous reports on T4MO. The desaturase activity afforded by this enzyme also mirrors similar desaturation chemistry proposed by other peroxodiiron(III) intermediates, adding further support to our tentative assignment of the diiron(III) transient as such a species.

ACKNOWLEDGEMENTS

Most of the credit for the work reported in this chapter goes to the Newcomb lab at the University of Illinois at Chicago. Data analysis, method development, and substrate synthesis were carried out there. Duplicate experiments were performed at M.I.T. and confirmed qualitatively that desaturation of norcarane occurred to an appreciable level during oxidation reactions with ToMO, MMO, and PH.

REFERENCES

1. Austin, R. N.; Chang, H.-K.; Zylstra, G. J.; Groves, J. T., *J. Am. Chem. Soc.* **2000,** *122* (47), 11747-11748.

2. Auclair, K.; Hu, Z.; Little, D. M.; Ortiz de Montellano, P. R.; Groves, J. T., *J. Am. Chem. Soc.* **2002,** *124* (21), 6020-6027.

3. Newcomb, M.; Shen, R.; Lu, Y.; Coon, M. J.; Hollenberg, P. F.; Kopp, D. A.; Lippard, S. J., *J. Am. Chem. Soc.* **2002,** *124* (24), 6879-6996.

4. Newcomb, M.; Shen, R.; Lu, Y.; Coon, M. J.; Hollenberg, P. F.; Kopp, D. A.; Lippard, S. J., *J. Am. Chem. Soc.* **2006,** *128* (4), 1394.

5. Moe, L. A.; Hu, Z.; Deng, D.; Austin, R. N.; Groves, J. T.; Fox, B. G., *Biochemistry* **2004,** *43* (50), 15688-15701.

6. Brazeau, B. J.; Austin, R. N.; Tarr, C.; Groves, J. T.; Lipscomb, J. D., *J. Am. Chem. Soc.* **2001,** *123* (48), 11831-11837.

7. Groves, J. T., *J. Inorg. Biochem.* **2006,** *100* (4), 434-447.

8. Merkx, M.; Kopp, D. A.; Sazinsky, M. H.; Blazyk, J. L.; Müller, J.; Lippard, S. J., *Angew. Chem., Int. Ed.* **2001,** *40* (15), 2782-2807.

9. Baik, M.-H.; Newcomb, M.; Friesner, R. A.; Lippard, S. J., *Chem. Rev.* **2003,** *103* (6), 2385-2419.

10. Newcomb, M.; Toy, P. H., *Acc. Chem. Res.* **2000,** *33* (7), 449-455.

11. Newcomb, M.; Lansakara-P., D. S. P.; Kim, H.-Y.; Chandrasena, R. E. P.; Lippard, S. J.; Beauvais, L. G.; Murray, L. J.; Izzo, V.; Hollenberg, P. F.; Coon, M. J., *J. Org. Chem.* **2007,** *72* (4), 1128-1133.

12. Kawabata, N.; Naka, M.; Yamashita, S., *J. Am. Chem. Soc.* **1976,** *98* (9), 2676-2677.

13. Chan, J. H. H.; Rickborn, B., *J. Am. Chem. Soc.* **1968,** *90* (23), 6406-6411.

14. Chini, M.; Crotti, P.; Flippin, L. A.; Gardelli, C.; Macchia, F., *J. Org. Chem.* **1992,** *57* (6), 1713-1718.

15. Denmark, S. E.; Edwards, J. P., *J. Org. Chem.* **1991,** *56* (25), 6974-6981.

16. Dauben, W. G.; Berezin, G. H., *J. Am. Chem. Soc.* **1963,** *85* (4), 468-472.

17. Friedrich, E. C.; Holmstead, R. L., *J. Org. Chem.* **1972,** *37* (16), 2550-2554.

18. Charette, A. B.; Francoeur, S.; Martel, J.; Wilb, N., *Angew. Chem., Int. Ed.* **2000,** *39* (24), 4539-4542.

19. Cafaro, V.; Scognamiglio, R.; Viggiani, A.; Izzo, V.; Passaro, I.; Notomista, E.; Dal Piaz, F.; Amoresano, A.; Casbarra, A.; Pucci, P.; DiDonato, A., *Eur. J. Biochem.* **2002,** *269* (22), 5689-5699.

20. Sazinsky, M. H.; Bard, J.; DiDonato, A.; Lippard, S. J., *J. Biol. Chem.* **2004,** *279* (29), 30600-30610.

21. Jin, Y.; Lipscomb, J. D., *J. Biol. Inorg. Chem.* **2001,** *6* (7), 717-725.

22. Halgren, T. A.; Roberts, J. D.; Horner, J. H.; Martinez, F. N.; Tronche, C.; Newcomb, M., *J. Am. Chem. Soc.* **2000,** *122* (13), 2988-2994.

23. Baik, M.-H.; Gherman, B. F.; Friesner, R. A.; Lippard, S. J., *J. Am. Chem. Soc.* **2002,** *124* (49), 14608-14615.

24. Beauvais, L. G.; Lippard, S. J., *J. Am. Chem. Soc.* **2005,** *127* (20), 7370-7378.

25. Fox, B. G.; Lyle, K. S.; Rogge, C. E., *Acc. Chem. Res.* **2004,** *37* (7), 421-429.

APPENDIX A

PRELIMINARY STUDIES OF PHOTOINDUCED ELECTRON TRANSFER TO OXIDIZED MMOH

INTRODUCTION

Dioxygen activation at non-heme carboxylate-bridged diiron(III) centers is incompletely understood. For example, the peroxide moiety in the conserved peroxo-bridged diiron(III) cluster is proposed to bind in either a μ-1,2 or μ-η^2:η^2 fashion.[1-4] The high-valent species Q in MMOH has been assigned as both a symmetric and asymmetric di(μ-oxo)diiron(IV) cluster.[5,6] The conversion of $MMOH_{peroxo}$ to Q is proposed to proceed by either homolytic[3,4] or heterolytic[7] O–O bond cleavage, the latter facilitated by protonation of the peroxide moeity. A detailed, complete mechanistic understanding of dioxygen activation in MMOH, and by extension other non-heme diiron enzymes, is therefore lacking. No intermediates are observed prior to the peroxodiiron(III) transient and after reacting the reduced diiron(II) protein with dioxygen-saturated buffer. Only oxygen isotope effects[8] and kinetic models[9] have been experimentally applied to infer information about these early steps.

In the MMO system, computational methods predict that a short-lived mixed-valent superoxodiiron(II,III) transient forms prior to $MMOH_{peroxo}$.[4] In agreement with this prediction, the rate constants obtained from RFQ EPR, Mössbauer, and stopped-flow optical experiments suggest the presence of such an intermediate because the rate of decay of the diiron(II) signal at g = 16 is faster than the rate of formation of the peroxodiiron(III) species.[10,11] Thus far, the techniques employed to probe the dioxygen activation in these systems rely on rapid mixing of two solutions. Photochemical methods, such as photoreduction of the active site of metalloproteins[12-15] or rapid photodissociation of dioxygen[16] from small inorganic complexes, however, are limited by the rate of the photochemical process rather than the mixing time (~ 1 ms). Such a strategy might allow us to interrogate the diiron center prior to the formation of $MMOH_{peroxo}$. We therefore attempted to use a tris(bipyridyl)ruthenium(II) complex tethered to MMOB to photoreduce the diiron active site in MMOH. The shortcomings of this strategy and possible future directions are described.

EXPERIMENTAL METHODS

General Considerations. MMO component proteins were expressed either in *E. coli* (MMOB and MMOR) or in *M. caps.* (MMOH) and isolated as described elsewhere.[17,18] Plasmids for recombinant expression of mutant forms of MMOB were supplied by Matthew Sazinsky. For all batches of MMOH isolated, the iron content determined by the ferrozine assay ranged from 3.8 to 4.2 Fe atoms per MMOH dimer. The specific activities determined by monitoring NADH consumption and with propylene as substrate ranged from 300 to 400 mU/mg of hyrdoxylase, similar to those reported elsewhere.[19] LC/MS ESI(+) analyses for proteins were carried out at the Biopolymers facility at M.I.T. as described in Chapter 2. Instrumentation for GC analyses and optical spectroscopy have been reported previously.[17] Reagents and materials were purchased from Sigma Aldrich Chemical Company.

Synthesis of Labeled MMOB. The MMOB mutants, N101C, C89A/H35C, and C89A/D22C, were modified according to the following procedure. The reagent (4-bromomethyl-4′-methyl-2,2′-bipyridyl)(bisbipyridyl)ruthenium(II) hexafluorophosphate, $[Ru(bpy)_3']$$(PF_6)$ was prepared according to literature procedures[20] and characterized by ESI(+)-MS. An aliquot of the MMOB mutant protein (300 μL of 1mM) was exchanged into 50 mM Tris/HCl pH 8.0 buffer by serial dilution and concentration steps. The buffer-exchanged protein (300 μL) was mixed with an aliquot (800 μL) of 5 mM $[Ru(bpy)_3']$$(PF_6)$ in distilled water and stirred in the dark. The reaction mixture was allowed to stand at room temperature for 4 h, after which it was loaded onto a BioGel PD10 desalting column (BioRad Labs, CA), equilibrated with 25mM MOPS pH 7.0. Fractions were eluted with the equilibration buffer, and those that eluted prior to the retention volume (8 mL) were collected, pooled, and loaded on a DEAE Sepharose CL-6B ion exchange column. The $Ru(bpy)_3'$-MMOB conjugate was eluted with a linear gradient of NaCl from 0 to 250 mM over 200 mL in 25 mM MOPS pH 7.0. SDS-PAGE and optical absorption spectral analysis of the fractions were recorded.

Fractions that absorbed at 452 nm and contained MMOB were pooled, concentrated to 100 μL, and drop-frozen in liquid nitrogen. All purified $Ru(bpy)_3'$–MMOB constructs, RuMMOB, were submitted to the Biopolymers Lab (M.I.T.) for LC/MS ESI(+). The steady-state activity and product composition for propylene as substrate were determined for the MMOB constructs.

Effect of $MMOH_{ox}$ on Fluorescence of RuMMOB. Degassed solutions of RuMMOB (2.5 μM) with or without MMOH (1.4 μM) were transferred to a fluorescence cuvette. The fluorescence at 600nm was recorded at 25.0 ± 0.2 °C for excitation at 337nm or 450nm using a Hitachi F-3010 Fluorescence Spectrophotometer.

EPR Sample Preparation. Solutions of MMOH, MMOB, and RuMMOB N101C were made anaerobic by repeated cycles of vacuum degassing and purging with nitrogen. The protein solutions and aniline were transferred to a Vacuum Atmospheres MO-20 anaerobic chamber. A standardized solution of sodium dithionite was used to reduce a portion of $MMOH_{ox}$ to $MMOH_{mv}$ as described previously[21] using methyl viologen as the mediator. All samples were made in duplicate and contained either oxidized or mixed valent MMOH (250 μM). MMOB (0.5 mM), RuMMOB N101C (0.5 mM), and aniline (1 mM) were either individually added or omitted. One of each pair of identical samples was exposed to a flash from a SunPak auto 433AF flash lamp. All samples were frozen and stored in liquid nitrogen. The EPR spectra were recorded at 5 K, 0.201mW, and 9.376GHz on a Bruker EMX (X-Band) spectrometer with ER 4102ST cavity. Spectra were modeled to obtain *g*-values using the software package Simfonia (Bruker).

RESULTS

Characterization of RuMMOB Constructs. The experimentally determined molecular weights for the RuMMOB constructs are given in Table 1. Only one product peak was observed in the LC trace for RuMMOB N101C, and deconvolution of the ion envelope indicated it to be the 1:1 conjugate of MMOB N101C with $[Ru(bpy)_3']^{2+}$ (Figure A.1). Three major peaks were observed in

Table A.1. Simulated *g*-values and Intensities of EPR Signals in MMOH Samples.

MMOH	MMOB	Aniline	Flash	*g* values	Intensity Limits
ox	WT	Y	N	1.88, 1.77, 1.62	1237, -1304
ox	WT	Y	Y	1.92, 1.77, 1.62	1923, -1527
ox	Ru	Y	Y	1.91, 1.77, 1.62	2461, -2086
mv	WT	N	N	1.88, 1.76, 1.62	15088, -10643
mv	WT	Y	N	1.88, 1.77, 1.62	10191, -9745
mv	WT	Y	Y	1.89, 1.78, 1.62	10241, -9695
mv	-	Y	N	1.89, 1.82, 1.78	37995, -13333
mv	-	Y	Y	1.92, 1.86, 1.74	41027, -13355

ox - $MMOH_{ox}$; mv - $MMOH_{mv}$; WT – MMOB; Ru – RuMMOB N101C; Y – included; N – omitted

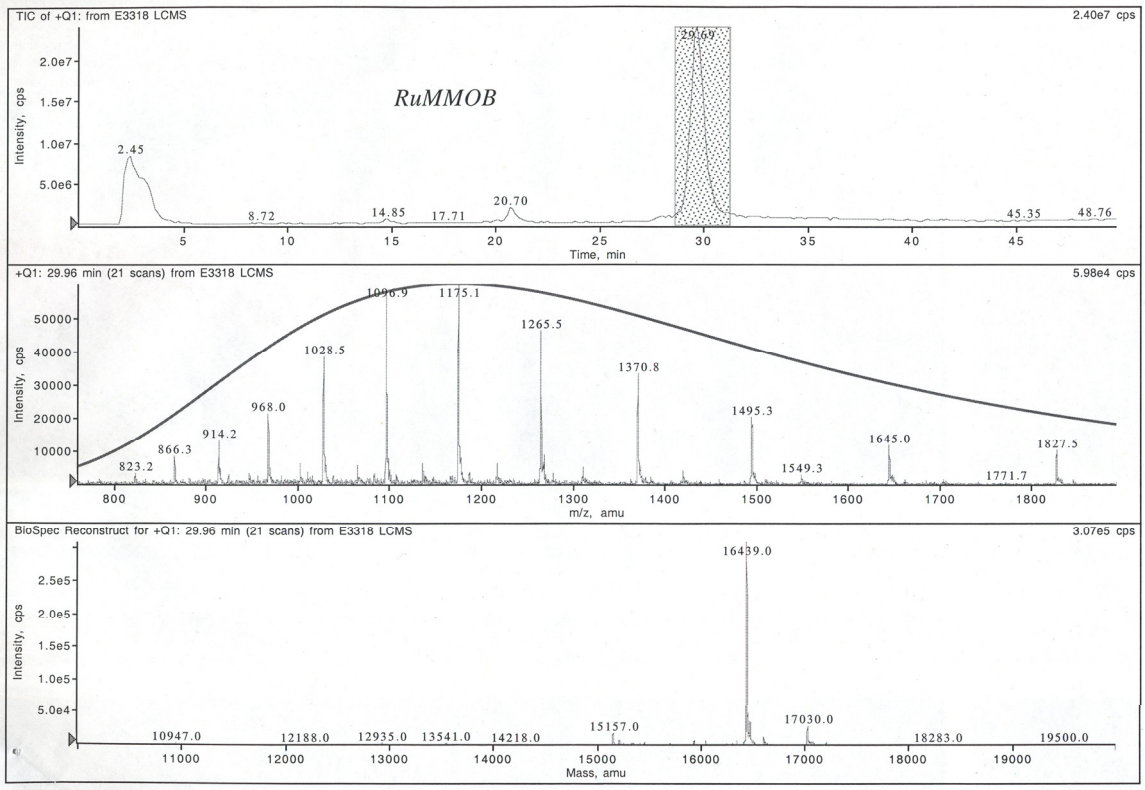

Figure A.1. LC trace and deconvoluted MS data for RuMMOB N101C. Only one major product is observed in the LC trace (top panel) with a retention time at 29.7 min. The LC trace is given as ion counts per second as opposed to an optical signal. The ion envelope for the species corresponding to the major product (middle panel) agrees with the LC trace with only one contributor to the envelope. The experimentally determined mass of RuMMOB, deconvoluted from the ion envelope (bottom), is 16439 Da, which agrees with the expected value of 16435 Da.

the LC trace of the purified RuMMOB C89A/D22C. Bands corresponding to proteins with a lower molecular weight than MMOB were observed on the SDS-PAGE gel for fractions from the DEAE

ion exchange column. For MMOB C89A/H34C, the experimentally determined molecular weight of the conjugate was 50 Da greater than the predicted molecular mass. RuMMOB N101C, therefore, was used in further experiments. The concentration was estimated by using an extinction coefficient of 13500 $M^{-1}cm^{-1}$ at 452 nm. This value corresponds to the $[Ru(bpy)_3']^{2+}$ center and assumes that the optical properties of this complex are unchanged upon ligation to the protein. The steady-state consumption of NADH in the absence of propylene for RuMMOB N101C was significantly higher than for native MMOB. Product analysis by GC, however, indicated that substrate was oxidized to propylene oxide even though NADH consumption and substrate oxidation appeared to be uncoupled. The fluorescence of RuMMOB N101C was unperturbed in the presence of $MMOH_{ox}$ with excitation at either 337 nm or 450 nm.

Photoreduction of MMOH by RuMMOB. A rhombic EPR signal was observed for $MMOH_{mv}$ with g = 1.88, 1.77, and 1.62, which is similar to previously reported values for this species.[22] Weak EPR signals corresponding to $MMOH_{mv}$ were observed in samples containing $MMOH_{ox}$, MMOB, and aniline (Table A.1). The presence of a minor amount of $MMOH_{mv}$ has been noted previously in EPR studies on MMOH.[22] These signals do not increase significantly in samples that contained RuMMOB N101C and were excited by the flash lamp. Photoinduced electron transfer therefore does not occur to an appreciable extent under these experimental conditions.

DISCUSSION

Photochemical methods for the reduction of metal cofactors in enzyme active sites have been applied extensively to heme systems, such as cytochrome P450cam[14] or to monitor electron transfer events in cytochrome *c* oxidase.[12,20] These one-electron processes are readily amenable to this methodology. The work pioneered here attempted to extend this technique to two-electron processes in the CBDI systems, specifically MMOH.

The steady-state activity of RuMMOB N101C exhibited uncoupled NADH consumption and substrate hydroxylation compared to native MMOB. This uncoupling could arise either from a perturbation of protein–protein interactions, or the redox active center conjugated to MMOB may influence electron shuttling into MMOH by MMOR. The site of mutagenesis, N101C, is likely to be close to the contact surface between MMOH and MMOB.[23,24] The introduction of the positively charged ruthenium moiety may therefore adversely affect the formation of the MMOH–MMOB complex. As mentioned in Chapter 1, this complex is crucial for efficient coupling of electron consumption to substrate hydroxylation. Moreover, the nature of the interacting surface of this complex is not completely understood, with experimental evidence indicating both electrostatic[25] and hydrophobic[26] interactions. Weaker binding of RuMMOB N101C to MMOH could allow for MMOR to displace the regulatory protein during dioxygen activation. Substrate hydroxylation would, as a consequence, compete with reductive quenching of oxygenated intermediates. Under constant irradiation, fluorescence quenching of RuMMOB N101C proteins in the presence of MMOH was not observed. Binding of MMOH to RuMMOB N101C might be expected to quench the fluorescence, at least partially, if the attachment site of the fluorophore is near the binding interface. The absence of a fluorescence change therefore lends support to the aforementioned hypothesis that protein–protein interactions between the hydroxylase and regulatory protein are disrupted by the ruthenium complex.

The intensity of EPR signals corresponding to $MMOH_{mv}$ did not increase significantly for photoexcited samples containing $MMOH_{ox}$, RuMMOB, and aniline. Reduction of $MMOH_{ox}$ to $MMOH_{mv}$ should be more facile than reduction of $MMOH_{mv}$ because of the reduction potentials reported for these species.[27] We predict therefore that photoinduced electron transfer would not be observed for samples containing $MMOH_{mv}$ because this process was not observed for samples containing $MMOH_{ox}$ and RuMMOB N101C.

The experimental design reported here requires electron transfer from $[Ru(bpy)_3']^{2+}$ through the MMOB–MMOH interface to the diiron cluster in MMOH. The estimated distance for this ET event

is in excess of 20 Å. According to Marcus theory,[28] ET rates decrease by approximately an order of magnitude for every 2 Å increase in the distance between cofactors. Therefore, the fastest possible ET rate would be in the range of 10 s^{-1}. This technique was pursued to observe the diiron active on a timescale faster than that of conventional mixing methods. These reduction rates, however, would be slower than the dead times of rapid mixing techniques.

FUTURE DIRECTIONS

Alternative strategies to photoreduce MMOH might entail tethering the photoreductant to either the ferredoxin domain of MMOR, or a small peptide that binds to MMOH. The first two strategies have been utilized previously for studying ET from the Rieske center to the ferric heme in the cytochrome bc_1 complex[12] and for tyrosyl radical generation in ribonucleotide reductase.[29] MMOR-Fd constructs that can be used for the former strategy were previously reported.[30,31] A small inhibitory peptide, DEDVITAALRQ, which bears sequence homology to MMOR and competes with MMOB for binding sites on MMOH,[32] could be modified with electron donors to explore the second strategy. Rapid photochemical release of dioxygen under anaerobic conditions in the presence of $MMOH_{red}$ and MMOB could circumvent these difficulties. The reaction of reduced cytochrome *c* with dioxygen has been successfully examined with this approach.[16] Electron transfer from photoreductants tethered to substrate analogues has afforded rapid reduction of the ferric heme in cytochrome P450cam.[14]

The large substrate access channel in ToMOH could allow for a similar strategy to be employed as hexapolyethylene glycol can bind within this channel in an extended conformation.[33] Photoreduction from an electron donor, positioned near to the protein surface at the channel entrance, to the diiron center would require ET to occur at a distance of 35 Å or more.[34] Such a large distance may hinder rapid and efficient photoinduced ET and negate the advantage of photochemical methods.

REFERENCES

1. Skulan, A. J.; Brunold, T. C.; Baldwin, J.; Saleh, L.; Bollinger, J. M., Jr.; Solomon, E. I., *J. Am. Chem. Soc.* **2004,** *126*(28), 8842-8855.

2. Yun, D.; García-Serres, R.; Chicalese, B. M.; An, Y. H.; Huynh, B. H.; Bollinger, J. M., Jr., *Biochemistry* **2007,** *46*(7), 1925-1932.

3. Rinaldo, D.; Philipp, D. M.; Lippard, S. J.; Friesner, R. A., *J. Am. Chem. Soc.* **2007,** *129*(11), 3135-3147.

4. Gherman, B. F.; Baik, M.-H.; Lippard, S. J.; Friesner, R. A., *J. Am. Chem. Soc.* **2004,** *126*(9), 2978-2990.

5. Lippard, S. J., *Philosophical Transactions of the Royal Society A* **2005,** *363*(1829), 861-877.

6. Lipscomb, J. D.; Que, L., Jr., *J. Biol. Inorg. Chem.* **1998,** *3*(3), 331-336.

7. Lee, S.-K.; Lipscomb, J. D., *Biochemistry* **1999,** *38*(14), 4423-4432.

8. Stahl, S. S.; Francisco, W. A.; Merkx, M.; Klinman, J. P.; Lippard, S. J., *J. Biol. Chem.* **2001,** *276*(7), 4549-4553.

9. Liu, Y.; Nesheim, J. C.; Lee, S.-K.; Lipscomb, J. D., *J. Biol. Chem.* **1995,** *270*(42), 24662-24665.

10. Lee, S.-K.; Nesheim, J. C.; Lipscomb, J. D., *J. Biol. Chem.* **1993,** *268*(29), 21569-21577.

11. Liu, K. E.; Wang, D.; Huynh, B. H.; Edmondson, D. E.; Salifoglou, A.; Lippard, S. J., *J. Am. Chem. Soc.* **1994,** *116*(16), 7465-7466.

12. Engstrom, G.; Xiao, K.; Yu, C.-A.; Yu, L.; Durham, B.; Millett, F., *J. Biol. Chem.* **2002,** *277*(34), 31072-31078.

13. Therien, M. J.; Selman, M.; Gray, H. B., *J. Am. Chem. Soc.* **1990,** *112*(6), 2420-2422.

14. Wilker, J. J.; Dmochowski, I. J.; Dawson, J. H.; Winkler, J. R.; Gray, H. B., *Angew. Chem., Int. Ed.* **1999,** *38*(1-2), 89-92.

15. Winkler, J. R.; Nocera, D. G.; Yocom, K. M.; Bordignon, E.; Gray, H. B., *J. Am. Chem. Soc.* **1982,** *104*(21), 5798-5800.

16. Van Eps, N.; Szundi, I.; Einarsdóttir, Ó., *Biochemistry* **2000,** *39*(47), 14576-14582.

17. Gassner, G. T.; Lippard, S. J., *Biochemistry* **1999,** *38*(39), 12768-12785.

18. Valentine, A. M.; Stahl, S. S.; Lippard, S. J., *J. Am. Chem. Soc.* **1999,** *121*(16), 3876-3887.

19. Beauvais, L. G.; Lippard, S. J., *J. Am. Chem. Soc.* **2005,** *127*(20), 7370-7378.

20. Liu, R. Q.; Geren, L.; Anderson, P.; Fairris, J. L.; Peffer, N.; McKee, A.; Durham, B.; Millett, F., *Biochimie* **1995,** *77*(7-8), 549-561.

21. DeWitt, J. G.; Bentsen, J. G.; Rosenzweig, A. C.; Hedman, B.; Green, J.; Pilkington, S.; Papaefthymiou, G. C.; Dalton, H.; Hodgson, K. O.; Lippard, S. J., *J. Am. Chem. Soc.* **1991,** *113*(24), 9219-9235.

22. Davydov, R.; Valentine, A. M.; Komar-Panicucci, S.; Hoffman, B. M.; Lippard, S. J., *Biochemistry* **1999,** *38*(13), 4188-4197.

23. Sazinsky, M. H.; Dunten, P. W.; McCormick, M. S.; DiDonato, A.; Lippard, S. J., *Biochemistry* **2006,** *45*(51), 15392-15404.

24. Zheng, H.; Lipscomb, J. D., *Biochemistry* **2006,** *45*(6), 1685-1692.

25. Balendra, S.; Lesieur, C.; Smith, T. J.; Dalton, H., *Biochemistry* **2002,** *41*(8), 2571-2579.

26. Walters, K. J.; Gassner, G. T.; Lippard, S. J.; Wagner, G., *Proc. Natl. Acad. Sci. U.S.A.* **1999,** *96*(14), 7877-7882.

27. Astier, Y.; Balendra, S.; Hill, H. A. O.; Smith, T. J.; Dalton, H., *Eur. J. Biochem.* **2003,** *270*(3), 539-544.

28. Marcus, R. A.; Sutin, N., *Biochim. Biophys. Acta* **1985,** *811*(3), 265-322.

29. Reece, S. Y.; Seyedsayamdost, M. R.; Stubbe, J.; Nocera, D. G., *J. Am. Chem. Soc.* **2007,** *129*(27), 8500-8509.

30. Blazyk, J. L.; Lippard, S. J., *Biochemistry* **2002,** *41*(52), 15780-15794.

31. Blazyk, J. L.; Gassner, G. T.; Lippard, S. J., *J. Am. Chem. Soc.* **2005,** *127*(49), 17364-17376.

32. Rosenzweig, A. C.; Brandstetter, H.; Whittington, D. A.; Nordlund, P.; Lippard, S. J.; Frederick, C. A., *Proteins* **1997,** *29*(2), 141-152.

33. McCormick, M. S.; Sazinsky, M. H.; Condon, K. L.; Lippard, S. J., *J. Am. Chem. Soc.* **2006,** *128*(47), 15108-15110.

34. Sazinsky, M. H.; Bard, J.; DiDonato, A.; Lippard, S. J., *J. Biol. Chem.* **2004,** *279*(29), 30600-30610.

APPENDIX B

ELECTRON TRANSFER FROM REDUCED TOMOC

TO THE OXIDIZED HYDROXYLASE

INTRODUCTION

ET processes between redox partners in proteins are controlled by the surrounding protein framework, which prevents undesired reactions. Interprotein ET in particular requires protein recognition and binding events to ensure a pathway-specific process.[1] Metalloenzymes that activate dioxygen, such as cytochromes P450,[2] the CBDI enzyme family,[3] and Rieske dioxygenases,[4] cycle between redox states, and cellular reducing agents, such as NADH, supply the necessary electrons for this process. In the CBDI enzyme family, the diiron active site is housed in the catalytic protein, which does not contain any other redox cofactors.[5] Other components of these enzyme systems must bind to this protein and transfer electrons to the diiron center to initiate the catalytic cycle. A spatially homologous hydrogen-bonding network in the BMMs, RNR-R2, and Δ^9D is proposed to function as the ET pathway. In RNR-R2, W48 within this network donates an electron to the μ-1,2-peroxodiiron(III) intermediate.[6] The binding site for the ferredoxin protein that reduces Δ^9D was determined to be in close proximity to an analogous hydrogen bonding network.[7] In the BMMs, this network is strongly conserved, spanning ~ 12 Å from the protein surface to the diiron center.[6]

Of the BMMs, the ET and protein interactions involved in the reduction of the diiron center have been studied the most extensively in MMO.[8-11] In this system, $MMOH_{peroxo}$ and Q form only in the presence of the regulatory protein.[12-14] Although MMOB facilitates the oxidative phase of the catalytic cycle, it inhibits ET from reduced MMOR or its ferredoxin domain, MMOR-Fd, to MMOH.[9-11] Hysteresis has been proposed for the interaction of MMOB and MMOH, where conformational changes in the hydroxylase are retained after dissociation of the protein complex.[9] Allosteric changes resulting from protein–protein interactions could be transmitted across the dimer interface and manifested as this hysteresis. Previously, kinetic models for steady-state catalysis and component complex formation have invoked ternary complexes, with MMOB and MMOR binding on the same face of the MMOH dimer, or half-sites reactivity, where MMOB and MMOR bind

exclusively to opposite faces of the dimer.[11] The half-sites model requires the oxidative and reductive phases of the catalytic cycle in each active site of the dimer to be out of phase with respect to one other.

Initial characterization of ET from reduced ToMOC to oxidized ToMOH under pre-steady-state conditions revealed that the regulatory protein is required for rapid ET.[15] Incubation of the hydroxylase with the regulatory protein prior to reaction with reduced ToMOC increased the ET rate by between one and two orders of magnitude. ToMOD could cause a conformational change on the hydroxylase either to favor binding of $ToMOC_{red}$ or perturb the reduction potentials of the diiron core. The latter effect is observed in MMO except that reduction of the hydroxylase is thermodynamically less favorable in the presence of MMOB.[16-19] More intriguing, however, was the observation in these experiments that only ~ 50% of reduced Rieske protein was consumed in the reaction. Half-sites reactivity has been previously proposed in CBDI proteins, such as RNR-R2,[20] Δ^9D,[21] and MMO.[11] To investigate the ET chemistry in this system, we monitored the thermodynamic distribution of electrons in mixtures containing $ToMOC_{red}$, ToMOH, and ToMOD by EPR spectroscopy. We compared these results to spectra of samples prepared by reduction of ToMOH with sodium dithionite in the presence of ToMOD. The results suggest that protein-protein interactions play a pivotal role in gating ET to the diiron centers of the oxidized hydroxylase, with $ToMOC_{red}$ favoring the complete reduction of one active site and chemical reduction being indiscriminate.

EXPERIMENTAL METHODS

General Considerations. ToMO component proteins were expressed and purified as described in Chapter 2. Iron assays and steady state activities were conducted as described elsewhere.[11,22] The iron content of the hydroxylases determined by the ferrozine assay was between 3.8 and 4.5 Fe:ToMOH dimer. Instrumentation for UV/visible absorption spectroscopy and anaerobic sample

preparation were as reported in Chapters 2 and 3. Chemical reagents were purchased from Sigma Aldrich Chemical Company.

EPR Sample Preparation and Data Acquisition for Mixtures Containing ToMOC$_{red}$. Samples were prepared in the anaerobic chamber with deoxygenated solutions of ToMOC, ToMOH, and ToMOD. A solution of ToMOC (500 μL, 350 μM) was reduced with excess sodium dithionite and dialyzed twice against 500 mL of 25 mM MOPS, pH 7.0, for 1 h each. Aliquots of ToMOC$_{red}$ were added to mixtures of ToMOH:2ToMOD. The combined protein solutions were each diluted to a final volume of 200 μL with anaerobic 25 mM MOPS buffer, pH 7.0. The concentration of ToMOH:2ToMOD in all samples was 100 μM, with ToMOC$_{red}$ concentrations ranging from 0 to 200 μM. Samples were allowed to equilibrate for 10 min at room temperature after which they were transferred to quartz EPR tubes. The tubes were capped with rubber septa, removed from the anaerobic chamber, and immersed in liquid nitrogen. Spectra were acquired on a Bruker EMX Spectrometer with an ER 4102ST cavity and an Oxford ESR 900 liquid helium cryostat at 10 K. Data were acquired with a microwave frequency of 9.379 GHz, a power of 0.2 mW, and a modulation amplitude and frequency of 10 G and 100 kHz, respectively.

EPR Sample Preparation of Chemically Reduced Hydroxylase. A solution of sodium dithionite was standardized with potassium ferricyanide as described elsewhere.[23] Samples were prepared as described above, except that varying equivalents of sodium dithionite were added to mixtures containing ToMOH:2 ToMOD (200 μM) instead of ToMOC. The equivalents reported for this experiment were determined from the iron content, and not the hydroxylase concentration. Protein solutions were allowed to stand for 20 min after addition of the reductant. Acquisition parameters were identical to those reported previously.

RESULTS

Reduction of $ToMOH_{ox}$ by Sub-stoichiometric $ToMOC_{red}$ Results in Diiron(II) Centers. To investigate the distribution of electrons in solutions containing $ToMOC_{red}$ and $ToMOH_{ox}$, EPR spectra of samples containing variable ratios of $ToMOC_{red}$ to ToMOH premixed with two equiv. of ToMOD were measured. Spectral features with *g*-values > 16 and < 2 have previously been attributed to diiron(II) and mixed-valent diiron(II,III) clusters at CBDI centers, respectively.[16] These features are absent in the spectrum of a sample containing the oxidized hydroxylase and regulatory protein, which is expected for an antiferromagnetically-coupled diiron(III) center (Figure B.1, top panel). As $ToMOC_{red}$ is added, a signal at g = 16 forms and increases in intensity, even at substoichiometric ratios of $ToMOC_{red}$ to $ToMOH_{ox}$. Unreacted $ToMOC_{red}$ dominates the region at g = 2.0 at ratios of ToMOC to ToMOH greater than 1:1. The reduced Rieske cluster has an anisotropic signal with g = 2.01, 1.91, and 1.75, which is typical of the diiron(II,III) form of these centers.[24,25] The signal from unreacted $ToMOC_{red}$ could therefore obscure the mixed-valent signals from $ToMOH_{mv}$. Weak features corresponding to the mixed-valent hydroxylase are observed in the spectrum of a sample containing one equiv. of $ToMOC_{red}$ and 2 equiv. of $ToMOH_{ox}$.

Generation of Mixed-Valent Diiron(II,III) ToMOH by Chemical Reduction. Titration of oxidized hydroxylase with sodium dithionite generated mixed-valent diiron(II,III) centers as evidenced by a rhombic signal with *g*-values of 1.93, 1.87, and 1.73, which are similar to those reported for $MMOH_{mv}$.[16] Chemical reduction afforded a mixture of hydroxylases in which one active site was reduced by two electrons, or both active sites were reduced by one electron, as increasing equiv of electrons were added to the hydroxylase. The sample spectra also contained a signal at g = 4.3 from high-spin ferric ions (not shown). The intensity of this signal decreased by almost 50% as increasing equiv. of electrons were added. As a consequence of reduction of adventitious free iron(III) in the sample, the effective concentration of reductant was lower than the calculated value.

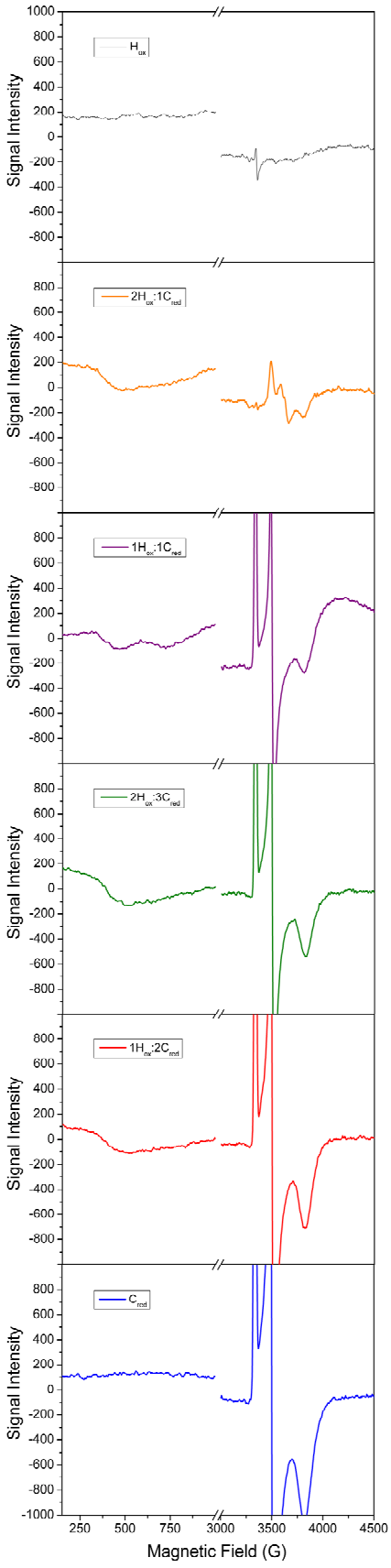

Figure B.1. EPR specta for mixtures containing variable ratios of $ToMOC_{red}$ to ToMOH:2ToMOD. The EPR spectrum of $ToMOH_{ox}$ (top) shows no signals around at 420 G (g ~ 16) and 3350 G (g ~ 2). As equivalents of $ToMOC_{red}$ were added, a signal at g = 16 was observed even at low ratios of reduced Rieske protein to $ToMOH_{ox}$. The features in the vicinity of g = 2 for ratios higher than 1:1 are similar to that of $ToMOC_{red}$ (bottom). The spectrum for 2 H_{ox}:C_{red} shows a signal at near g = 2 that differs from the reduced Rieske center, and is analogous to signals for $MMOH_{mv}$. Features at g = 16 arise from diiron(II) centers in the hydroxylase.

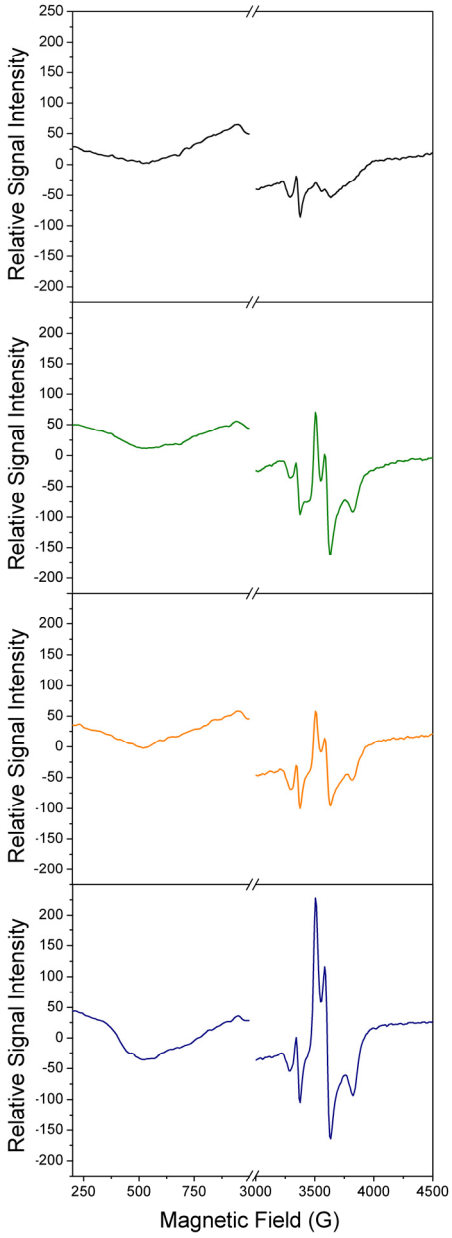

Figure B.2. EPR Spectra of ToMOH:2ToMOD mixtures reduced with one (top), two (green), three (orange), and four (blue) equivalents of electrons from sodium dithionite. The signals at $g \sim 16$ (420 G) are from the reduced diiron(II) centers, and signals near $g < 2.0$ (3350 G) from the mixed-valent diiron(II,III) centers. Addition of increasing electrons to $ToMOH_{ox}$ results in a distribution of mixed-valent and reduced centers. Chemical reduction contrasts that afforded by $ToMOC_{red}$ as a significant mixed-valent hydroxylase concentration is observed.

DISCUSSION

Reduction to Oxidized ToMOH Proceeds Through a Half-Sites Mechanism. When allowed to equilibrate, electron transfer from $ToMOC_{red}$ to $ToMOH_{ox}$ forms predominantly the reduced diiron(II) centers in the hydroxylase (Figure B.1). The mixed-valent hydroxylase is observed only at the lowest measured ratio of $ToMOC_{red}$ to ToMOH. Protein-protein interactions between ToMOC and ToMOH may favor reduction of the oxidized hydroxylase to form diiron(II) sites, instead of

mixed-valent centers. One possibility is that ToMOH:ToMOC complex formation increases the reduction potential, greatly favoring electron transfer to a mixed-valent diiron(II,III) core. In T4MO, binding between the regulatory and the Rieske proteins was reported,[26] suggesting that this complex might be relevant to reduction of the di(μ-hydroxo)diiron center in the hydroxylase. Binding of ToMOD to ToMOC could ensure accurate localization of the Rieske iron-sulfur cluster relative to the diiron center in the hydroxylase.

An appreciable amount of the Rieske protein remains unreacted and dominates the spectrum at $g \sim 2.0$. The reason that the reduced Rieske protein is not completely consumed in these samples, even at substoichiometric ratios of ToMOC to ToMOH, is unclear. In single-turnover experiments, dissociation of the coordinated hydroxylated product from the oxidized hydroxylase is enhanced by reduction of the ferric ions (Chapter 3). Product or substrate bound to the diiron center, or within the active site cavity, may gate electron transfer, as observed for mononuclear iron enzymes, such as cytochromes P450[2,27] and α-ketoglutarate.[28] Given the strong signals from the Rieske protein, low yields of the mixed-valent state would be undetected and their presence cannot be excluded.

By comparison, chemical reduction with sodium dithionite forms significantly greater quantities of the mixed-valent hydroxylase (Figure B.2). Even under these conditions and at low ratios of electrons to hydroxylase, reduction still affords diiron(II) sites within the hydroxylase. Because diiron(II) sites form in the absence of ToMOC–ToMOH protein interactions, assembly of this protein complex may dictate, only partially, the distribution of electrons to diiron(III,III) or diiron(III,II) centers. In the PHH-PHM structure, the environment around the diiron center in the protomer to which PHM is not bound shows similar helical distortions as those for the protomer to which PHM is bound.[29] Such features could arise from allosteric changes transmitted across the dimer interface as a consequence of regulatory protein binding. MMOB is proposed to bind to MMOH at the analogous site on the hydoxylase,[30] suggesting that regulatory proteins across the BMM family may bind at

spatially homologous loci on the hydroxylases. We postulate that ToMOD might modulate the potentials of the diiron center in the opposite protomer through allosteric effects. Protonation of the bridging hydroxide ligands in the oxidized hydroxylase active site is required, presumably during reduction, because these species are absent in crystal structures of reduced or Mn(II)-reconstituted forms of this protein.[6,31] Structural changes at the diiron center arising from ToMOD binding to the opposite face of the hydroxylase may open a conserved pore, facilitating proton entry and favoring reduction. Mössbauer samples prepared in an analogous manner, where the hydroxylase is ^{57}Fe-enriched, with or without other components present, would provide a more accurate probe of the electron distribution within the hydroxylase upon reduction by either sodium dithionite or ToMOC.

Half-sites Reductive and Oxidative Phases in ToMO. Half-sites reactivity during the oxidative phase of the catalytic cycle has been proposed for other members of the CBDI enzyme family. For example, the BMMs only form oxygenated intermediates in ~ 50% yield, with unreacted diiron(II) protein decaying by alternate uncharacterized pathways to the resting state.[14,32] In Δ^9D, the four-electron reduced desaturase forms a μ-1,2-peroxodiiron(III) intermediate quantitatively at both active sites, yet this intermediate is incapable of substrate desaturation under these conditions.[21] Similar control of the reductive phase has not been reported. In a half-sites mechanism in the BMMs, cellular reducing equivalents are used inefficiently if these hydroxylases are reduced by four electrons, because both active sites cannot simultaneously oxidize substrate. Therefore, strict control over the reducing factors prevents the complete reduction of the hydroxylases, ensuring maximal coupling of substrate hydroxylase to NADH consumption.

FUTURE DIRECTIONS

Here we present the first evidence that reduction of the diiron(III) centers in $ToMOH_{ox}$ in complex with ToMOD by $ToMOC_{red}$ affords predominantly two-electron reduction of a single active site, instead of one-electron reduction of both diiron(III) cores. Characterization of the electron

transfer reaction by RFQ EPR and stopped-flow optical spectroscopy with varying amounts of substrate, product, or other protein components, will further elucidate the functions of protein-protein interactions on this half of the catalytic cycle.

REFERENCES

1. Hake, R.; McLendon, G., *Chem. Rev.* **1992,** *92* (3), 481-490.

2. Denisov, I. G.; Makris, T. M.; Sligar, S. G.; Schlichting, I., *Chem. Rev.* **2005,** *105* (6), 2253-2277.

3. Merkx, M.; Kopp, D. A.; Sazinsky, M. H.; Blazyk, J. L.; Müller, J.; Lippard, S. J., *Angew. Chem., Int. Ed.* **2001,** *40* (15), 2782-2807.

4. Mason, J. R.; Cammack, R., *Annu. Rev. Microbiol.* **1992,** *46* 277-305.

5. Kurtz, D. J., Jr., *J. Biol. Inorg. Chem.* **1997,** *2* (2), 159-167.

6. Sazinsky, M. H.; Lippard, S. J., *Acc. Chem. Res.* **2006,** *39* (8), 558-566.

7. Sobrado, P.; Lyle, K. S.; Kaul, S. P.; Turco, M. M.; Arabshahi, I.; Marwah, A.; Fox, B. G., *Biochemistry* **2006,** *45* (15), 4848-4858.

8. Kopp, D. A.; Berg, E. A.; Costello, C. E.; Lippard, S. J., *J. Biol. Chem.* **2003,** *278* (23), 20939-20945.

9. Blazyk, J. L.; Gassner, G. T.; Lippard, S. J., *J. Am. Chem. Soc.* **2005,** *127* (49), 17364-17376.

10. Kopp, D. A.; Gassner, G. T.; Blazyk, J. L.; Lippard, S. J., *Biochemistry* **2001,** *40* (49), 14932-14941.

11. Gassner, G. T.; Lippard, S. J., *Biochemistry* **1999,** *38* (39), 12768-12785.

12. Liu, Y.; Nesheim, J. C.; Lee, S.-K.; Lipscomb, J. D., *J. Biol. Chem.* **1995,** *270* (42), 24662-24665.

13. Lee, S.-K.; Nesheim, J. C.; Lipscomb, J. D., *J. Biol. Chem.* **1993,** *268* (29), 21569-21577.

14. Liu, K. E.; Wang, D.; Huynh, B. H.; Edmondson, D. E.; Salifoglou, A.; Lippard, S. J., *J. Am. Chem. Soc.* **1994,** *116* (16), 7465-7466.

15. Cadieux, E.; McCormick, M. S.; Sazinsky, M. H.; Lippard, S. J., unpublished results.

16. Liu, K. E.; Lippard, S. J., *J. Biol. Chem.* **1991,** *266* (20), 12836-12839.

17. Kazlauskaite, J.; Hill, H. A. O.; Wilkins, P. C.; Dalton, H., *Eur. J. Biochem.* **1996,** *241* (2), 552-556.

18. Liu, Y.; Nesheim, J. C.; Paulsen, K. E.; Stankovich, M. T.; Lipscomb, J. D., *Biochemistry* **1997,** *36* (17), 5223-5233.

19. Astier, Y.; Balendra, S.; Hill, H. A. O.; Smith, T. J.; Dalton, H., *Eur. J. Biochem.* **2003,** *270* (3), 539-544.

20. Sjöberg, B.-M.; Karlsson, M.; Jörnvall, H., *J. Biol. Chem.* **1987,** *262* (20), 9736-9743.

21. Broadwater, J. A.; Ai, J.; Loehr, T. M.; Sanders-Loehr, J.; Fox, B. G., *Biochemistry* **1998,** *37* (42), 14664-14671.

22. Cafaro, V.; Scognamiglio, R.; Viggiani, A.; Izzo, V.; Passaro, I.; Notomista, E.; Dal Piaz, F.; Amoresano, A.; Casbarra, A.; Pucci, P.; DiDonato, A., *Eur. J. Biochem.* **2002,** *269* (22), 5689-5699.

23. Palmers, G.; Lambeth, D. O., *J. Biol. Chem.* **1973,** *248* (17), 6095-6103.

24. Baymann, F.; Giusti, F.; Picot, D.; Nitschke, W., *Proc. Natl. Acad. Sci. U.S.A.* **2007,** *104* (2), 519-524.

25. Salernoa, J. C.; McCurley, J. P.; Dong, J.-H.; Doyle, M. F.; Yu, L.; Yu, C.-A., *Biochem. Biophys. Res. Commun.* **1986,** *136* (2), 616-621.

26. Moe, L. A.; McMartin, L. A.; Fox, B. G., *Biochemistry* **2006,** *45* (17), 5478-5485.

27. Davydov, R.; Perera, R.; Jin, S.; Yang, T.-C.; Bryson, T. A.; Sono, M.; Dawson, J. H.; Hoffman, B. M., *J. Am. Chem. Soc.* **2005,** *127* (5), 1403-1413.

28. Grzyka, P. K.; Ryle, M. J.; Monterosso, G. R.; Liu, J.; Ballou, D. P.; Hausinger, R. P., *Biochemistry* **2005,** *44* (10), 3845-3855.

29. Sazinsky, M. H.; Dunten, P. W.; McCormick, M. S.; DiDonato, A.; Lippard, S. J., *Biochemistry* **2006,** *45* (51), 15392-15404.

30. Walters, K. J.; Gassner, G. T.; Lippard, S. J.; Wagner, G., *Proc. Natl. Acad. Sci. U.S.A.* **1999,** *96* (14), 7877-7882.

31. McCormick, M. S.; Sazinsky, M. H.; Condon, K. L.; Lippard, S. J., *J. Am. Chem. Soc.* **2006,** *128* (47), 15108-15110.

32. Murray, L. J.; García-Serres, R.; Naik, S.; Huynh, B. H.; Lippard, S. J., *J. Am. Chem. Soc.* **2006,** *128* (23), 7458-7459.

LESLIE JUSTIN MURRAY

EDUCATION

Ph.D. Inorganic Chemistry 2002-2007	Massachusetts Institute of Technology, Cambridge, MA Advisor: Professor Stephen J. Lippard
B.A. Chemistry 1998-2002	Swarthmore College, PA
B.A. Biology 1998-2002	Swarthmore College, PA

HONORS & AWARDS

2005	Martin Family Society of Fellows for Sustainability, Massachusetts Institute of Technology
2002	Presidential Fellow, Massachusetts Institute of Technology
2002	Phi Beta Kappa, Philadelphia Chapter
2002	American Chemical Society Scholastic Achievement Award, Swarthmore College
1997	National Scholarship, Government of Trinidad & Tobago

PUBLICATIONS

Murray, L. J., García-Serres, R., Naik, S., Huynh, B. H., and Lippard, S. J. (2006) Dioxygen activation at non-heme diiron centers: characterization of intermediates in a mutant form of toluene/*o*-xylene monooxygenase hydroxylase, *J. Am. Chem. Soc. 128*, 7458-7459.

Newcomb, M., Chandrasena, R. E. P., Lansakara-P., D. S. P., Kim, H.-Y., Lippard, S. J., Beauvais, L. G., Murray, L. J., Izzo, V., Hollenberg, P. F., and Coon, M. J. (2007) Desaturase reactions complicate the use of norcarane as a mechanistic probe. Unraveling the mixture of twenty-plus products formed in enzyme-catalyzed oxidations of norcarane, *J. Org. Chem. 72*, 1121-1127.

Newcomb, M., Lansakara-P., D. S. P., Kim, H.-Y., Chandrasena, R. E. P., Lippard, S. J., Beauvais, L. G., Murray, L. J., Izzo, V., Hollenberg, P. F., and Coon, M. J. (2007) Products from Enzyme-Catalyzed Oxidations of Norcarenes, *J. Org. Chem. 72*, 1128-1133.

Murray, L. J., and Lippard, S. J. (2007) Substrate trafficking and dioxygen activation in bacterial multicomponent monooxygenases, *Acc. Chem. Res. 40*, 466-474.

Murray, L. J., Naik, S. G., Ortillo, D. O., García-Serres, R., Lee, J. K., Huynh, B. H., and Lippard, S. J. (2007) Characterization of the arene-oxidizing intermediate in ToMOH as a diiron(III) species, submitted.

Murray, L. J., García-Serres, R., McCormick, M. S., Davydov, R., Naik, S., Kim, S.-H., Hoffman, B. M., Huynh, B. H., and Lippard, S. J. (2007) Dioxygen activation at non-heme diiron centers: oxidation of a proximal residue in the I100W variant of ToMOH, submitted.

PRESENTATIONS

234th American Chemical Society National Meeting & Exposition, Boston, MA, Aug. 19-23, 2007. Short talk title: Dioxygen Activation at the non-heme diiron center of the hydroxylase component of toluene/*o*-xylene monooxygenase.

Inorganic Reaction Mechanisms Gordon Research Conference, Ventura, CA, Feb. 18-23, 2007. Poster title: Dioxygen Activation in the Toluene/*o*-Xylene Monooxygenase System.